

**Characterization and immunogenicity of novel
MVA-based vaccines against *Chlamydia
trachomatis* in different mouse models**

Inaugural dissertation

for the attainment of the title of doctor in the Faculty of Mathematics
and Natural Sciences
at the Heinrich Heine University Düsseldorf

presented by

Giuseppe Andreacchio

from Messina, Italy

Düsseldorf, April 2025

from the institute for Virology
at the Heinrich Heine University Düsseldorf

Published by permission of the Faculty of Mathematics and Natural
Sciences at
Heinrich Heine University Düsseldorf

Supervisor: Prof. Dr. med Ingo Drexler
Co-supervisor: Prof. Dr. rer. nat. Kalscheuer.

Date of the oral examination: **18th June 2025**

The data presented in this work supported the publication of the following manuscript:
Viral vector-based *Chlamydia trachomatis* vaccines encoding CTH522 induce distinct immune responses in C57BL/6J and HLA transgenic mice. Vaccines (Basel). 2024 Aug 22;12(8):944. doi: 10.3390/vaccines12080944.

The publication provides a detailed account of the authors' contributions. In summary, Andreacchio G. contributed most of the raw data for the manuscript, performed most of the experiments, drafted the initial version of the manuscript, and was involved in all aspects of subsequent revisions and finalization. The co-authors contributed by editing the manuscript, experimental design, data curation, data analysis, methodology, investigation, supervision and securing funding.

Table of contents

List of abbreviations	1
Summary	3
1. Introduction	5
1.1. Adaptive immune response	5
1.1.1. Humoral immune response.....	5
1.1.2. Cellular-mediated immune response.....	8
1.2. Vaccines	14
1.2.1. Principles of vaccination and vaccine development.....	14
1.2.2. Poxviruses	14
1.2.3. Modified Vaccinia Virus Ankara	15
1.3. Chlamydia trachomatis	16
1.3.1. Biology of Chlamydia trachomatis	16
1.3.2. Epidemiology of C. trachomatis.....	18
1.3.3. Mouse models for investigating C. trachomatis infection and immune response	19
1.3.4. Adaptive immune response to C. trachomatis infection.....	22
1.3.5. Vaccine research addressing C. trachomatis infection.....	24
2. Aim of the thesis	26
3. Materials.....	27
3.1. Plasmids.....	27
3.2. Primers.....	28
3.3. Antibodies.....	28
3.4. Peptides.....	29
3.5. Enzymes	29
3.6. Bacteria.....	30
3.7. Cell lines	30
3.8. Viruses	30
3.9. Mice.....	31
3.10. Buffers	31

Homemade Buffers	31
Commercial Buffers	32
3.11. Media.....	32
3.12. Chemicals	33
3.13. Kits	34
3.14. Instruments	34
4. Methods.....	35
4.1. Shuttle plasmid vector construction	35
4.2. Bacteria transformation for plasmid amplification.....	37
4.3. Recombinant Bacterial Artificial Chromosome (BAC) construction.....	38
4.4. Isolation of recombinant BAC.....	39
4.5. Rescue of recombinant MVA.....	40
4.6. Purification of MVA.....	42
4.7. Titration of MVA	43
4.8. Sequencing of target DNA inserted in recombinant MVA genomes	43
4.9. Eukaryotic cell culture.....	44
4.10. In vitro infection.....	44
4.11. SDS-PAGE and Western Blot analysis	45
4.12. Immunofluorescence Microscopy	46
4.13. Immunization of mice.....	47
4.14. Isolation of splenocytes, blood and vaginal washes	48
4.15. Ex vivo T-cell activation	48
4.16. Intracellular cytokines staining (ICS).....	48
4.17. Enzyme-Linked Immunosorbent Assay (ELISA)	49
5. Results.....	51
5.1. Generation of recombinant MVA-CTH522 and MVA-spCTH522.....	51
5.2. In vitro characterization of MVA-CTH522 and MVA-spCTH522	54
5.2.1. Analysis of the stability passage of MVA-CTH522 and MVA-spCTH522.....	54
5.2.2. Kinetics of CTH522 and spCTH522 antigen synthesis.....	56

5.2.3.	Growth kinetics analysis of MVA-CTH522 and MVA-spCTH522.....	59
5.2.4.	Localization of spCTH522.....	60
5.3.	Ex-vivo analysis of CTH522-specific immune response in C57BL/6J mice	62
5.3.1.	MVA-spCTH522 and MVA-CTH522:B7 induced CD4 ⁺ but not CD8 ⁺ T-cell responses in C57BL/6J mice	62
5.3.1.	MVA-CTH522:B7 but not MVA-spCTH522 induces antibody responses in C57BL/6J mice.....	66
5.4.	Ex-vivo analysis of CTH522-specific immune responses in HLA-A2.DR1 mice70	
5.4.1.	Single dose of MVA-spCTH522 and MVA-CTH522:B7 induces T-cell responses in HLA-A2.DR1 mice	70
5.4.1.	A booster dose of MVA-spCTH522 and MVA-CTH522:B7 increased T-cell responses in HLA-A2.DR1 mice	75
5.4.2.	MVA-CTH522:B7 but not MVA-spCTH522 induce antibody responses in HLA-A2.DR1 mice	80
6.	Discussion	82
7.	Conclusion.....	94
	References.....	95
8.	Appendix.....	106
8.1.	Supplementary material.....	106
8.2.	List of Figures.....	112
8.3.	List of Tables.....	114
	Acknowledgement	115
	Declaration.....	116

List of abbreviations

aa	amino acids
ADCC	antibody dependent cellular cytotoxicity
APCs	antigen-presenting cells
APS	Ammonium Persulfate
ASCs	antibody-secreting cells
BAC	Bacterial Artificial Chromosome
BCR	B-cell receptor
BFA	Brefeldin A
BSA	Bovine serum albumin
CAM	chloramphenicol
CD(n)	cluster of differentiation
C _D	constant domains
CEF	chicken embryo fibroblasts
CPE	cytopathic effects
CTLs	cytotoxic T lymphocytes
CVA	Chorioallantois Vaccinia virus Ankara
DCs	dendritic cells
DMSO	Dimethyl sulfoxide
EB	elementary body
ELISA	Enzyme-Linked Immunosorbent Assay
ER	endoplasmic reticulum
ERAP	endoplasmic reticulum aminopeptidase
Fab	antigen-binding fragment
FACS	fluorescence-activated cell sorting
FBS	Fetal bovine serum
Fc	crystallizable fragment
FDCs	Follicular dendritic cells
Fwd	Forward
GFP	green fluorescent protein
H.P.I.	hours post infection
HCl	Hydrogen chloride
HeLa	Henrietta Lacks
HIV	Human Immunodeficiency Virus
HLA	Human Leucocytes Antigens
I.P.	intraperitoneal
ICS	intracellular cytokine staining
IFN	Interferon
Ig	immunoglobulin
IL	Interleukin
IU	infectious units
LGV	lymphogranuloma venereum
MHC	Major Histocompatibility Complex
MOI	multiplicity of infection
MOMP	major outer membrane protein

MVA	Modified Vaccinia virus Ankara
nAbs	neutralizing antibodies
NK	natural killer
NLRs	nucleotide-binding oligomerization domain-like receptors
OD	Optical density
ORF	open reading frames
OVA	ovalbumin
PA	polyallomer
PAGE	polyacrylamide gel electrophoresis
PAMPs	pathogen-associated molecular patterns
PBMCs	peripheral blood mononuclear cells
PBS	Phosphate-buffered saline
PCR	Polymerase Chain Reaction
pNPP	p-nitrophenyl phosphate
PRRs	pattern recognition receptors
RB	reticulate body
Rev	Reverse
RFV	rabbit fibroma virus
SARS-CoV-2	Severe Acute Respiratory Syndrome coronavirus 2
SDS	Sodium Dodecyl Sulfate
STDs	sexually transmitted diseases
STING	stimulator of interferon genes
TAP	Transporter associated with Antigen Processing
TB	Tuberculosis bacterium
TBE	TRIS-Borate-EDTA
TCID	tissue culture infectious dose
TCM	central memory T-cells
TCR	T-cell receptor
TEM	effector memory T-cells
Tfh	T follicular helper cells
Th	T helper cell
TLR	Toll-like receptor
TNF	Tumor necrosis factor
VACV	Vaccinia virus
V _D	variable domains
WGA	wheat germ agglutinin

Summary

Chlamydia trachomatis is a leading cause of sexually transmitted infections worldwide and a major public health concern due to its prevalence and potential complications, including infertility and pelvic inflammatory disease, requiring innovative vaccine solutions. Modified Vaccinia Virus Ankara (MVA) is a well-established, safe and highly immunogenic vaccine vector, making it a promising candidate for *C. trachomatis* vaccine development. The MVA vector was engineered to express the *C. trachomatis* MOMP-based CTH522 antigen, a known target for immune responses against *C. trachomatis*. The vaccines were designed with two variations of the antigen: one in a secreted form (MVA-spCTH522) and the other in a membrane-anchored form (MVA-CTH522:B7). These variations were used to investigate how the localization of the antigen affects the immune response. The vaccine candidates were tested in two different mouse models: C57BL/6J mice, a standard strain widely used in immunological research, and HLA transgenic mice, which express human leukocyte antigen (HLA) molecules to better mimic human immune responses. This dual model evidenced how immune responses differ in a standard inbred mouse system compared to one that more closely associates with human immunology. In the C57BL/6J mouse model, both vaccines successfully induced CD4⁺ T cell responses, a critical component of the adaptive immune system. However, they did not induce significant antigen-specific CD8⁺ T-cell responses, which are often associated with the clearance of intracellular pathogens such as *C. trachomatis*. Notably, the membrane-anchored form of the vaccine, MVA-CTH522:B7, induced a more robust antibody response, particularly in the form of IgG2b and IgG2c antibodies, which are indicative of a Th1-directed immune response. This finding suggests that localization of the antigen to the cell membrane may enhance its immunogenicity. In the HLA transgenic mouse model, both vaccines demonstrated the ability to stimulate Th1-directed CD4⁺ T cells and multifunctional CD8⁺ T cells. However, only the MVA-CTH522:B7 vaccine induced a detectable antibody response in this model. This observation further confirms the importance of antigen localization in determining the nature and strength of the humoral immune response. The results of the study emphasize the critical role of antigen design for vaccine efficacy. The form and localization of the antigen significantly influenced the immune response, with the membrane-anchored form showing greater potential to induce both humoral and cellular immunity. The research also highlights the importance of selecting appropriate animal models for preclinical testing, as immune responses can vary widely between different systems. These results provide valuable insights into the development of vaccines against *C. trachomatis*. While the study provides a strong foundation for further research, it also highlights the complexity of vaccine development and the importance of using animal models which allow for immune responses that closely

mimic the human immune response to better predict vaccine performance in humans. Future studies should investigate the efficacy of these vaccines in preventing *C. trachomatis* infection, assess their protective potential in challenge models, and evaluate different immunization strategies, including mucosal and systemic routes of administration. The research represents a significant step forward in addressing a pressing global health challenge and lays the groundwork for the development of effective vaccines against *C. trachomatis*.

1. Introduction

1.1. Adaptive immune response

The adaptive immune response is one of the two main components of the immune system, the other being the innate immune response. Together, they form the most sophisticated defense mechanism in the human body. It is characterized by its ability to recognize specific pathogens, respond with precision, and remember these invaders for future protection. Vaccines harness this extraordinary system and train it to defend against infectious diseases without causing the illness itself¹.

1.1.1. Humoral immune response

1.1.1.1 B-cell lymphocytes

The humoral component of the adaptive immune response is responsible for the production and function of antibodies, also known as immunoglobulins. This arm of the immune response is orchestrated primarily by B-cells, a subtype of lymphocytes. After infection or vaccination, B-cells that recognize specific antigens are activated and transform into antibody-secreting cells (ASCs) that produce neutralizing antibodies (nAbs), or transform into memory B-cells². This process begins as the antigen travels to the secondary lymphoid organs, such as draining lymph nodes, where B-cells equipped with surface B-cell receptors (BCR) bind specific antigens and undergo rapid activation³. In the extrafollicular response, B-cells rapidly mature into ASCs, known as plasma cells. Although short-lived, plasma cells play a critical role in clearing active infections, since they produce large quantities of antigen-specific antibodies within the first few weeks after infection or vaccination⁴. The follicular response is initiated when activated CD4⁺ helper T-cells, discussed later, provide co-stimulatory signals to B-cells, prompting them to enter or initiate the germinal center response. B-cells increase expression of CXCR5 in order to migrate toward higher concentrations of CXCL13 produced by follicular dendritic cells (FDCs) and T follicular helper cells (Tfh) within the B-cell follicle⁵. Within the germinal center, activated B-cells undergo rapid proliferation and somatic hypermutation in the dark zone to develop higher affinity BCR. B-cells with newly acquired mutations in the BCR then migrate to the light zone to test the BCR against antigens presented by FDCs. Tfh cells signal B-cells to return to the dark zone for further somatic hypermutation or differentiation. Finally, B-cells with high affinity BCRs are selected for further differentiation into memory B-cells or plasma cells⁶. Plasma cells migrate to the bone marrow where they continuously produce high affinity antibodies, while memory B-cells monitor secondary

lymphoid organs for their specific antigen. Upon encountering their antigen during a secondary infection or vaccination, memory B-cells rapidly differentiate into plasma cells or even more potent memory B-cells with enhanced affinity BCRs. Together, long-lived plasma cells and memory B-cells are critical in providing protective immunity against pathogens⁷.

1.1.1.2 Antibodies

Antibodies are Y-shaped protein complexes composed of two identical heterodimers, each consisting of a heavy chain and a light chain linked by disulfide bonds⁸ (Fig. 1). Both heavy and light chains contain variable regions (V_H and V_L) and constant regions (C_{H1-H3} and C_L). Antibodies have diverse functions based on two distinct domains: the antigen-binding fragment (Fab) and the crystallizable fragment (Fc). Each antibody consists of two identical Fab domains linked by a flexible hinge region to a single Fc domain. The Fab domain incorporates the variable regions of the Ig heavy and light chains, which together form the antigen binding site. These variable regions arise by V(D)J recombination during B-cell development and can be further optimized by somatic hypermutation upon encountering antigens, thereby increasing their affinity for specific targets⁹. In IgG, a family of antibodies which primarily protect against infectious diseases, the Fab fragment binds specific region of pathogenic antigen in order to neutralize pathogens. This function is critical for preventing their entry into host cells and controlling their replication and dissemination. The specificity and affinity of the Fab region are key factors influencing the neutralizing efficacy of antibodies. The Fc domain consists of the constant regions of two heavy chains and facilitates non-neutralizing antibody functions by interacting with various receptors or complement. In mice, the IgG family is divided into five subclasses: IgG1, IgG2a, IgG2b, IgG2c and IgG3^{10,11}. The subclasses differ mainly in the amino acid composition of the flexible hinge regions and in the different glycosylation patterns in the Fc regions, which together define the effector functions of the IgG. Different strains of mice produce either IgG2a or IgG2c¹².

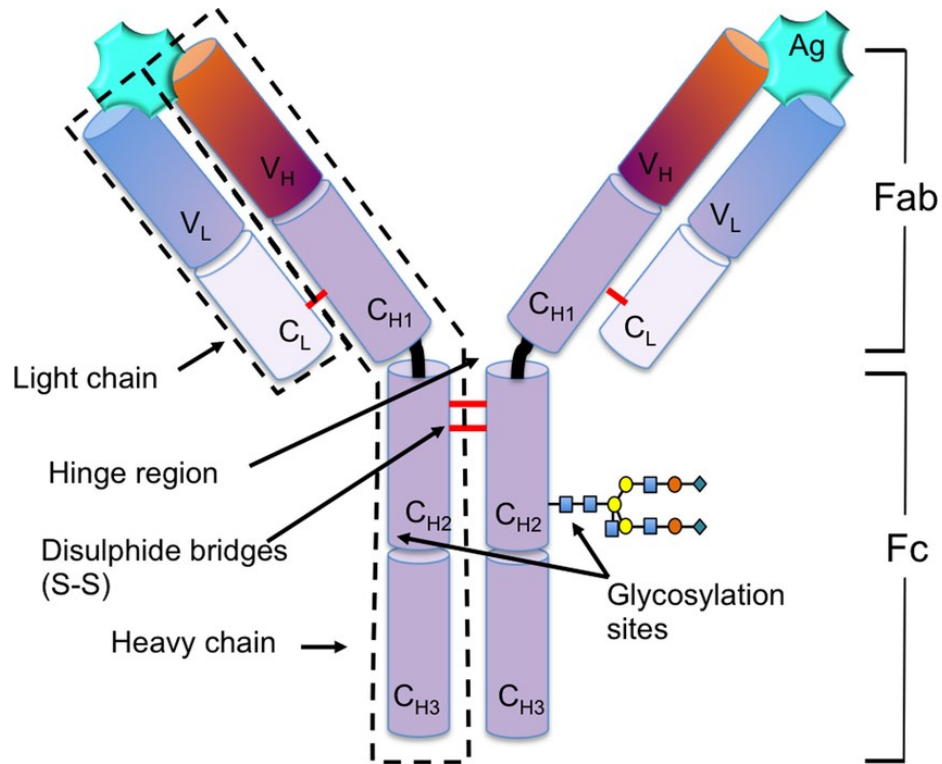


Figure 1. Schematic structure of antibodies.

The antibody molecule is composed of four polypeptide chains: two identical heavy chains and two identical light chains, which are held together by disulfide bonds, depicted here in red. Each light chain consists of two regions: a variable light region (V_L) and a constant light region (C_L). Similarly, each heavy chain contains a variable heavy region (V_H) and three constant regions, designated as C_{H1}, C_{H2}, and C_{H3}. The Fc region of the IgG molecule plays a critical role in mediating effector functions of the immune system, such as engaging Fc receptors on immune cells and activating the complement system. Image source: *Antibody Technology Journal* volume 6, 17–32¹³.

Another important class of antibodies is immunoglobulin A (IgA), which plays a critical role in maintaining mucosal homeostasis in the gastrointestinal, respiratory and genitourinary tracts. As the dominant antibody in mucosal immunity, IgA is the second most abundant immunoglobulin in the body and provides essential defense against mucosal-associated pathogens. In humans and primates, serum IgA is predominantly monomeric, whereas in other animals it is predominantly dimeric. In mucosal sites, IgA is produced by local plasma cells primarily as dimeric IgA (dIgA), which consists of two monomers linked by a J chain. This form of dimeric IgA binds to the polymeric immunoglobulin receptor (pIgR) on the basolateral side of epithelial cells, facilitating its transport across the epithelium. Upon reaching the luminal side, pIgR is cleaved, leaving a fragment known as the secretory component (SC), which binds to dIgA to form secretory IgA (SIgA). The secretory component is a hydrophilic, highly glycosylated, negatively charged molecule that protects SIgA from enzymatic

degradation in luminal secretions, thereby ensuring its stability and efficacy in mucosal immunity¹⁴.

Antibodies perform a variety of critical functions in the immune response¹⁵, including:

- Neutralization: antibodies have the ability to directly bind to pathogens, such as viruses or bacteria, and inhibit their ability to infect host cells.
- Opsonization: antibodies can target pathogens for engulfment by immune cells such as macrophages and neutrophils.
- Complement activation: antibodies can activate the complement system, a cluster of proteins that amplify the immune response by promoting inflammation, cell lysis, and phagocytosis.
- Antibody dependent cellular cytotoxicity (ADCC): antibodies can recruit natural killer (NK) cells and other immune cells to eliminate infected or abnormal cells.

The humoral segment of the adaptive immune response is a critical defense mechanism against extracellular pathogens, including bacteria and bloodstream viruses, and toxins. It confers durable protection and is an integral part of vaccination strategies. Vaccines are designed to stimulate the production of precise antibodies without causing disease, thereby preparing the immune system to respond effectively to future encounters with the same pathogens¹⁶.

1.1.2. Cellular-mediated immune response

The cellular component of the adaptive immune system consists of lymphocytes, which are further subdivided into B-cells, mentioned before, and T-cells¹⁷. These lymphocytes mature in specific locations, with B-cells maturing in the bone marrow and T-cells maturing in the thymus^{18,19}. Each cell type carries a receptor, either the B-cell receptor or the T-cell receptor (TCR). Similar to the BCR, the TCR exhibits a high degree of diversity, generated from a limited number of receptor genes by processes such as V(D)J recombination and the random addition of nucleotides during cell development²⁰. Because of the partially random nature of this process, each receptor is specific and unique to a clonal cell. What distinguishes the adaptive immune system from the innate immune system is its ability to recognize a wide range of specific components of pathogens, such as membrane and secreted proteins, through BCRs and TCRs, rather than relying on the recognition of conserved pathogen components, such as LPS^{21,22}. The BCRs can recognize full length antigens of pathogens, whereas TCRs recognize processed antigens as peptides presented on major histocompatibility complex

(MHC) molecules^{23,24}. T-cells can be further subdivided into CD4⁺ (helper T-cells) and CD8⁺ (cytotoxic T-cells), which interact with different types of MHCs and have different functions²⁵. MHC class I is expressed by almost all nucleated cells and consists of a heavy chain and a soluble β 2 microglobulin. The α 1 and α 2 domains of the heavy chain form a peptide-binding groove for 8-11 amino acid long peptides. MHC class II, on the other hand, is mainly expressed by professional antigen-presenting cells (APCs), including B-cells, dendritic cells (DCs), and macrophages. It is composed of an α chain and a β chain and binds longer peptides (12-14 amino acids) within a peptide-binding groove open at both ends²⁶. The differences between peptides presented on MHC class I and class II extend beyond their length to include their production process and source. Peptides presented on MHC class I usually originate from intracellular synthesized proteins that are degraded by the proteasome, a cytosolic multi-subunit complex of proteases. The resulting peptides are then transported by the transporter associated with antigen processing (TAP) protein complex to the endoplasmic reticulum (ER), where they are further truncated by aminopeptidases such as endoplasmic reticulum aminopeptidase I (ERAP I). The peptides are then loaded onto MHC class I molecules, which assemble with β 2 microglobulin. The newly formed MHC class I/peptide complexes are then transported to the cell surface where they present the peptides to CD8⁺ T-cells²⁷. MHC class I molecules are expressed on all nucleated cells, allowing CD8⁺ T-cells to recognize infected cells through the presentation of endogenously produced pathogen-derived epitopes^{28,29} (Fig. 2). In contrast, MHC class II molecules usually present epitopes that derive from extracellular proteins taken up by professional APCs such as DCs, macrophages and B-cells³⁰. The process of uptake of the extracellular proteins occurs through several cellular internalization mechanisms, such as phagocytosis, endocytosis or macropinocytosis. After internalization, extracellular antigens are degraded into peptides by acidic proteases such as cathepsins within endosomes. MHC class II molecules are transported from the endoplasmic reticulum to the endosomes. To prevent premature binding of self-peptides, MHC II complexes are loaded with a placeholder peptide called invariant chain. The vesicles containing MHC class II/invariant chain complexes fuse with the peptides containing endosomes, and the invariant chain is replaced by a peptide produced in the endosome. The fully assembled MHC class II/peptide complexes are then transported to the cell surface where patrolling CD4⁺ T-cells can recognize their respective epitopes³¹. Over the past decade, numerous studies have demonstrated the involvement of several alternative mechanisms in antigen processing and presentation. Through a process known as cross-presentation, epitopes derived from phagocytosed proteins can also be presented on MHC class I, while autophagy, a degradation pathway that delivers cellular organelles and proteins to lysosomes to maintain homeostasis, also plays a critical role in antigen presentation by transporting pathogen-derived

intracellular antigens to lysosomal compartments for processing, thereby enhancing MHC class II presentation to CD4⁺ T cells.^{32,33} (Fig. 2).

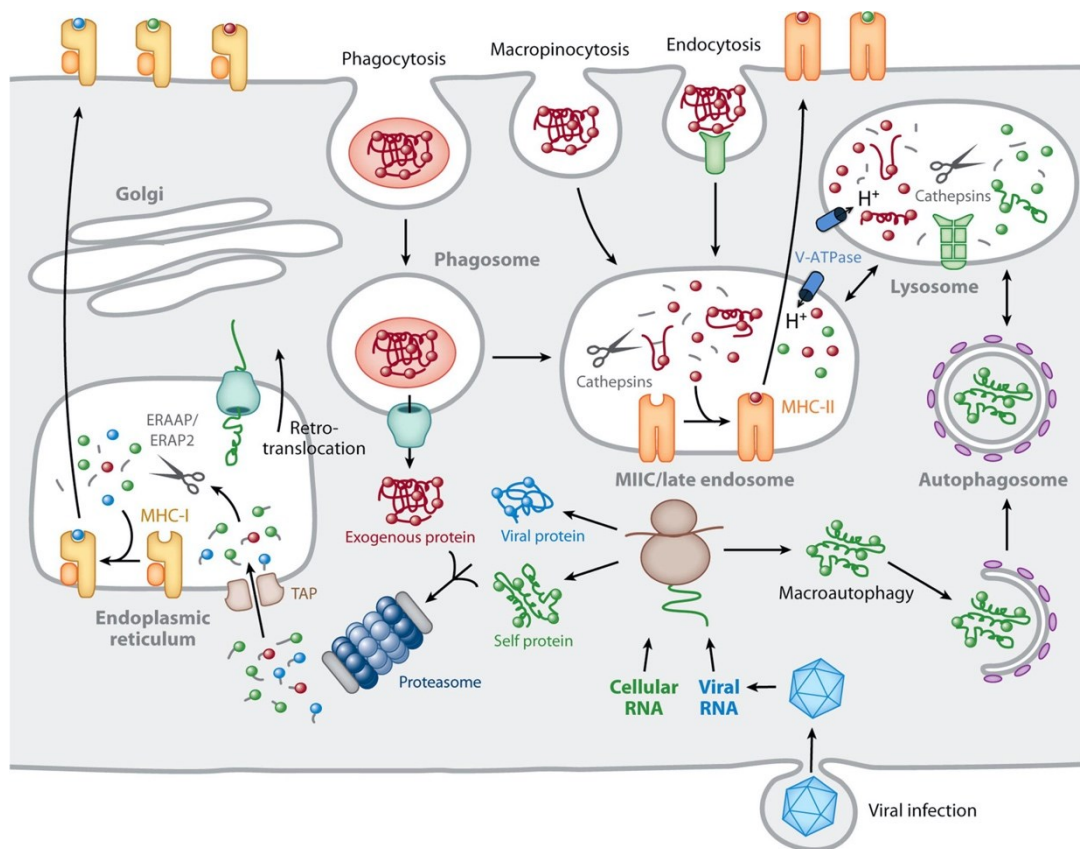


Figure 2. Pathways of antigen processing and presentation.

In MHC-I-mediated presentation, proteins synthesized in the cytosol are degraded into small peptides by the proteasome. Peptides are then transported into the ER lumen by TAP to bind to newly synthesized MHC I molecules. Within the ER, peptides can be further truncated by ERAAP1 and ERAAP2 to a final length of 8-10 amino acids. Fully assembled MHC-I peptide complexes exit the ER and are transported to the plasma membrane where they are recognized by CD8⁺ T cells. In MHC-II-mediated presentation, proteins are internalized into endosomes by various mechanisms and degraded into peptides in late endosomes. These endosomes are rich in proteases known as cathepsins, which function optimally at acidic pH. MHC-II molecules are targeted from the ER to these compartments via their association with the invariant chain, a chaperone (not shown). In late endosomes, the invariant chain is proteolytically degraded, allowing MHC-II molecules to bind exogenously derived peptides. After a series of peptide processing steps, immunodominant MHC-II peptide complexes are transported to the plasma membrane for recognition by CD4⁺ T cells. Among the mechanisms for antigen processing for MHC-II-mediated presentation, autophagy provides processed peptides by encapsulating cytosolic proteins in a double-membrane autophagosome that matures by fusion with lysosomes to form proteolytic autophagolysosomes. In specialized antigen-presenting cells (APCs), such as DCs, proteins taken up by endocytosis or phagocytosis are retro-translocated to the cytosol for proteasomal degradation and subsequent binding to MHC-I in a process called cross-presentation. Although the mechanism of retro-translocation remains undefined, it is depicted here as a channel involved in ER-associated degradation (ERAD) that can be recruited from the ER to the phagosome. Image source: *Microbiol Spectr.* Volume 4(3), 2016³⁴.

1.1.2.1 T-cell activation

To fulfil their role, T-cells must undergo an initial activation process to become epitope-specific effector T-cells. This activation occurs through a mechanism known as antigen presentation, which is carried out by specialized APCs³⁵. Antigen presentation triggers the activation of naive T-cells, which have T-cell receptors specific for antigen-derived epitopes. In general, macrophages, B-cells and DCs are considered professional APCs because they have the ability to activate both CD4⁺ and CD8⁺ T-cells, with DCs being particularly proficient in this role³⁵. T-cell activation requires the contribution of specific and orchestrated signals as well as the physical interaction between different types of immune cells. One of these signals is TCR engagement, which results from the initial interaction between the APC and T-cell³⁶. This interaction involves binding between the MHC-I/peptide or MHC-II/peptide complex of the APC and the TCR as well as the CD3 complex of CD8⁺ or CD4⁺ T-cells, respectively. In addition to MHC presentation of the peptide, co-stimulatory signals are essential to prevent anergic responses³⁷. These co-stimulatory signals are mediated by specific ligands, such as CD80 and CD86, that are expressed on the surface of APCs and interact with the CD28 receptor on the surface of T-cells³⁸. In addition, the interaction between CD40 on APCs and CD40 ligand on T-cells is recognized as critical for proper T-cell activation³⁹. The activation and differentiation of CD8⁺ T-cells is further influenced by an additional signal that depends on the secretion of different cytokines by APCs and the spatial co-interaction of CD4⁺, CD8⁺ and APCs⁴⁰. In fact, CD4⁺ T-cells can enhance the CD8⁺ T-cell response by 'licensing' DCs. This licensing process involves CD40-CD40L interactions between DCs and CD4⁺ T-cells, leading to the functional maturation of DCs^{41,42}. Simultaneously, CD4⁺ T-cells contribute to the enhancement of CD8⁺ T-cell responses by aiding the spatial access and interaction between the licensed DCs and CD8⁺ T-cell. Licensed DCs can then interact with CD8⁺ T-cells which initiate a robust response. This is achieved through CD4⁺ T-cell inducing the production of CCL3/4/5 and IL-12 by licensed DCs and an increased expression of the chemokine receptor CCR5 on CD8⁺ T-cells⁴³. Licensed DCs-produced IL-12 interacts with CCR5 on CD8⁺ T cell, which in turn induces the expression of CD25, also known as IL-2 receptor, in CD8⁺ T cells. Increased CD25 can subsequently interact with CD4⁺ T cells-produced IL-2, which promotes the proliferation and survival of CD8⁺ T cells^{44,45} (Fig. 3).

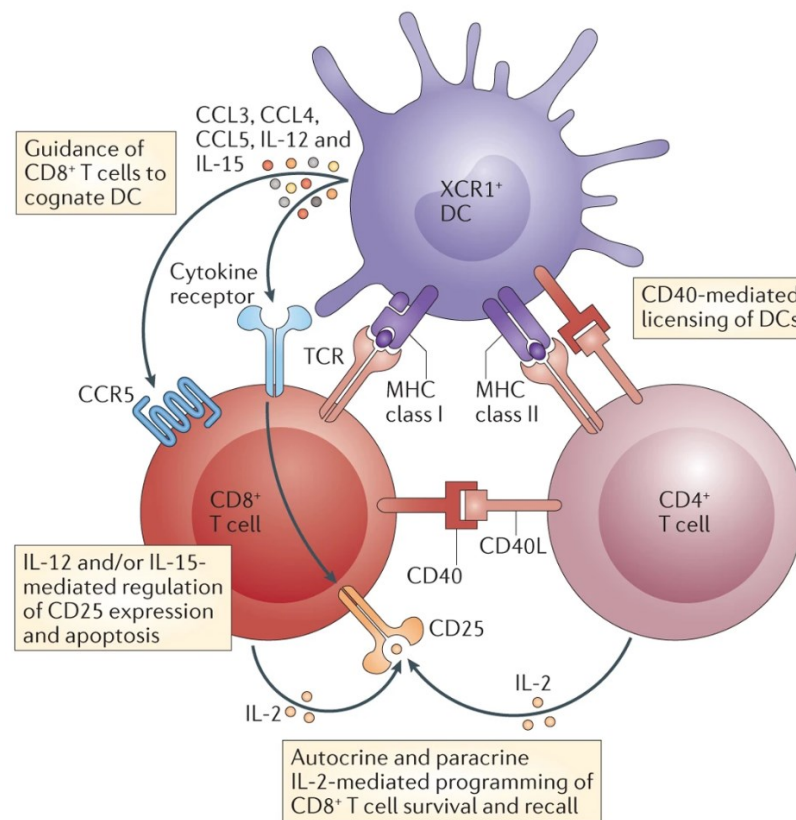


Figure 3. The multifaceted role of CD4⁺ T-cells in CD8⁺ T-cell activation.

CD4⁺ T-cells are activated and subsequently engage in a CD40-dependent process to license XCR1⁺ DCs. These licensed DCs exhibit increased expression of MHC and co-stimulatory molecules, enabling them to attract CD8⁺ T-cells to their cognate DC by releasing CCL3, CCL4 and CCL5. Licensed DCs also secrete interleukin-12 (IL-12) and interleukin-15 (IL-15), which increase CD25 expression (IL-2 receptor) on CD8⁺ T-cells and promote their survival. Increased CD25 expression enhances the response of CD8⁺ T-cells to IL-2, further promoting their survival and proliferation in subsequent encounters with the antigen. Notably, both CD4⁺ and CD8⁺ T-cells can serve as sources of IL-2 and are also capable of direct interactions via CD40-CD40 ligand (CD40L) signaling when exposed to cellular antigens. Image source: Nat. Rev. Immunol. volume 16, 2016, 102–111⁴⁶.

1.1.2.2 CD4⁺ T-cells

After proliferation, the majority of T-cells undergo terminal differentiation into end-stage effector cells and die after clearance of the infection⁴⁷. CD4⁺ T-cells differentiate into different types of T helper cells depending on cytokine production. Briefly, Th1-skewed CD4⁺ T-cells primarily produce IFN- γ , IL-2 and TNF- α to directly stimulate immune cells to kill pathogen-infected cells, such as cytotoxic effector CD8⁺ T-cells. Th2-skewed CD4⁺ T-cells and Tfh cells primarily produce IL-4 and IL-5 and serve as T helper cells that assist B-cells in antibody production⁴⁸.

1.1.2.3 CD8⁺ T-cells

Viral or intracellular bacterial infections require the differentiation of CD8⁺ T-cells into effector cytotoxic T lymphocytes (CTLs) that mediate clearance of the infection by inducing the death of infected cells⁴⁹. Cytotoxic CD8⁺ T-cells eliminate infected cells by releasing death-inducing granules that contain perforin and granzymes, and by releasing cytokines such as IFN- γ and TNF- α ⁵⁰. When a cell is infected with an intracellular pathogen, it attempts to signal the immune system about the infection by degrading pathogen-associated proteins and presenting the resulting peptides on its surface via MHC-I molecules. If effector CD8⁺ T-cells have been previously activated by APCs, they can recognize the infected cells and initiate their killing⁵¹. Traditionally, activated cytotoxic T-cells have been associated with killing pathogen-infected cells through perforin-granzyme-mediated apoptotic pathways and Fas-FasL signalling²⁸. However, recent research has shown that CD8⁺ T-cells can also use alternative cytotoxic mechanisms, such as ferroptosis and pyroptosis, to kill cells⁵². Interactions between CD8⁺ T-cells and their target cells are characterized by sustained motility of the T-cells over the target cell surface. These mechanical forces facilitate pore formation in the target cell membrane, allowing effective killing via the secretion of granzymes, perforin, cathepsin C and granulysin, which fuse with the target cell membrane⁵³. This complex of granulysin, perforin and granzymes can also be endocytosed by the target cell. Within the endosomal compartment of the target cell, granulysin and perforin form pores, releasing granzymes into the cytoplasm⁵⁴. In addition, CD8⁺ T-cells induce target cell death by expressing FasL on cell surface. FasL binds to Fas receptors on target cells and initiates death domain signaling via FADD. This cascade activates caspases and endonucleases, culminating in DNA fragmentation and target cell death⁵⁵.

1.1.2.4 Memory T-cells

A small fraction of effector T-cells remaining after pathogen clearance further differentiate into memory T-cells⁵⁶. The two primary subsets of memory T-cells are effector memory T-cells (TEM), which are characterized by low levels of the surface markers CD62L and CCR7 and typically reside in non-lymphoid tissues, and central memory T-cells (TCM), which express high levels of CD62L, CCR7, and CD127 and typically reside in secondary lymphoid organs and bone marrow⁵⁷. Upon re-exposure to a specific pathogen-associated antigen, memory T-cells, including those generated by vaccination, rapidly differentiate into large numbers of effector T-cells⁵⁸. This rapid transformation allows the immune system to mount

an effective and immediate response, neutralizing the pathogen before it can cause significant damage. This mechanism plays a critical role in adaptive immunity, enabling the body to respond effectively to previously encountered pathogens and providing enhanced protection against infection or disease recurrence. Vaccine-induced memory T-cells are particularly valuable because they 'remember' the antigen introduced by the vaccine before pathogen encounter and are primed for rapid activation and expansion⁵⁹.

1.2. Vaccines

1.2.1. Principles of vaccination and vaccine development

Edward Jenner provided the world with the first solid scientific evidence that protection against infectious agents could be achieved by intradermal inoculation of cowpox, which effectively conferred immunity to smallpox its highly virulent but antigenically close relative^{60,61}. Subsequently, in the late 19th century, Louis Pasteur demonstrated that infectious agents could be weakened and rendered harmless for use in vaccination⁶². To this day, vaccines remain a fundamental discipline within the field of medicine and are recognized as the most cost-effective public health measure for reducing morbidity and mortality from infectious agents in both animals and humans⁶³. The efficacy or performance of a vaccine depends on several factors, including the specific disease, the strain of the pathogen, individual characteristics (such as ethnicity, age and genetic predisposition) and the method of vaccine delivery⁶⁴⁻⁶⁸. While all of these factors play a critical role in vaccine development, particular emphasis is placed on the composition of the antigen and the means of vaccine delivery. Recent scientific and technological advances, including genome sequencing and innovative vaccine delivery platforms, have had a profound impact on the field of vaccine development⁶⁹. Traditionally, vaccines have been designed to induce antibody responses. However, newer vaccine platforms, such as viral vectored vaccines, are being explored to stimulate also T-cell responses against infectious pathogens^{70,71}. Among these platforms, recombinant adenoviruses and modified vaccinia virus Ankara (MVA) have emerged as extensively studied viral vectors for the expression of foreign antigens, known for their ability to induce potent, antigen-specific antibody and T-cell responses against a wide range of infectious diseases, including HIV, TB, and influenza.

1.2.2. Poxviruses

Poxviruses, particularly the prototypical *orthopoxvirus* vaccinia virus (VACV), have emerged as valuable recombinant expression systems for vaccine development following the eradication of human smallpox in 1980⁷². They possess numerous characteristics that make them advantageous as vaccine platforms⁷³. In particular, poxviruses have the ability to integrate substantial amounts of DNA, including foreign genes, into their extensive genomes⁷⁴. Importantly, because their entire replication cycle occurs exclusively within the host cell cytoplasm, gene expression occurs without potential integration of viral DNA into the host genome. This is made possible by the tight regulation of virus-specific transcription and RNA modification systems⁷⁵⁻⁷⁷. In addition, poxviruses have the ability to induce robust adaptive immunity involving both humoral and cellular responses^{78,79}. It's worth noting, however, that the use of poxviruses as vector vaccines, such as vaccinia virus, has occasionally been associated with severe side effects, particularly in immunocompromised individuals⁸⁰⁻⁸³. Consequently, Modified Vaccinia virus Ankara (MVA) virus has gained prominence as a viral vector system due to its inability to replicate efficiently in mammalian cells, resulting in an exceptional safety profile in humans and animals^{84,85}.

1.2.3. Modified Vaccinia Virus Ankara

MVA was developed by over 570 passages of Chorioallantois Vaccinia virus Ankara (CVA) in chicken embryo fibroblasts (CEF). CVA was derived from material collected from skin lesions after intracutaneous inoculation of calves and donkeys and was initially used as a smallpox vaccine in Turkey⁸⁶. CVA was then brought to Germany in 1953, where it was also used as a smallpox vaccine. After the passages in CEF cells, the virus failed to replicate in most mammalian cell lines, including human cells, and exhibited a highly attenuated phenotype *in vivo* while retaining strong immunogenicity⁸⁷. MVA's high safety profile is attributed to its genome being 15% smaller than that CVA⁸⁸. Indeed, it contains six large deletion sites in the viral genome and various truncations and point mutations in viral genes^{89,90}. As a result of these genetic changes, MVA has lost a significant number of virulence factors and host range genes responsible for host cell tropism^{91,92}. After infection of mammalian cells, the viral replication cycle is arrested following the formation of immature virions. For this reason, cell lines are classified into three groups based on the ability of MVA to replicate in them: permissive cells (e.g. DF-1 cells), semi-permissive cells (e.g. Vero cells), and non-permissive cells (e.g. HeLa cells)^{93,94}. Despite its reduced genome, MVA exhibits remarkable genetic stability, as confirmed by several independent genome sequence analyses.

Due to the presence of six deletion sites and its ~178 kb long genome, MVA can incorporate a substantial number of different sequences of recombinant DNA, allowing a high degree of variability in foreign protein expression^{87,95}. MVA promoters can be categorized as early, intermediate and late, with specific early-late promoters capable of sustaining transcription and translation of gene products for extended periods of time⁹⁶⁻⁹⁸. In most mammalian cells, both early and late proteins are produced without leading to maturation of infectious virions. Indeed, MVA infects the host cell and initiates its replication cycle, which is arrested late in the virion assembly stage⁹⁹. Because replication occurs largely independently of host cell transcription and translation and viral gene expression is regulated by specific viral promoters, the viral transcription complex can be activated at all stages of the viral life cycle^{100,101}. This allows MVA to produce viral or recombinant proteins with minimal hindrance. Thus, MVA has the essential characteristics of a successful vaccine platform. Its safety was convincingly demonstrated during the smallpox eradication program in Germany in the 1970s^{86,102}. In addition, early clinical trials of recombinant MVA vaccines against diseases such as Ebola and HIV reported no significant adverse effects^{103,104}. In 2020, the European Medicines Agency (EMA) approved the use of a heterologous adenovirus/MVA vaccine against Ebola virus in children and adults, administered with a 56-day interval. This regimen includes a priming dose of Ad26.ZEBOV, a monovalent, recombinant, replication-incompetent adenovirus type 26 (Ad26) vector-based vaccine encoding the glycoprotein of the Mayinga strain of Ebola virus, followed by a booster dose of MVA-BN-Filo, a multivalent, recombinant MVA vector-based vaccine. MVA-BN-Filo encodes glycoproteins from the Ebola Mayinga, Sudan virus Gulu and Marburg Musoke strains and the Taï Forest virus nucleoprotein. Clinical trials have demonstrated the safety and immunogenicity of the vaccination regimen¹⁰⁵⁻¹⁰⁹. Recent preclinical studies have provided compelling evidence for the immunogenicity and efficacy of recombinant MVA expressing the Severe Acute Respiratory Syndrome coronavirus 2 (SARS-CoV-2) Spike protein^{110,111}. Several studies have also shown that intranasal vaccination of mice with MVA-based vaccines induces a potent local immune response that confers protection against SARS-CoV-2 infection^{112,113}. Therefore, MVA has significant potential as a safe vaccine platform against a broad range of pathogens, including those that affect the mucosal tract.

1.3. Chlamydia trachomatis

1.3.1. Biology of Chlamydia trachomatis

Chlamydia trachomatis is a sexually transmitted obligate intracellular bacterium that represents a major public health problem worldwide due to its high prevalence¹¹⁴. Within the *C. trachomatis* species, nineteen serotypes can be identified on the basis of their major outer membrane protein (MOMP) genetic characteristics: serovars A, B/Ba and C, which cause ocular trachoma; serovars D/Da, E, F, G/Ga, H, I/Ia, J and K, which are responsible for urogenital infections; serovars L1, L2, L2a and L3, which cause lymphogranuloma venereum¹¹⁵. All species of *Chlamydia* follow a common developmental cycle characterized by the alternation of two distinct forms: the extracellular, infectious elementary body and the intracellular, non-infectious highly replicative reticulate body¹¹⁶. Elementary bodies enter mucosal cells and transform into reticulate bodies within a membrane-bound compartment known as the inclusion body. After several rounds of replication, the reticulate bodies revert to the elementary bodies form and are released from the host cell, ready to infect neighboring cells. *Chlamydia* spp. have a significantly reduced genome compared to other Gram-negative bacteria. *C. trachomatis* has a genome of 1.04 Mb encoding 895 open reading frames and lacks many metabolic enzymes, making it dependent on the host cell for many metabolic needs¹¹⁷. The two forms, elementary bodies and reticulate bodies, are both morphologically and functionally distinct. Elementary bodies can withstand the harsh extracellular environment; their spore-like cell wall is reinforced by a network of disulphide bond-linked proteins called the outer membrane complex, which provides resistance to osmotic and physical stress. This cross-linking is subsequently reduced during differentiation to provide the membrane fluidity necessary for replication¹¹⁸. Reticulated bodies are specialized for nutrient acquisition and replication, and divide by binary fission within the expanding inclusion. Infection by multiple elementary bodies within a single cell creates individual inclusions that eventually fuse by homotypic fusion^{119,120}. In later stages of infection, reticulate bodies transition to elementary bodies in an asynchronous manner, possibly triggered by their detachment from the inclusion membrane. The developmental cycle of *C. trachomatis* can be temporarily halted by environmental and stress factors, including nutrient depletion, exposure to host cytokines, and antibiotics that target cell wall synthesis. Under such conditions, reticulate bodies transform into enlarged, non-dividing persistent forms¹²¹. This persistence may serve as a stealth strategy to evade the host immune system. However, whether persistence occurs *in vivo* remains controversial, although it may contribute to the chronic inflammation and scarring observed in chlamydial disease¹²² (Fig. 4).

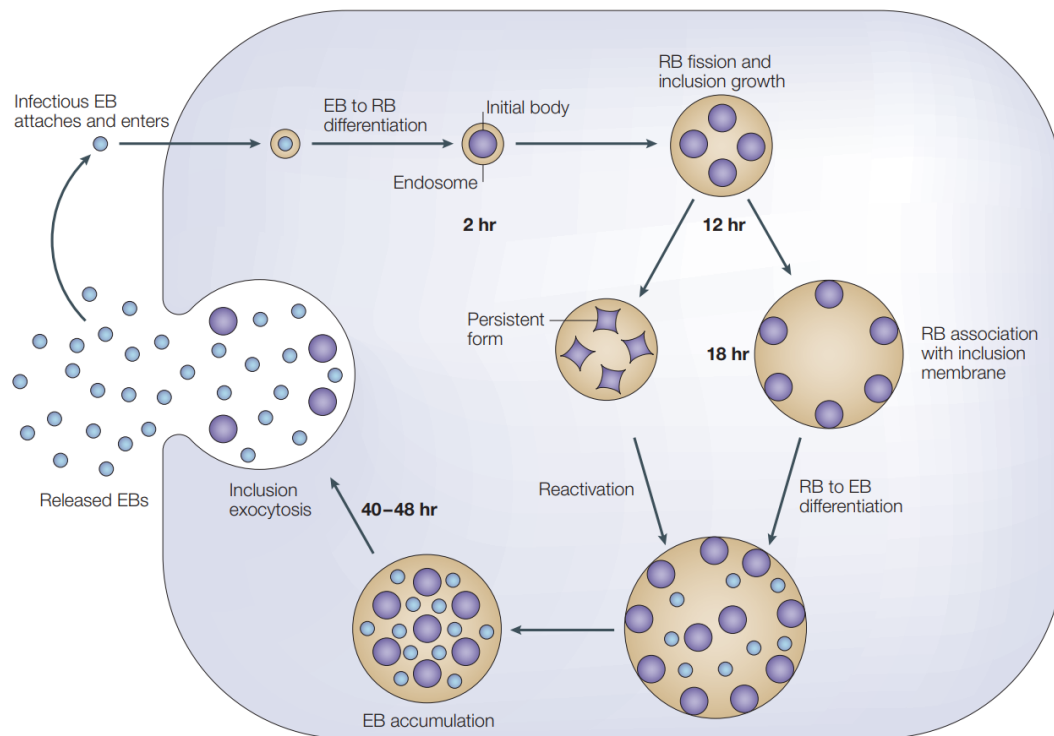


Figure 4. The life cycle of *C. trachomatis*.

C. trachomatis, an intracellular pathogen, undergoes a biphasic cycle within mucosal epithelial cells. The infectious elementary body (EB) is engulfed and forms an inclusion, a specialized vacuole. Within the inclusion, the EB transforms into a replicative reticulate body (RB) that divides by binary fission. After 40-48 hours, the RBs revert to infectious EBs that are released to infect neighboring cells. In the presence of growth inhibitors, such as interferon- γ , *C. trachomatis* adopts a non-replicating, persistent form and reverts to infectious forms upon inhibitor removal. Image source: Molecules, volume 20(3), 2015, 4180-4203¹²³

1.3.2. Epidemiology of *C. trachomatis*

The World Health Organization reported that around 128.5 million new cases of chlamydia infection occurred worldwide in 2020¹²⁴. The asymptomatic nature of the infection can lead to undetected disease transmission, with approximately 80% of women and 50% of men being asymptomatic. Female urogenital chlamydia infection is particularly affecting young and sexually active women, with the highest incidence observed in individuals aged 14-24 years¹²⁵. Several significant risk factors have been identified, including having multiple or new sexual partners, infrequent use of condoms, and a history of or current sexually transmitted diseases (STDs)^{126,127}. The likelihood of *C. trachomatis* transmission varies according to the type of sexual contact, the number of sexual acts and the duration of the partnership. It has been estimated that the probability of transmission is 2.0% per vaginal sex act and 5.8% per anal sex act for both male-to-female and female-to-male transmission¹²⁸.

1.3.3. Mouse models for investigating *C. trachomatis* infection and immune response

Mice are the most widely used animal model for the study of genital chlamydial infections, primarily because of their small size, ease of handling, widespread availability, and cost-effectiveness¹²⁹. The female mouse genital tract is susceptible to infection by both *Chlamydia muridarum* (*C. muridarum*) and *C. trachomatis*. *C. muridarum*, formerly identified as *C. trachomatis* mouse pneumonitis biovar or MoPn, is a naturally occurring mouse pathogen that causes pneumonitis and was originally isolated from the lungs of mice¹³⁰. Intravaginal inoculation of *C. muridarum* in mice causes an infection of the genital tract that is similar to the acute genital infection caused by *C. trachomatis* in women¹³¹. It has been shown that *C. muridarum* infection in the cervical epithelium is followed by ascension to upper genital tract tissues, especially uterine horns and fallopian tubes¹³². The ascension of *C. muridarum* infection often results in hydrosalpinx, fibrosis, and infertility, mimicking common post-infection sequelae of *C. trachomatis* infection in women. In contrast, intravaginal inoculation of *C. trachomatis* in mice typically results in a mild genital tract infection that resolves relatively quickly and rarely ascends to the upper genital tract¹³³. Notably, *C. trachomatis* infection results in post-infection sequelae only when high doses are inoculated directly into the uterus, uterine horns, or ovarian bursa¹³³. The course and outcome of chlamydia infection can vary depending on the mouse strain, inoculation dose, age of the animal, and hormone levels present. The C3H mouse strain has a more severe disease course and a higher rate of infection-driven infertility than other strains for both *C. muridarum* and *C. trachomatis* infection^{134–136}. The infectious dose of chlamydia also influences the course of infection and bacterial ascent in the reproductive tract of mice. Establishing infection requires more infectious units for *C. trachomatis* than for *C. muridarum*. In addition, the oestrous cycle appears to play an important role in the pathogenesis of infection, with mice being less susceptible to upper genital tract infection during the follicular phase than during the luteal phase¹³⁷. For such reason, for both *C. muridarum* and *C. trachomatis* infections, mice are typically pre-treated with progesterone to induce a prolonged diestrus, thereby increasing the initial infection rate¹³⁸. However, this pre-treatment with progesterone could disrupt the hormonal balance and subsequent immunologic state, making it difficult to assess native hormonal contributions to infection progression and resolution^{139–141}. Although commonly used, progesterone pre-treatment is not essential for *C. muridarum* infection in mice, whereas the *C. trachomatis* mouse model relies heavily on progesterone treatment¹⁴². *C. muridarum* exhibits greater virulence in mice compared to *C. trachomatis*, and upper genital tract pathology in *C. muridarum*-infected mice closely resembles that observed in women with post-chlamydial infection sequelae¹⁴³. While this similarity makes it a valuable animal model

for studying chlamydial pathogenesis and protective immunity, the *C. muridarum* model primarily recapitulates the acute phases of human *C. trachomatis* infection and falls short in mimicking the chronic phases responsible for human disease¹⁴⁴. On the other hand, intravaginal infection of mice with *C. trachomatis* closely mimics in many respects the course and outcome of chlamydia infection in most women, characterized by an asymptomatic and self-limiting infection that rarely leads to severe upper genital tract sequelae¹⁴⁵. However, neither *C. muridarum* nor *C. trachomatis* infection allows the development of chronic infections in mice that are observed in humans¹⁴⁶. Another suitable mouse model for studying the adaptive immune response, particularly the T-cell-mediated response, following chlamydia infection is the humanized mouse model known as HLA-A2.DR1¹⁴⁷. This transgenic mouse model has undergone deletion and replacement of its major histocompatibility complexes I and II (H-2) with equivalent human genes, namely HHD, HLA-DRA*01.01, and HLA-DRB*01.01 (Fig. 5). HHD encodes a monochain class I molecule consisting of the α -1 and α -2 domains of HLA-A*02:01 covalently linked to human β 2 microglobulin, together with the α -3 transmembrane and cytoplasmic domains of H-2Db. Both the H-2Db and mouse β 2-microglobulin genes are disrupted, resulting in HLA-A2.DR1 mice lacking classical (class I) and non-classical (class I-b) restricted antigen presentation. In addition, HLA-A2.DR1 mice lack cell surface expression of conventional class II molecules namely H-2 I-A and I-E due to inactivation of the H-2 IA β b gene, and because H-2 IE α is a pseudogene in mice with H-2b haplotype. As a result, these mice are deprived of cell surface expression of both H-2 class I and class II molecules, and cellular immunity is completely restricted to human HLA molecules, with a complete absence of immune responses restricted by mouse MHC molecules. The lack of competition between mouse and human MHC complexes facilitates the characterization of T-cell-mediated immune responses to human pathogens and the study of epitopes in human vaccines that require cooperation between HLA-restricted CD4⁺ T helper cells and HLA-restricted CD8⁺ T cytolytic cells¹⁴⁸⁻¹⁵⁴.

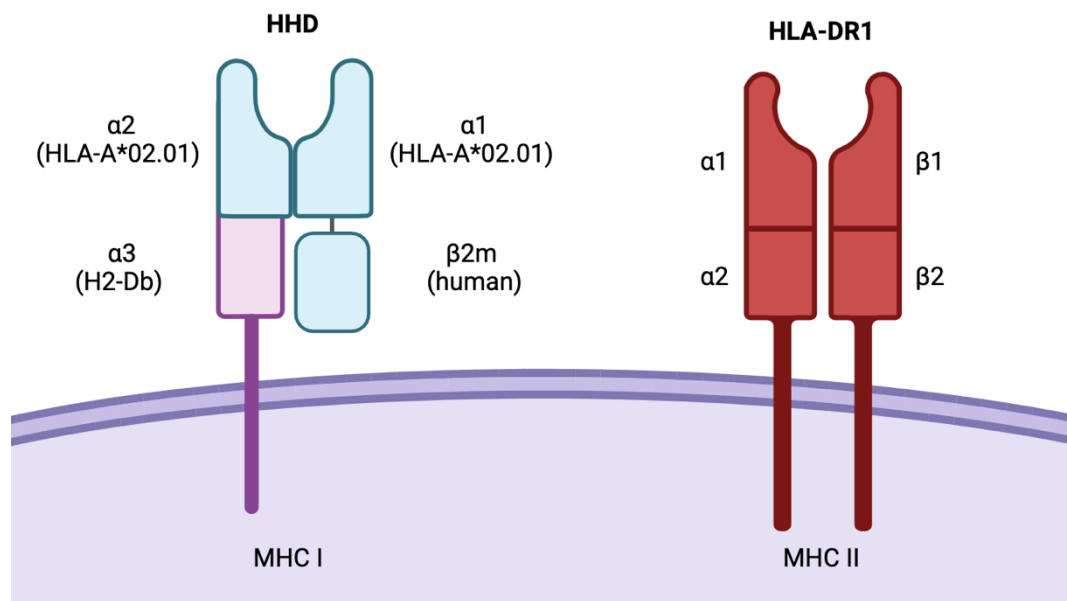


Figure 5. Schematic representation of the HHD and HLA-DR1 molecules.

HLA-A2.DR1 mice express only two MHC molecules. The first is the HHD molecule (MHC class I), which consists of the epitope binding domains $\alpha 1$ and $\alpha 2$ from HLA-A*02:01, the $\alpha 3$ domain from mouse H-2Db, and is covalently linked to human $\beta 2m$. The second is the fully human HLA-DR1 heterodimeric molecule (MHC class II) expressed on antigen presenting cells (APCs). These mice lack murine MHC class I and II molecules, ensuring that all immune responses are restricted to HLA-A*02:01 and HLA-DR1. Image created with BioRender.

To date, no studies have reported infection of HLA-A2.DR1 mice with *C. trachomatis* but with *Chlamydia pneumoniae*¹⁵⁵. After intranasal infection with the *C. pneumoniae*, HLA-A2.DR1 mice demonstrated the ability to clear the infection within a time frame comparable to C56BL/6J mice. However, the transgenic mice exhibited an increased number of bacteria in the lungs during the first weeks after challenge. Notably, acquired protection against repeated *C. pneumoniae* challenges was observed in the HLA-A2.DR1 mice. These mice had 10-1000 times lower lung bacterial counts at 2-4 weeks after rechallenge as compared to the bacterial count determined within the same time frame after the primary challenge. This suggests that the protective immunity acquired during the primary challenge was effective in the HLA-restricted murine immune system. When immunized with *C. pneumoniae*-derived antigens, HLA-A2.DR1 mice demonstrated the ability to process and present chlamydial antigens to CD8⁺ cells. This suggests that CD8⁺ T-cells in HLA-A2.DR1 mice can recognize *C. pneumoniae* antigens in an HLA-A*02:01-restricted manner. Thus, the HLA-A2.DR1 mouse model seems to be useful to identify human CD8⁺ epitopes from chlamydial antigens.

1.3.4. Adaptive immune response to *C. trachomatis* infection

The immune response to *C. trachomatis* infection involves both humoral and cellular immune responses that target the extracellular and intracellular stages of the invading pathogen¹¹⁵. *C. trachomatis* can trigger various components of the adaptive immune system despite being obligate intracellular bacteria.

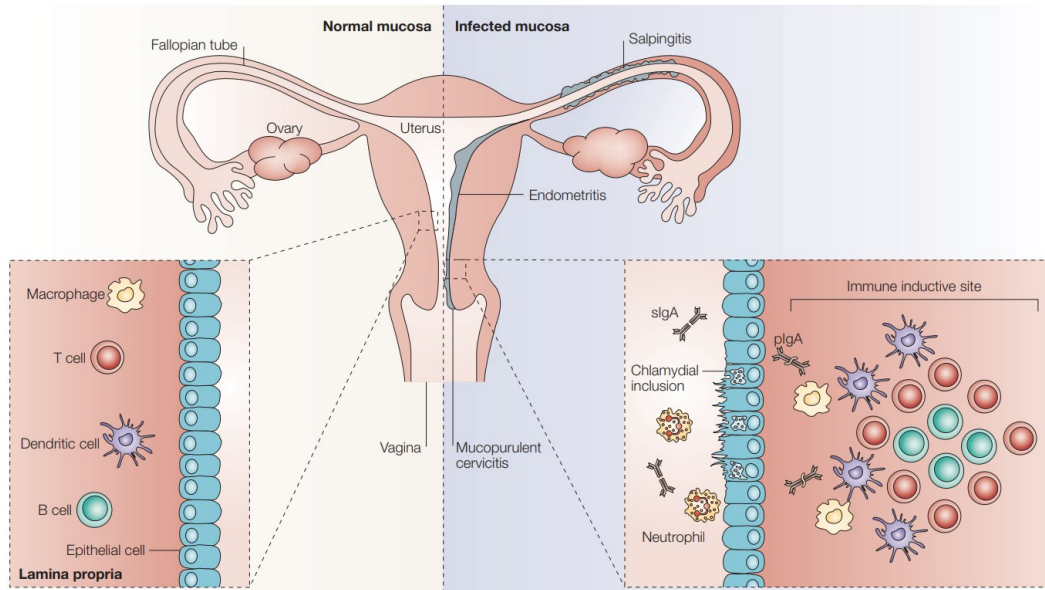


Figure 6. The mucosal immune response to *C. trachomatis* infection.

The infection caused by *C. trachomatis* initiates the recruitment of macrophages and neutrophils, while B-cells, T-cells, DCs and macrophages collaborate to activate an acquired immune response, including the secretion of IgAs (sIgA). pIgA, polymeric IgA. Image source: Nat. Rev. Immun. volume 5, 2005, 149–161¹⁵⁶

Antigen-presenting cells, particularly DCs, play a critical role in initiating the adaptive immune response, contributing to the establishment of immune memory and thus, to the success of vaccines. They are essential for priming both CD4⁺ and CD8⁺ T-cell responses to *C. trachomatis*¹⁵⁷. Upon uptake of *C. trachomatis* into DCs, Toll-like receptor 2 (TLR2), stimulator of interferon genes (STING) and nucleotide-binding oligomerization domain-like receptors (NLRs) are activated¹⁵⁸. This activation leads to the production of pro-inflammatory cytokines such as IL-6, TNF- α , CCR7, CXCL10, IL-1 α and IL-12, which are critical for inducing maturation and optimal antigen presentation in DCs. During antigen uptake, DCs preferentially produce IL-12, which plays a key role in activating and guiding the differentiation of naive CD4⁺ T lymphocytes predominantly into the Th1 phenotype¹⁵⁹. This Th1 polarization is critical for providing primary protection against *C. trachomatis* infection.

The critical role of DCs in inducing polarized CD4⁺ T-cells was also demonstrated in infection models, where DCs pulsed with UV-inactivated *C. muridarum* EBs elicit a weaker protective immune response compared to those pulsed with live EBs¹⁶⁰. This suggests that active infection with live EBs interferes with the development of robust protective immunity, although the exact mechanism of interference remains unclear. CD8⁺ T-cells are thought to play a critical role in responding to intracellular pathogens by directly targeting the intracellular environment required for pathogen replication^{161,162}. *In vitro* studies have shown that CD8⁺ T-cells, recognizing specific *C. trachomatis* proteins such as Cap1 and CrpA, can eliminate target cells in an antigen-dependent manner^{163,164}. Furthermore, adoptive transfer of transgenic NR23.4 T-cells recognizing CrpA or vaccination with recombinant vaccinia virus expressing CrpA demonstrate their ability to confer protection against *C. trachomatis* in murine models¹⁶⁵. Typically, resolution of the primary infection results in the establishment of a stable memory T-cell population, ensuring a more rapid and extensive response to secondary infection¹⁶⁶. However, the CD8⁺ T-cell response to *C. trachomatis* infection shows variability, with fewer *C. trachomatis*-specific CD8⁺ T-cells observed during the secondary response¹⁶⁷. This phenomenon appears to be influenced by an excess of cytokines following *C. trachomatis* infection¹⁶⁸. If, on the one hand, IL-12 produced by DCs favors the generation of Th1-skewed CD4⁺ T-cells, on the other hand, it may be hindering the development of effector memory CD8⁺ T-cells. Indeed, it has been shown that IL-12 promotes the generation of short-lived *C. trachomatis*-specific effector T-cells while inhibiting the development of effector T-cell memory progenitors. In addition to the role of pro-inflammatory cytokines in preventing effector memory T-cells against *C. trachomatis*, the PD-1/PD-L1 immunomodulatory pathway also contributes to this inhibition¹⁶⁹. PD-L1 is upregulated on uterine epithelial cells and DCs after *C. trachomatis* infection and promotes a central memory phenotype in *C. trachomatis*-specific CD8⁺ T-cells. Blocking PD-L1 shifts the T-cell population towards an effector memory phenotype, resulting in faster clearance of *C. trachomatis*. It is worth noting that blocking immunoinhibitory molecules such as PD-L1, whilst potentially aiding bacterial clearance when targeted, can also contribute to increased inflammation. In *C. muridarum*-infected mice, blocking PD-L1 and TIM3 increases uterine and oviduct pathology, highlighting the delicate balance between promoting T-cell activation and preventing excessive inflammation¹⁷⁰. A study examining T-cell-mediated inflammation in wild-type or OT-I mice suggests that the CD8⁺ T-cell response to *C. muridarum* infection may contribute to the pathology of the genital tracts¹⁷¹. OT-I mice express an engineered T-cell receptor. The transgenic T-cell receptor is specifically designed to recognize exclusively the OVA-derived peptide SIINFEKL in the context of H2-Kb. This leads to the development of uniquely OVA-specific CD8⁺ T-cells in the T cell pool. OT-I mice did not develop hydrosalpinx after intravaginal infection with chlamydia, whereas the transfer of CD8⁺ T-cells

derived from the spleen or mesenteric lymph nodes of chlamydia-infected C57BL/6J mice to chlamydia-infected OT-I mice appeared to induce tissue damage in the OT-I mice¹⁷². However, given the impaired protective function of CD8⁺ T-cells caused by chlamydial infection, this approach may not fully elucidate the true role of CD8⁺ T-cells in chlamydial protection. In fact, it appears that bystander non-protective CD8⁺ and CD4⁺ T-cells recruited to the site of chlamydial infection via CXCR3 play an important role in the immunopathology¹⁷³. Interestingly, mice lacking CXCR3 and CCR5 show increased susceptibility to *C. trachomatis* infection. In these CXCR3 and CCR5 knockout mice, chlamydia-specific CD4⁺ T-cells are unable to migrate and persist in genital tract tissues, resulting in reduced clearance of infection compared to wild-type mice¹⁷³.

1.3.5. Vaccine research addressing *C. trachomatis* infection

Efforts to develop a vaccine to protect against trachoma, caused by *C. trachomatis*, began more than a century ago and continue to this day. In the first attempt, dating back to 1913, Nicolle's research group in Tunis conducted vaccine studies in both humans and non-human primates¹⁷⁴. The results were mixed, with some individuals showing resistance to rechallenge and others showing inconclusive results. Subsequent human vaccine trials initially focused on ocular inoculation with whole inactivated bacteria, primarily for the treatment of trachoma¹⁷⁵⁻¹⁷⁷. However, the significant discovery of vaccine-induced exacerbation of inflammatory disease in trial participants and non-human primates prompted a shift from whole-cell vaccination to subunit vaccination strategies. The first evidence of a subunit chlamydia vaccine protecting mice against genital challenge was an acellular vaccine consisting of the outer membrane complex of *C. trachomatis*¹⁷⁸. Subsequent studies focused on recombinant MOMP as a vaccine antigen, which demonstrated protection against vaginal shedding and infertility, albeit with some variability in results¹⁷⁹. The major outer membrane protein (MOMP), a 40-kDa protein that makes up a substantial portion of the chlamydia outer membrane proteins, played a key role in vaccine development. The structural features of MOMP, including four variable domains (VDs) alternating with five constant domains (CDs) and its trimeric structure with disulphide cross-links, were identified^{180,181}. MOMP emerged as an immunodominant antigen with multiple T-cell and B-cell epitopes in humans, leading to the exploration of subunit vaccination strategies^{182,183}. Various vaccine formulations, including detergent-extracted chlamydial outer membrane complex, incomplete Freund's adjuvant, and cationic liposomes, showed promising results in animal models^{184,185}.

Recent advances have included the development of a multivalent vaccines containing specific MOMP regions from different *C. trachomatis* serovars¹⁸⁶. These constructs, adjuvated with CAF01, elicited serovar-specific immune responses and demonstrated protection against vaginal shedding and inflammatory responses in challenged mice¹⁸⁷.

In 2019, a significant milestone was reached with the clinical testing of a multivalent vaccine called CTH522, the first human vaccine candidate since the 1970s. CTH522 is a chimeric protein that combines a partial sequence of the MOMP from serovar D (aa 56-349) with the external VD4 domain from serovars E (aa 282-349), F (aa 283-351), and G (aa 283-351), representing the most common serovars¹⁸⁸⁻¹⁹⁰. The Phase I safety and efficacy trial yielded promising results, demonstrating vaccine-induced immunogenicity, increased antigen-specific mucosal IgG and IgA, antibody neutralization and enhanced antigen-specific CD4⁺ T cells-mediated IFN- γ production^{191,192}. These results provide valuable insight into the potential of MOMP as a vaccine candidate and its ability to induce antigen-specific immune responses in humans.



Figure 7. Schematic representation of the CTH522 antigen

CTH522 contains a partial sequence of the MOMP from serovar D (aa 56-349) and the external VD4 domains from serovars E (aa 282-349), F (aa 283-351), and G (aa 283-351).

2. Aim of the thesis

The aim of this work was to develop, characterize, and evaluate the immunogenicity of MVA-based vaccines against *C. trachomatis*. Specifically, the MVA vector was genetically engineered to express three different antigens: CTH522, spCTH522 and CTH522:B7, designated MVA-CTH522, MVA-spCTH522 and MVA-CTH522:B7, respectively. Compared to CTH522, the spCTH522 construct includes the N-terminal sequence of MOMP (amino acids 1-55) to investigate the potential presence of T-cell epitopes within MOMP. The CTH522:B7 construct is a cell membrane anchored form of CTH522. To localize CTH522 to the cell surface, the N-terminus of the antigen was fused to the signal sequence of the murine IgG κ chain to promote protein secretion, while the C-terminus was extended with the transmembrane region and cytoplasmic domain of murine CD80 (also called B7-1) to anchor the protein to the cell surface membrane. The MVA-CTH522:B7 vector was developed and characterized by Sara Moreno Mascaraque, who did her PhD in the laboratory of Prof. Ingo Drexler. This vector is included in this thesis for comparison with MVA-CTH522 and MVA-spCTH522 vectors, as well as for further investigation.

The immunogenicity of these vaccines was evaluated in two different mouse models: the widely used C57BL/6J and HLA-A2.DR1 mouse models. The primary goal of the study is to compare the immune responses elicited by these vaccines in the two models, with a focus on the potential role of MHC molecules for shaping specific epitope presentation, for T-cell activation and for the subsequent development of adaptive immunity. The research aims to determine how the genetic background of the host, specifically the expression of murine versus human MHC molecules, influences the type, magnitude and quality of immune responses to the vaccine. By analyzing differences in both humoral and cellular-mediated immunity, the study aims to provide insight into how vaccines encoding CTH522 antigens can be optimized for clinical application. In addition, the study highlights the importance of using HLA transgenic mice for preclinical vaccine testing, as these models more accurately mimic human antigen presentation and induction of T-cell responses against pathogen-associated epitopes observed in or relevant for humans. By bridging the gap between the mouse and human immune systems, the study contributes to the development of more effective vaccines against *C. trachomatis*.

Ultimately, this work aims to provide antigen design strategies to develop effective MVA based vaccines and improve our understanding of host-specific factors that influence vaccine efficacy, with the broader goal of advancing vaccines for clinical use.

3. Materials

3.1. Plasmids

Name	Description	Source
pcDNA3.3-CTH522	Plasmid vector carrying CTH522 ORF (coding for the amino acid sequence of MOMP SvD (aa 56-349) fused with MOMP SvE (aa 282-349), MOMP SvF (aa 283-351), and MOMP SvG (aa 283-351), supplementary table 1) used for generation of recombinant MVA-CTH522	Invitrogen
pcDNA3.3-spCTH522	Plasmid vector carrying spCTH522 ORF (coding for the amino acid sequence of MOMP SvD (aa 1-349) fused with MOMP SvE (aa 282-349), MOMP SvF (aa 283-351), and MOMP SvG (aa 283-351), supplementary table 1) used for generation of recombinant MVA-spCTH522	Invitrogen
pEP-MVA-dVI-CTH522	Plasmid vector carrying CTH522 expression cassette used for BAC recombination	This study
pEP-MVA-dVI-spCTH522	Plasmid vector carrying spCTH522 expression cassette used for BAC recombination	This study

3.2. Primers

Primer Name	Sequence
MVA-DelVI-5'-Rev	CCTGGACATTTAGTTTGAGTGTTTCCTGAAT
MVA-DelVI-3'-Fwd	CTCCGCATCTAGTTGATATTCCAACCTCTT
<i>Bam</i> HI-CTH522-Fwd	AAGGATCCATGGGAGATGCCATTT
<i>Af</i> III-CTH522-Rev	CTTTGCAATTGAATTAAGAGAAAAG
<i>Bam</i> HI-spCTH522-Fwd	TCGGATCCGCCACCATGAAGAAA
CTH522-1-Fwd	GCACTTTGGGAGCAACTTCTG
CTH522-4-Rev	ACATTCCCACAAAGCAGCCC
GFP-Fwd	TTGTACAGCTCGTCCATGCCGAG
GFP-Rev	GCAAGGCCGGATCTGGGAATTC
RFV-Fwd	AAAGATGCGTACATTGGACCC
RFV-Rev	GTTCGAGACTAGAAAAGCGCC

3.3. Antibodies

Antibody	Cat. Number	Company	Technic	Conjugate
Rat anti-mCD8	48-0081-82	Thermofisher	FACS	eFluor405
Rat anti-mCD4	100528	Biolegend	FACS	PE/Cyanine7
Rat anti-mCD107	12-1071-82	Thermofisher	FACS	PE
Rat anti-mIFN- γ	554411	BD	FACS	FITC
Rat anti-mTNF- α	506344	Biolegend	FACS	APC-Cy7
Rat anti-mIL-2	560544	BD	FACS	PerCP-Cy5.5
Mouse anti- <i>C. trachomatis</i> L2 MOMP	CT602	Chlamydia Biobank	WB	unconjugated
Mouse anti-m β -actin	A228	Sigma-Aldrich	WB	unconjugated
Rabbit anti-VACV H3 antibody	-	In house	WB	unconjugated
Goat anti-rabbit IgG	111-035-003	Jackson Immuno Research	WB	Horseradish peroxidase

Goat anti-mouse IgG	115-035-003	Jackson Immuno Research	WB	Horseradish peroxidase
Rabbit anti-Calnexin	ab225062	ABCAM	Confocal microscopy	Alexa Fluor 647
Wheat Germ Agglutinin (WGA)	W11262	Invitrogen	Confocal microscopy	Alexa Fluor 594
Donkey anti-mouse IgG (H+L) Highly Cross- Adsorbed	A-21202	Invitrogen	Confocal microscopy	Alexa Fluor 488

3.4. Peptides

Peptide name	MHC restriction	Sequence
VACV B8 ₂₀₋₂₇	H2-K ^b	TSYKFESV
OVA ₂₅₇₋₂₆₄	H2-K ^b	SIINFEKL
VACV B5 ₄₆₋₆₀	I-A ^b	FTCDQGYHSSDPNAV
OVA ₃₂₃₋₃₃₉	I-A ^b	ISQAVHAAHAEINEAGR
VACV B8 ₂₀₋₂₇	HLA-A*02:01	TSYKFESV
Flu M1 ₅₈₋₆₆	HLA-A*02:01	GILGFVFTL
VACV A10 ₂₉₃₋₃₀₇	HLA-DR1	SMRYQSLIPRLVEFF
Flu M1 ₁₇₋₃₀	HLA-DR1	SGPLKAEIAQRLED
MOMP^D ₂₈₂₋₂₉₀	HLA-A*02:01	NMFTPYIGV
MOMP^D ₂₀₀₋₂₀₉	HLA-A*02:01	ALWECGCATL

3.5. Enzymes

Name	Cat. Number	Company
BamHI-HF	R3136	NEB
AflII	R0520	BD
PacI	R0547	NEB

3.6. Bacteria

Name	Description	Source
XL-1-Blue	Chemically competent <i>E. Coli</i>	Stratagene
GS1783	Electrocompetent <i>E. Coli</i> carrying pMVAF-DX, in a self-excising BAC	¹⁹³

3.7. Cell lines

Cell line	Specificity	Organism	ATCC
DF-1	Fibroblasts	Chicken	CRL-12203
HeLa	Cervical carcinoma	Human	CCL-2

3.8. Viruses

Name	Description	Source
MVA-sB, here referred as MVA-WT	Non-recombinant MVA obtained with the BAC-MVA method	Ronny Tao
MVA-CTH522	Recombinant MVA carrying the CTH522 expression cassette in the Deletion VI region of MVA genome	This study
MVA-spCTH522	Recombinant MVA carrying the spCTH522 expression cassette in the Deletion VI region of MVA genome	This study
MVA-CTH522:B7	Recombinant MVA carrying the CTH522:B7 expression cassette in the Deletion VI region of MVA genome. The CTH522:B7 construct is a cell membrane-anchored form of CTH522, generated by adding the signal sequence of the murine IgG κ chain at the N-terminus and the	Sara Moreno Mascaraque

	cytoplasmic domain of murine CD80 at the C-terminus
Rabbit fibroma virus (RFV)	Helper virus to rescue recombinant MVA from BAC ¹⁹⁴

3.9. Mice

Mice	Origin
C57BL/6J	Janvier
HLA-A2.DR1	ZETT HHU Düsseldorf

3.10. Buffers

Homemade Buffers

Name	Composition
Blocking buffer (for western blot)	5 % skimmed milk powder in TBS-t
Blocking buffer (for Immunofluorescence microscopy)	3 % BSA powder in PBS
DNA extraction buffer	75 mM Tris 20 mM (NH ₄) ₂ SO ₄ 1,2 mM MgCl ₂ Proteinase K (0,2 mg/mL) pH 8.8
FACS staining buffer	1 % BSA, 0.02 % NaN ₃ in PBS
Fixation buffer (for FACS)	2 % Paraformaldehyde in PBS
Fixation buffer (for Immunofluorescence microscopy)	4 % Paraformaldehyde in PBS
Separating gel buffer (4x)	1.5 M TRIS-Base HCl up to pH8.8
Sucrose cushion solution	36% sucrose

	10mM TRIS-Base (pH 9)
Stacking gel buffer (4x)	0.5 M TRIS-Base / HCl up to pH6.8
Running Buffer (1x)	25 mM TRIS-Base 0,2 M Glycine 0,1% SDS (w/v)
TBS-t (1x)	10 mM TRIS-Base HCl up to pH 8.0 1500 mM NaCl 0,05 % Tween-20
Transfer Buffer (1x)	50 mM TRIS-Base 40 mM Glycine
Tris 10 mM	10 mM TRIS-Base HCl up to pH 9
Tris 1 mM	1 mM TRIS-Base HCl up to pH 9

Commercial Buffers

Name	Cat. Number	Company
10x rCutSmart	B6004S	NEB
4x Laemmly Sample Buffer	161-07-47	BioRad
Pharm Lyse Buffer	555899	BD
RIPA buffer	89900	ThermoFisher Scientific
TBE (10X)	106177	Merck

3.11. Media

Name	Specification
RPMI 1640	Gibco

Fetal bovine serum (FBS)	PAN-Biotech
Cell culture medium	RPMI 1640 supplemented with 10% FBS
Bacteria LB-medium	20% LB in water (w/v)
Bacteria LB-agar	5% agar in LB-medium (w/v)
M2 medium	RPMI 1640, 50uM b-mercaptoethanol, 10% FBS
SOC Outgrowth Medium (NEB, cat #B9020S)	2% Vegetable Peptone 0.5% Yeast Extract 10 mM NaCl 2.5 mM KCl 10 mM MgCl ₂ 10 mM MgSO ₄ 20 mM Glucose

3.12. Chemicals

Name	Company
β-mercaptoethanol	Roth
Acetic acid	Merck
Agarose	Biozym
Ampicillin	Roth
Cytofix/Cytoperm	BD
Perm/Wash	BD
Brefeldin A	Sigma
Bromophenol Blue	Merck
Dimethyl sulfoxide (DMSO)	Sigma
EZ-Vision In-gel	VWR
Fetal Bovine Serum (FBS)	Merck
Fixable Viability Dye eFluor 660	eBioscience
Gel Loading Dye (6x)	NEB
Glycerol	Roth
Glycine	Roth
Kanamycin	Roth
LB Broth	Roth

Methanol	Merck
MitoTracker™ Red CMXRos	Invitrogen
Paraformaldehyde	Merck
Pierce™ ECL	ThermoFisher Scientific
Rotiphorese Gel (29:1)	Roth
Skimmed milk powder	Roth
Sodium Azide	Merck
Sodium Chloride	Roth
Sodium Dodecyl Sulfate (SDS)	Roth
TEMED	BioRad
TRIS-Base	Roth
Trypan Blue	Gibco
Trypsin-EDTA (0,05%)	Gibco
TurboFect™ Transfection Reagent	ThermoFisher Scientific
Tween 20	Merck
UltraPure Distilled Water	Invitrogen

3.13. Kits

Name	Cat. Number	Company
DreamTaq PCR Master Mix kit	K1082	ThermoFisher
Nucleospin Gel and PCR Clean-up	740609	Macherey-Nagel
Phusion® High-Fidelity PCR Master Mix with HF Buffer kit	M0531	NEB
QIAprep Spin Miniprep Kit	27104	Qiagen
QIAGEN Large-Construct Kit	12462	Qiagen
Quick Ligation™ Kit	M2200	NEB

3.14. Instruments

Name	Company
Centrifuge 5424 R	Eppendorf
ChemoStar Touch ECL Imager	Intas
Eppendorf Eporator®	Eppendorf
FACS Canto II	BD
Heracell 240i CO2 incubators	Thermo Scientific
Mars safety sterile benches	Labogene
MaxQ™ 4000 Benchtop Orbital Shaker	Thermo Scientific
Microscope CKX41	Olympus
Mini-PROTEAN Tetra Vertical Electrophoresis Cell	BioRad
Multiskan GO	Thermo Scientific
NanoDrop 2000	Thermo Scientific
Professional Trio Thermocycler	Biometra
Rocking shaker	CAT
Sonopuls HD 200	Bandelin
Sorvall ST 16R centrifuge	Thermo Scientific
Sorvall WX+ Ultra Series centrifuge	Thermo Scientific
ThermoMixer®	Eppendorf
Trans-Blot® SD Semi-Dry Transfer Cell	BioRad
Vortex-Genie 2	Scientific Industrie

4. Methods

4.1. Shuttle plasmid vector construction

DNA sequences encoding the CTH522 or spCTH522 antigens were synthesized by GeneArt® (ThermoFisher Scientific). To clone the open reading frames (ORF) of CTH522 or spCTH522 antigens downstream the modified pH5 promoter, the corresponding DNA sequences were PCR amplified with primers designed to produce *Bam*HI-CTH522-*Afl*III and *Bam*HI-spCTH522-*Afl*III (see 3.2). After restriction digest, the DNA fragments were inserted into the MVA transfer plasmids pVI-PmH5-dVI. The PCR reactions were carried out using Phusion high-fidelity PCR master mix kit according to the manufacturers' guidelines. The components used for the PCR reaction are listed in the Table 1.

Table 1. Reaction components for the Phusion PCR of CTH522 or spCTH522 open reading frames

Component	Volume	Final concentration
2x Phusion Master Mix	25 μ L	1X
<i>Bam</i> HI-CTH522-Fwd/ <i>Bam</i> HI-spCTH522-Fwd	2,5 μ L	500 nM
<i>Af</i> III-CTH522-Rev	2,5 μ L	500 nM
pcDNA3.3-CTH522/pcDNA3.3-spCTH522	1 μ L	100 ng
Water	Up to 50 μ L	-

PCR-generated DNA fragments were purified using the Nucleospin Gel and PCR Clean-up Kit following the manufacturers' instructions. The purified DNA fragments and pVI-PmH5-dVI plasmid DNA were then double-digested with *Bam*HI and *Af*III restriction enzymes. The components used for the digestion reaction are listed in the Table 2.

Table 2. Reaction components for the digestion of PCR derived DNA and pVI-PmH5-dVI plasmid DNA

Component	Volume	Final concentration
10x rCutSmart Buffer	5 μ l	1X
<i>Bam</i> HI-HF	1 μ L	4U/ μ g DNA
<i>Af</i> III	1 μ L	4U/ μ g DNA
DNA	-	5 μ g
Water	Up to 50 μ L	-

The double digestion was performed at 37°C for 2-3h, followed by inactivation of restriction enzymes at 65°C for 20 min. The digested PCR products and plasmid fragments were separated on 1% (w/v) agarose gels supplemented with fluorescent DNA Dye. After verifying the correct fragment length, target DNA fragments were cut out and extracted from the gel using the Nucleospin Gel and PCR Clean-up Kit according to the manufacturers' instructions. The purified DNA fragments were then quantified using a NanoDrop spectrophotometer. The purified DNA fragment containing the ORF of CTH522 or spCTH522 was then ligated to the pVI-PmH5-dVI plasmid DNA that has been digested with the same restriction enzymes to construct pVI-PmH5-CTH522 or pVI-PmH5-spCTH522, respectively, using the Quick Ligation™ Kit following the manufacturers' instructions.

4.2. Bacteria transformation for plasmid amplification

Chemically competent XL-1 Blue *E. Coli* cells were used for transformation. A 50 μ L aliquot of cells was thawed on ice for 20 minutes, then the ligation mixture was added and gently mixed. The tube was then incubated on ice for 20 minutes, followed by a 45 second heat shock at 42°C and immediately cooled on ice for 2 minutes. 500 μ L of pre-warmed SOC medium was then added and the mixture and incubated at 37°C with shaking at 800 rpm for 1 hour. Transformed cells were then plated onto pre-warmed LB agar plates containing 30ug/mL of kanamycin for selection and incubated overnight at 37°C. To verify successful transformation of pVI-PmH5-CTH522 or pVI-PmH5-spCTH522 into XL-1 Blue cells, colony PCR was performed. Ten colonies were picked from each plasmid transformed sample, resuspended in 50 μ L water and used for PCR amplification of CTH522 or spCTH522, using MVA-DelVI-3' and CTH522-4 primers (see 3.2). The PCR reactions were carried out using DreamTaq PCR master mix kit according to the manufacturers' instructions. The components used for the PCR reaction are listed in the Table 3.

Table 3. Reaction components for the colony PCR of pVI-PmH5-CTH522 or pVI-PmH5-spCTH522 transformed XL-1 blue *E. Coli* cells

Component	Volume	Final concentration
2x DreamTaq Master Mix	15 μ l	1X
MVA-DelVI-3' primer	1,5 μ L	500 nM
CTH522-4 primer	1,5 μ L	500 nM
DNA (bacteria suspended in water)	1 μ L	-
Water	Up to 30 μ L	-

PCR products were analyzed on a 1% agarose gel supplemented with fluorescent DNA dye. A single positive colony from each transformation was then inoculated into 5 mL of LB medium containing 30 ug/mL of kanamycin and incubated overnight at 37°C with shaking at 200 rpm. The next day, plasmid DNA was purified, quantified, and stored at -20°C. A glycerol stock was also prepared by mixing 500 μ L of 50% (v/v) glycerol with 500 μ L of the bacterial culture and stored at -80°C.

4.3. Recombinant Bacterial Artificial Chromosome (BAC) construction

To generate recombinant MVA, a suitable method is to create a recombinant self-excising BAC in the *E. Coli* strain GS1783. Specifically, this strain carries the MVA genome in the pBELO-BAC11 plasmid¹⁹³, renamed pMVAF-DX. In addition to the MVA genome, the BAC contains a chloramphenicol resistance cassette under a bacterial promoter and a GFP expression cassette under the poxviral late FP4B promoter. This *E. Coli* strain also contains the λ -red recombinase genes under a heat-inducible promoter and the *I-SceI* endonuclease gene under an L-arabinose-inducible promoter. To insert the PmH5-CTH522 and PmH5-spCTH522 expression cassettes into the MVA-BAC deletion VI region, pVI-PmH5-CTH522 and pVI-PmH5-spCTH522 plasmids were digested with *PacI* endonuclease to obtain linearized ~4.5 kb pVI-PmH5-CTH522 and ~4.7 kb pVI-PmH5-spCTH522 DNA fragments, respectively, each flanked by sequences homologous to the deletion VI site in the MVA genome. The components of the digest are described in Table 4.

Table 4. Reaction components for the *PacI* restriction digest of pVI-PmH5-CTH522 or pVI-PmH5-spCTH522 plasmid DNA

Component	Volume	Final concentration
10x rCutSmart Buffer	5 μ l	1X
<i>PacI</i>	1 μ L	4U/ μ g DNA
DNA	-	5 μ g
Water	Up to 50 μ L	-

The digestion was performed at 37°C for 2-3h, followed by inactivation of the restriction enzyme at 65°C for 20 min. The digested plasmid fragments were separated on 1% (w/v) agarose gels supplemented with fluorescent DNA dye. After verifying the correct fragment length, target DNA fragments containing the expression cassettes were extracted from the gel using the Nucleospin Gel and PCR Clean-up Kit according to the manufacturers' instructions. The purified linearized fragments were incubated with 50 μ l aliquots of electrocompetent *E. Coli* GS1783, thawed on ice for 20 min. Transformation was achieved by electroporation at 1.5 kV, 200 Ω , and 25 μ F. After pulsing, 900 μ l of antibiotic-free LB medium was immediately added and the bacteria were shaken for 2 hours before plating on LB agar with 30 μ g/ml chloramphenicol (CAM) and 30 μ g/ml kanamycin for 48 hours. Colonies with correct insertion of the recombinant DNA were identified by colony PCR using MVA-DelVI-3 and CTH522-4 primers. The PCR reactions were carried out using DreamTaq PCR master

mix kit according to the manufacturers' guidelines. The components used for the PCR reaction are listed in the Table 5. The PCR products were separated on 1% (w/v) agarose gels and verified for the correct length. For the second round of red recombination to remove the I-SceI/kanamycin cassette, the colonies with correct DNA integration were inoculated into 1 ml of LB containing 30 µg/ml CAM. After 4 hours of incubation at 32°C and 220 rpm, 1 ml of prewarmed LB containing 30 µg/ml CAM and 2% L-arabinose was added. Bacteria were shaken for 1 hour at 32°C, 220 rpm, then incubated at 42°C for 30 minutes, followed by another 2 hours at 32°C, 220 rpm. Bacterial growth density was measured at OD600nm, and based on the OD600nm values, 10 µl of the bacterial suspension was plated at 1:100 dilution (OD600nm < 0.5) or 1:1000 dilution (OD600nm > 0.5) on LB agar containing 30 µg/ml CAM and 1% L-arabinose. Plates were incubated at 32°C for 48 hours to allow for colony formation. Integration of the CTH522 and spCTH522 expression cassettes and deletion of the kanamycin cassette were confirmed by colony PCR using MVA-DelVI-5' and MVA-DelVI-3' primers (see 3.2), with sequence integrity verified by subsequent sequencing. The PCR reactions were carried out using DreamTaq PCR master mix kit according to the manufacturers' guidelines. The components used for the PCR reaction are listed in the Table 5.

Table 5. Reaction components for the colony PCR of GS1783 single colonies carrying recombinant BAC

Component	Volume	Final concentration
2x DreamTaq Master Mix	15 µl	1X
MVA-DelVI-3' primer	1,5 µL	500 nM
MVA-DelVI-5' primer	1,5 µL	500 nM
DNA (bacteria suspended in water)	1 µL	-
Water	Up to 30 µL	-

The PCR products were separated on 1% (w/v) agarose gels supplemented with fluorescent DNA dye and verified for the correct length.

4.4. Isolation of recombinant BAC

Single colonies of GS1782 *E. coli* containing the recombinant MVA-BAC with the CTH522 or spCTH522 expression cassette were grown in 5 mL LB medium containing 30 µg/mL chloramphenicol and incubated overnight at 32°C with shaking at 220 rpm. Recombinant MVA-BAC DNA was extracted from 4 mL of the bacterial culture, while the remaining 1 mL

was mixed with 1 mL of 100% glycerol to create a glycerol stock, which was stored at -80°C. The bacterial culture was centrifuged at 5000 rpm for 10 minutes at 4°C and the supernatant was removed. The bacteria pellet was resuspended in 250 µl of P1 buffer from the QIAGEN Large-Construct Kit and then transferred to a 1.5 mL tube. Next, 350 µl of P2 lysis buffer was added to lyse the cells; samples were inverted 5-6 times and incubated at room temperature for 5 minutes. To stop the lysis, 350 µl of P3 neutralization buffer was added and the tubes were inverted 5-6 times, then incubated on ice for 10 minutes to precipitate the lysate. The samples were centrifuged at 13,000 rpm for 15 minutes at 4°C, and the supernatant was transferred to a new 2 mL tube. For DNA isolation, chloroform-isoamyl alcohol was added to the supernatant (1:1), gently mixed, and centrifuged at 14,000 rpm for 5 minutes at 4°C. The supernatant containing MVA-BAC DNA was transferred to new 2 mL tubes and isopropanol was added at a 1:0.8 ratio. The tubes were gently inverted to mix and then incubated on ice for 1 hour. The tubes were then centrifuged at 13,000 rpm for 30 minutes at 4°C to precipitate the DNA. The supernatant was discarded, and the DNA pellet was washed with 500 µl of 70% ethanol and centrifuged again at 13,000 rpm for 20 minutes at 4°C. After discarding the supernatant, the pellet was air dried for 20 minutes at room temperature and resuspended in 30 µl of DNase-free water. The DNA concentration was measured using a NanoDrop spectrophotometer.

4.5. Rescue of recombinant MVA

DF-1 cells were seeded in a 6-well plate one day prior to co-transfection/infection to rescue recombinant MVA, aiming to reach 70% confluence on the day of transfection. For transfection, 5 µg of recombinant MVA-BAC was combined with 6 µl TurboFect in 400 µl serum-free RPMI and incubated for 20 minutes at room temperature. After incubation, the mixture was filled up to 1 mL of 10% FBS supplemented RPMI. The culture medium was then removed from the DF-1 cells and the 1 mL transfection mixture was added. The cells were incubated at 37°C for 3 hours. After transfection, the cells were infected with helper rabbit fibroma virus (RFV), which provides the transcriptional machinery necessary for early gene transcription from MVA-BAC. RFV was diluted in RPMI supplemented with 5% FBS to obtain MOI of 1, and 100 µL of RFV was added to the culture medium of transfected DF-1 cells. The cells were incubated at 37°C with gentle shaking every 15 minutes for three rounds. After inoculation, the medium was replaced with 2 mL RPMI with 5% FBS and the cells were incubated at 37°C. After 48-72 hours, GFP production was observed through immunofluorescence microscopy to identify green fluorescent cells. GFP-positive wells were harvested by scraping and centrifuged at 4000 rpm for 10 minutes at 4°C. The supernatant was

discarded and the pellet was resuspended in 800 μ L of fresh medium. The recovered DF1 cells producing recombinant MVA were then subjected to three freeze-thaw cycles, sonicated three times for 1 minute each, and serially diluted (10^1 to 10^5) on 70% confluent DF-1 cells in 6-well plates. After a 1-hour inoculation, 1.5 mL of fresh medium was added and the plates were incubated at 37°C. Cells were assessed for GFP production and cytopathic effects (CPE) after 3-4 days. The well with the most pronounced CPE and minimal GFP expression was harvested by scraping and the above protocol was repeated for two additional passages to ensure viral replication. Samples containing virus were stored at -80°C. To isolate single clones of recombinant MVA-CTH522 and MVA-spCTH522, a limiting dilution infection was performed. One day before infection, 15.000 DF-1 cells/well were seeded in 96-well plates with 100 μ l RPMI containing 5% FBS. On the following day, limiting dilutions of recombinant virus (10^{-6} to 10^{-8}) were prepared from the 3rd passage. One full 96-well plate was used per dilution, with 100 μ l of each dilution added per well. After 6-7 days, cells were analyzed for GFP production and CPE. Wells negative for GFP but positive for CPE were harvested and total DNA was extracted. To extract DNA, cells were scraped from the selected wells and 100 μ l of the cell suspension was centrifuged at 15000 x g for 2 minutes at room temperature. The supernatant was discarded and the pellet was resuspended in 50 μ l DNA extraction buffer. Samples were incubated at 56°C for 3 hours to facilitate extraction, followed by Proteinase K inactivation at 96°C for 20 minutes. The extracted DNA was analyzed by PCR using GFP-Fwd/GFP-Rev, RFV-Fwd/RFV-Rev and MVA-DeI_{VI}3'/CTH522-4 primer combinations to detect GFP, RFV and either the CTH522 or spCTH522 expression cassette, respectively. The PCR reactions were carried out using DreamTaq PCR master mix kit according to the manufacturers' guidelines. The components used for the PCR reaction are listed in the Table 6.

Table 6. Reaction components for the PCR analysis of MVA-CTH522 and MVA-spCTH522 single clones

Component	Volume	Final concentration
2x DreamTaq Master Mix	15 μ l	1X
MVA-DeI_{VI}3'/GFP-Fwd/RFV-Fwd primer	1,5 μ L	500 nM
CTH522-4/GFP-Rev/RFV-Rev primer	1,5 μ L	500 nM
DNA (recombinant MVA-derived DNA in water)	1 μ L	-
Water	Up to 30 μ L	-

The PCR products were separated on 1% (w/v) agarose gels supplemented with fluorescent DNA dye and verified for the correct length. A single clone lacking GFP and RFV but containing the expression cassette for CTH522 or spCTH522 was selected for further amplification, while the remaining samples were stored at -80°C. Positive clones were expanded by infecting DF-1 cells to obtain high amounts of recombinant MVAs.

4.6. Purification of MVA

To amplify recombinant MVA, a single clone obtained from a limiting dilution (see 4.5), lacking the GFP cassette and the RFV but containing the CTH522 or spCTH522 expression cassette, was expanded through serial passaging. This process started with a single well of a 96-well plate and was scaled up to a 6-well plate and then to a T75 flask. For large scale virus stock production, DF-1 cells pre-seeded in forty T182.5 flasks were infected with virus from the expanded T75 culture for 3-4 days. For harvesting, the cells were scraped and transferred to ultracentrifuge buckets. The weight of the buckets containing the cell suspension was balanced with ice-cold 10 mM Tris (pH 9) and centrifuged at 16000 rpm for 90 minutes at 4°C using a pre-chilled ultracentrifuge rotor (A-621). The supernatant was discarded and the pellets were resuspended three times in 10 ml of 10 mM Tris. The pooled virus suspension was subjected to three freeze-thaw cycles to rupture cells and release virus particles. Using an ultrasonic needle disinfected with 80% ethanol and UV light, the suspension was sonicated three times for 15 seconds at 76% power while the suspension was kept on ice. After sonication, the suspension was centrifuged at 4000 rpm for 10 minutes at 4 °C and the supernatant was collected in a new 50 ml tube. The pellet was resuspended in 30 ml of 10 mM Tris and sonicated again three times for 15 seconds. After a second centrifugation at 4000 rpm for 10 minutes at 4 °C, the supernatant was combined with the first. Ultracentrifuge buckets for AH 626-36 and AH 626-17 rotors were pre-cooled at 4 °C and UV-irradiated prior to use. The virus supernatant was evenly distributed into 36 ml sterile polyallomer (PA) vials previously filled with 25 ml of 36% sucrose solution in 10 mM Tris. The vials were balanced with 10 mM Tris and centrifuged at 13500 rpm for 1 hour at 4°C using an AH 626-36 rotor. After centrifugation, the supernatant was discarded and the virus pellets were resuspended in 12 ml of 10 mM Tris and transferred to a 50 ml Falcon tube. The resuspended virus was then divided into 17 ml PA vials, each previously filled with 12 ml of 36% sucrose solution. The vials were balanced with 10 mM Tris and centrifuged at 13500 rpm for 1 hour at 4°C using an AH 626-17 rotor. The supernatant was discarded and the pellet was resuspended in 3 ml of 1 mM Tris (pH 9). The purified virus was aliquoted, titrated and stored at -80 °C.

4.7. Titration of MVA

DF-1 cells were seeded at a density of 15,000 cells/well in 96-well plates in RPMI medium supplemented with 5% FBS, one day prior to titration. For titration of MVA in purified stock (see 4.6), 10-fold serial dilutions from 10^{-6} to 10^{-11} were prepared in RPMI supplemented with 2% FBS. To infect the cells, 100 μ l of the 10^{-6} virus dilution was added to the first column of the 96-well plate, while 100 μ l of the 10^{-7} to 10^{-11} virus dilutions were added to two columns each. For titration in replication kinetics experiments, 10-fold serial dilutions from 10^{-1} to 10^{-6} were prepared. In all titration assays, the last column of the 96-well plate received RPMI with 2% FBS as a negative control. Plates were incubated at 37°C and plaque formation was assessed 7 days after titration. The TCID₅₀ was calculated using the following equation:

$$\text{TCID}_{50} = 10^{a+0,5+\Sigma\left(\frac{b}{n}\right)} \times 10$$

where '**a**' is the highest dilution factor with all wells showing CPE, '**b**' is the number of wells showing CPE at subsequent dilutions and '**n**' is the total number of wells per dilution.

4.8. Sequencing of target DNA inserted in recombinant MVA genomes

Viral DNA was isolated from the purified recombinant MVAs using a DNA extraction buffer containing proteinase K. Approximately 5 μ L of purified virus sample was incubated with 50 μ L of extraction buffer at 56°C for 3 hours. Proteinase K was then inactivated by heating at 96°C for 20 minutes. Next, 1 μ L of the extracted DNA was used for PCR amplification of the deletion VI region in the recombinant MVA using specific primers designed to anneal within the deletion VI. (see 3.2). The PCR reactions were carried out using Phusion high-fidelity PCR master mix kit according to the manufacturers' guidelines. The components used for the PCR reaction are listed in the Table 7.

Table 7. Reaction components for the Phusion PCR specific for deletion VI of MVA-CTH522 and MVA-spCTH522

Component	Volume	Final concentration
2x Phusion Master Mix	25 μ L	1X
MVA-DelVI-5'-Rev	2,5 μ L	500 nM

MVA-DelVI-3'-Fwd	2,5 µL	500 nM
Viral DNA	1 µL	-
Water	Up to 50 µL	-

The PCR products were separated on 1% (w/v) agarose gels. After verifying the correct fragment length, target DNA fragments were extracted from the gel using the Nucleospin Gel and PCR Clean-up Kit according to the manufacturers' instructions. The purified DNA fragments were then quantified using a NanoDrop spectrophotometer. The PCR products were then mixed with MVA-DelVI-5'-Rev, MVA-DelVI-3'-Fwd, CTH522-1-Fwd, and CTH522-4-Rev primers (see [3.2](#)) and sequenced by Eurofins Genomics, GmbH.

4.9. Eukaryotic cell culture

Eukaryotic cell cultures were maintained at 37°C with 5% CO₂. HeLa and DF-1 cells were cultured in RPMI medium supplemented with 10% FBS. When cell confluence reached 80-90%, the cells were passaged. The old culture medium was removed, the cells were rinsed with PBS and then detached by trypsinization using 0.05% trypsin-EDTA solution. After 5 minutes, the trypsin was neutralized with fresh culture medium and the cells were split before being transferred to fresh medium.

4.10. In vitro infection

For protein synthesis and replication kinetics analyses, DF-1 and HeLa cells were seeded in 6-well plates at a density of 7×10^5 cells per well one day before infection. On the day of infection, the culture medium was removed and the cells were washed with PBS. Viruses were thawed at room temperature, sonicated for 1 minute and kept on ice. Based on the desired MOI for each experiment, the required volume of purified virus was diluted with FBS-free medium to obtain a final virus suspension of 500 µL per well. PBS was removed from the cells, 500 µL of virus suspension was added and the plates were incubated at 37°C with gentle shaking three times every 15 minutes. For mock infection controls, FBS-free RPMI was added to the cells. After one hour of incubation, the virus suspension was removed, the cells were washed with PBS to remove excess virus, and fresh RPMI containing 10% FBS was added. Cells were then maintained at 37°C.

To analyse protein synthesis and replication kinetics, infections were monitored at different time points: for protein synthesis kinetics, samples were taken at 0, 4, 8, 24, 48 and 72 hours post infection, while for replication kinetics, samples were taken at 0, 24, 48 and 72 hours. At each time point, cells were scraped and collected. For protein synthesis analysis, cells were pelleted by centrifugation at $600 \times g$ for 5 minutes, washed with PBS and centrifuged again. Cell pellets were then processed for SDS-PAGE and western blot analysis as described in section 4.11. For replication kinetics, whole suspensions of infected cells were subjected to three freeze-thaw cycles followed by sonication for 1 minute, repeated three times, to release viral particles. Virus titers were then determined by MVA titration as described in section 4.7.

4.11. SDS-PAGE and Western Blot analysis

Pellets of infected cells were resuspended in 100 μ L of RIPA buffer and heated to 98°C for five minutes. The lysates then underwent three freeze-thaw cycles, followed by an additional five-minute incubation at 98°C. Afterward, samples were sonicated three times at 100% power for one minute each. Protein quantification was performed using the Pierce™ BCA Protein Assay Kit, in accordance with the manufacturer’s protocol. Whole-cell lysates were stored at -80°C until needed. For protein synthesis analysis, 30 μ g of cell lysate was resuspended in Laemmli sample buffer and loaded onto polyacrylamide gels. The compositions of the stacking and separating gels are provided in Table 8.

Table 8. Polyacrylamide gel components for SDS-PAGE, with volumes calculated for a single 10% gel

Component	Separating gel mix (5 mL)	Stacking gel mix (5 mL)
NF-Acrylamide/Bis-solution 30 (29:1)	1,7 mL	0.7 mL
1.5 M TRIS/HCl, pH 8.8	1.3 mL	-
0.5 M TRIS/HCl, pH 6.8	-	1.3 mL
Water	2.1 mL	3 mL
10% SDS	50 μ L	50 μ L
10% APS	50 μ L	50 μ L
TEMED	5 μ L	5 μ L

SDS-PAGE was conducted in an electrophoresis chamber containing running buffer, at 90 V and room temperature, until the bromophenol blue dye front of the Laemmli buffer reached

the edge of the gel. After SDS-PAGE, the proteins were transferred from the gel to a nitrocellulose membrane using a western blot sandwich setup. This sandwich consisted of six filter papers and an Amersham™ Protran™ nitrocellulose membrane. Each component was soaked in transfer buffer and the layers were assembled in the following order from anode to cathode: three filter papers, the nitrocellulose membrane, the gel, and three more filter papers. The assembled sandwich was placed in a Trans-Blot® SD Semi-Dry Transfer Cell and protein transfer was performed at 15 V for one hour at room temperature. After transfer, proteins on the membrane were visualized using Ponceau red staining to confirm successful transfer. The staining was then removed with TBSt. Following the transfer, membranes were blocked with 5% non-fat milk for one hour with gentle agitation at room temperature. After blocking, membranes were incubated with the primary antibody, either for one hour at room temperature or overnight at 4°C. The antibodies used included a mouse anti-*C. trachomatis* L2 species-specific MOMP antibody to detect CTH522 and spCTH522 proteins (diluted 1:10000), a mouse anti-β-actin antibody (diluted 1:50000), and a rabbit anti-VACV H3 antibody (diluted 1:500) diluted in 5% non-fat milk. After primary antibody incubation, the membranes were washed three times with TBSt for 10 minutes each and then incubated with either an HRP-conjugated anti-mouse antibody (diluted 1:3000) or an anti-rabbit antibody (diluted 1:5000) in 5% non-fat milk for one hour at room temperature. The membranes were then washed three times with TBSt for 10 minutes each. Protein detection was performed using Pierce™ ECL Western Blotting Substrate. The detection solution was applied to the membranes, which were then placed in the ECL ChemoStar and images captured using ChemoStarTS software. The membranes were exposed for 10 minutes and images were acquired every 30 seconds.

4.12. Immunofluorescence Microscopy

For confocal microscopy imaging, HeLa cells were seeded on microscope coverslips in 6-well plates at a density of 1.5×10^5 cells per well. The cells were infected with either MVA-WT or MVA-spCTH522 at a multiplicity of infection (MOI) of 5. During the first hour of infection, the plates were gently shaken every 15 minutes to ensure uniform virus distribution, and the cells were then incubated for a further 5 hours.

For mitochondrial staining, infected HeLa cells were incubated with MitoTracker™ Red CMXRos for 30 minutes before the end of the 6-hour infection period. The cells were then washed with PBS, permeabilized, and fixed with 100% ice-cold methanol for 15 minutes on ice. After fixation, the cells were washed with PBS and incubated in BSA blocking buffer for

1 hour at room temperature. Colocalization with spCTH522 proteins was then detected using a mouse monoclonal antibody against MOMP (diluted 1:2000) for 1 hour at room temperature. The secondary antibody staining procedure is described below.

For endoplasmic reticulum (ER) staining, infected HeLa cells were washed with PBS, permeabilized, and fixed with 100% ice-cold methanol for 15 minutes on ice. After fixation, cells were washed with PBS and incubated with BSA blocking buffer for 1 hour at room temperature. ER staining was performed using Alexa Fluor 647-conjugated rabbit anti-calnexin antibody for 1 hour at room temperature. Colocalization with spCTH522 proteins was detected using a mouse monoclonal anti-MOMP antibody (diluted 1:2000). The secondary antibody staining procedure is described below.

For cell surface colocalization staining, infected HeLa cells were fixed with 4% formaldehyde for 15 minutes at room temperature. After washing with PBS, the cell membrane was labelled with a wheat germ agglutinin (WGA) probe conjugated to the red fluorescent dye Alexa Fluor 594 (diluted 1:200). Colocalization with spCTH522 proteins was detected using a mouse monoclonal anti-MOMP antibody (diluted 1:2000). The secondary antibody staining procedure is described below.

In all staining protocols, bound anti-MOMP antibodies were detected with a secondary anti-mouse antibody conjugated to the green fluorescent dye Alexa Fluor 488 (diluted 1:200) for 30 minutes at room temperature. Cell nuclei were stained with DAPI (blue) after thorough washing. The coverslips containing stained cells were carefully removed from the wells, dried, mounted on microscope slides, and sealed with nail polish. Imaging of stained cells was performed using a ZEISS LSM 880 confocal laser scanning microscope, which provides high-resolution visualization of labelled components and allows detailed analysis of colocalization patterns or spCTH522 across mitochondria, ER and cell surface.

4.13. Immunization of mice

C57BL/6J or HLA-A2.DR1 mice aged 8-12 weeks were used in this study. Mice received an intraperitoneal (i.p.) vaccination of 1×10^7 IU (infectious units) of either MVA-WT, MVA-spCTH522 or MVA-CTH522:B7 in a 200 μ L volume of PBS. Vaccination was administered either as a single dose or in a prime/boost regimen, with the booster dose administered i.p. on day 28. In the prime/boost regimen, mice received a priming dose of 1×10^7 IU followed by a boosting dose of 1×10^8 IU. Spleens were harvested 8 days after priming or 28 days after

boosting to assess T-cell responses by intracellular cytokine staining (ICS). Blood samples and vaginal washings were collected 28 days post-boost to assess antibody responses by ELISA.

4.14. Isolation of splenocytes, blood and vaginal washes

Spleens were harvested and pressed through a 70 µm cell strainer to obtain a single cell suspension in M2 medium. These suspensions were then centrifuged at 1500 rpm for 5 minutes. To eliminate erythrocytes, cell pellets were resuspended with 5mL of 1:10 diluted BD Pharm Lyse™ lysis buffer for 1 minute at room temperature. Lysis was stopped by adding 45 mL of fresh M2 medium to the suspension. The cells were then passed through a second 70 µm cell strainer and counted using a Neubauer counting chamber. Finally, 2×10^6 cells were plated in 100 µL of M2 medium per well of a 96-well plate for peptide stimulation. Blood samples were obtained via retro-orbital bleeding and left to coagulate at room temperature for 20 minutes. The blood was subsequently centrifuged at 2.500 rpm for 30 minutes at 4°C, and the separated serum was aliquoted into tubes and stored at -80°C. Vaginal tracts were washed with 100 µL of PBS supplemented with protease inhibitors and stored at -80°C.

4.15. Ex vivo T-cell activation

T-cells activation was assessed by *ex vivo* peptide pulsing of splenocytes. For this, 2×10^6 splenocytes per well were plated in a V-bottom 96-well plate, as described in 4.3. Single peptides or the spCTH522 overlapping peptides pool (Supplementary table 2) diluted in 50 µL/well of M2 medium to a final concentration of 10 µg/mL were added to the splenocytes. Subsequently, 50 µL of Brefeldin A (BFA) diluted in M2 medium was added in each well to reach a final concentration of 1 µg/mL. The plate was incubated at 37°C for 4-5 hours to facilitate peptide stimulation of the splenocytes. Activation of T-cells within splenocytes suspensions was analyzed through intracellular cytokines staining (ICS).

4.16. Intracellular cytokines staining (ICS)

Peptide-pulsed splenocytes were centrifuged and washed with PBS. Dead cells were stained with eBioscience™ Fixable Viability Dye eFluor™ 660 for 20 minutes on ice, protected from light. Cells were then washed twice with FACS staining buffer and stained with a combination

of antibodies specific for surface markers (eFluor405 anti-mCD8, PE-Cy7 anti-mCD4, PE anti-mCD107) for 30 minutes on ice, also protected from light. After staining, the cells were centrifuged and washed twice with FACS staining buffer. Cells were then fixed and permeabilized with BD Cytofix™ Fixation Buffer for 15 minutes on ice, protected from light. After permeabilization/fixation, cells were centrifuged and washed with BD Perm Wash. Permeabilized cells were then stained with a panel of antibodies specific for intracellular cytokines (FITC anti-mIFN- γ , APC-Cy7 anti-mTNF- α , PerCP-Cy5.5 anti-mIL-2) for 30 minutes in the dark on ice. After intracellular staining, splenocytes were centrifuged, washed with FACS staining buffer and fixed in 1% paraformaldehyde. Flow cytometry analysis was performed using BD FACS Canto II. All centrifugation steps were performed at 1400 rpm for 2 minutes at 4°C.

4.17. Enzyme-Linked Immunosorbent Assay (ELISA)

This method was performed by Ms. Esmā Özü̇n during her four-month internship in the laboratory of Prof. Dr. med. Ingo Drexler as part of her bachelor thesis. Under my direct supervision, she focused on analyzing the humoral immune response to the vaccine candidates discussed here. The experiments were closely supervised and carried out in collaboration, and the results were included in her thesis and the above-mentioned publication.

MaxiSorp round-bottom 96-well plates were prepared for analysis by coating each well with 100 μ L of recombinant CTH522 at a concentration of 5 μ g/mL or MVA virus (10^5 TCID₅₀/well) in 0.1 M carbonate/bicarbonate buffer (pH 9.6). This coating step was performed overnight at 4°C to ensure optimal antigen binding to the well surface. The next day, the plates were washed three times with PBS containing 0.05% Tween-20 (PBST) to remove unbound material and then blocked with 3% BSA/PBST for 1 hour to prevent non-specific binding. Serum and vaginal wash samples collected from mice immunized with MVA-WT, MVA-spCTH522 or MVA-CTH522:B7 were serially diluted in 1% BSA/PBST. These diluted samples were added to the wells and incubated for 1 hour at room temperature to allow for antigen-specific antibody binding. After incubation, the plates were washed three times with PBST to remove unbound antibodies. To detect bound antibodies, the wells were incubated with alkaline phosphatase-conjugated goat anti-mouse secondary antibodies specific for either total IgG, IgG1, IgG2b, IgG2c, IgG3 or IgA. The secondary antibodies, diluted 1:1000, were incubated for 1 hour at room temperature. After further three washing steps with PBST, the enzyme substrate p-nitrophenyl phosphate (pNPP) was added to the

wells to initiate the enzymatic reaction and subsequent color development. The reaction was allowed to proceed for 30 minutes before being stopped by the addition of 2 M NaOH. The absorbance of the color reaction was measured at 405 nm using a spectrophotometer microplate reader. All experimental steps were performed at room temperature, unless otherwise stated.

5. Results

5.1. Generation of recombinant MVA-CTH522 and MVA-spCTH522

In order to generate recombinant MVA-CTH522 and MVA-spCTH522, the two-steps *en passant* recombination method was employed. In the first step, each expression cassette encoding for CTH522 or spCTH522 antigens (Fig. 8A) was cloned into the plasmid pVI-PmH5-dVI, a shuttle vector which contains homologous regions to the deletion VI of the MVA genome, and a kanamycin resistance cassette (Fig. 8B)

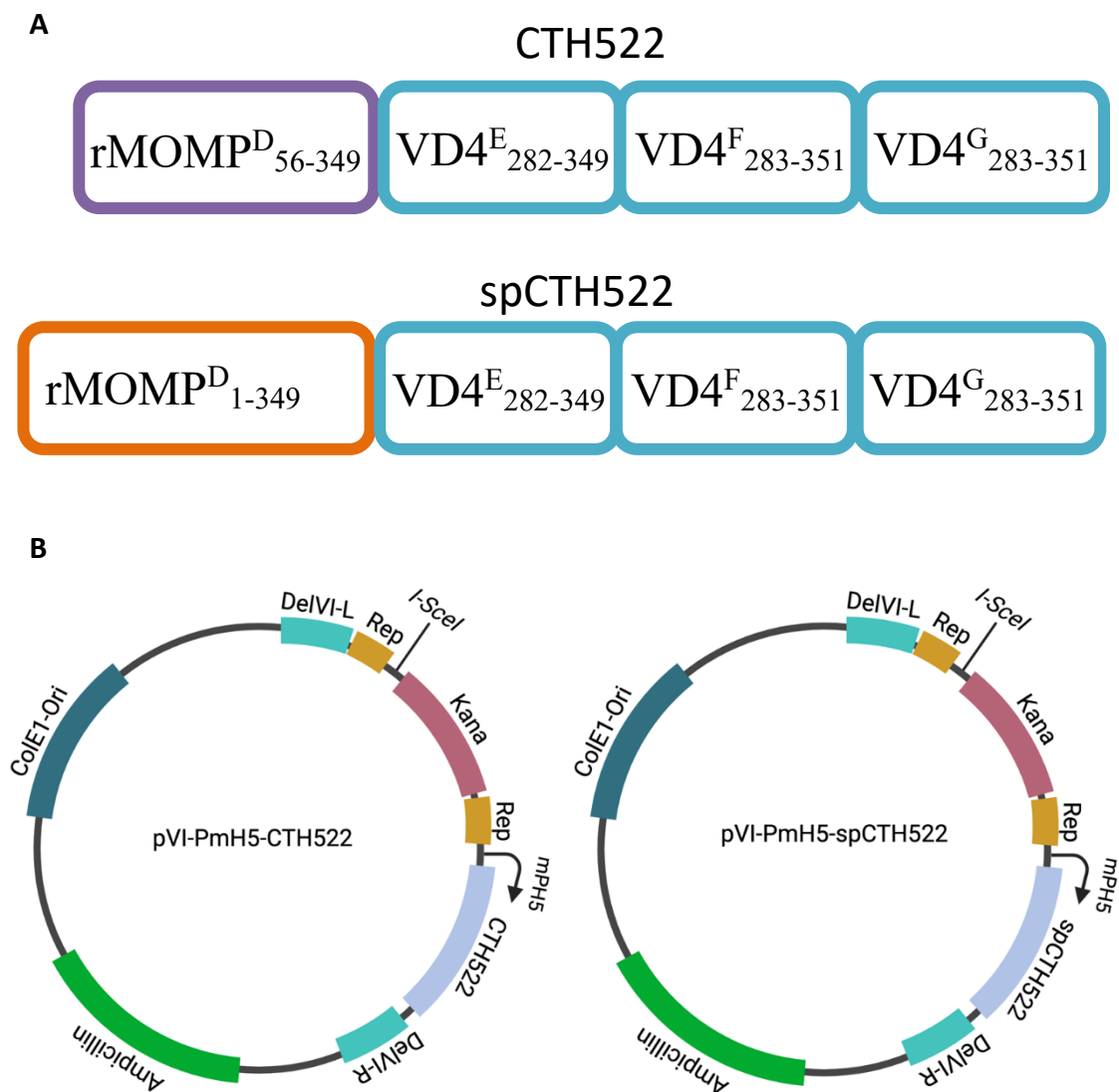


Figure 8. Schematic representation of the CTH522 and spCTH522 antigen and schematic map of the pVI-PmH5-CTH522 and pVI-PmH5-spCTH522 shuttle vectors.

A) The CTH522 antigen contains a partial sequence of the MOMP from serovar D (aa 56-349) and the external VD4 domains from serovars E (aa 282-349), F (aa 283-351), and G (aa 283-351), while the spCTH522 antigen contains a partial sequence of the MOMP from serovar D (aa 1-349) and the external VD4 domains from serovars E (aa 282-349), F (aa 283-351), and G (aa 283-351). B) The pVI-PmH5-CTH522 and pVI-PmH5-spCTH522 vector contains a ~650 bp DelVI-L sequence homologous to the left region of DelVI in the MVA genome, together with a kanamycin resistance expression cassette flanked by 50 bp homologous sequences (REP). The *I-SceI* restriction site is located between the initial REP sequence and the kanamycin cassette. Following the kanamycin cassette, the vector contains an expression cassette for the recombinant antigen of interest under the control of the mPH5 promoter, followed by a ~1000 bp DelVI-R sequence homologous to the right region of DelVI in the MVA genome.

After linearization, the shuttle vector was introduced into the electrocompetent *Escherichia coli* strain GS1783 by electroporation. This particular *E. coli* strain harbors the MVA genome in a bacterial artificial chromosome (BAC) and also contains the heat-inducible red recombinase system and the L-arabinose-inducible *I-SceI* endonuclease in its bacterial genome. Upon heat induction at 42°C, the red recombination system facilitated the integration of the linearized shuttle vector into BAC-MVA. This process occurred by homologous recombination between the deletion VI regions of the shuttle vector and the MVA genome. After induction with L-arabinose, the *I-SceI* endonuclease cleaved between the first REP sequence and the kanamycin cassette. Subsequently, upon heat induction, the Red recombinase system mediated the recombination of the homologous REP regions flanking the kanamycin cassette, as shown in Figure 9. Ultimately, a recombinant, markerless BAC-MVA carrying our expression cassette of interest was successfully generated. This method was used to generate two BAC-MVA constructs carrying the expression cassettes for either CTH522 or spCTH522.

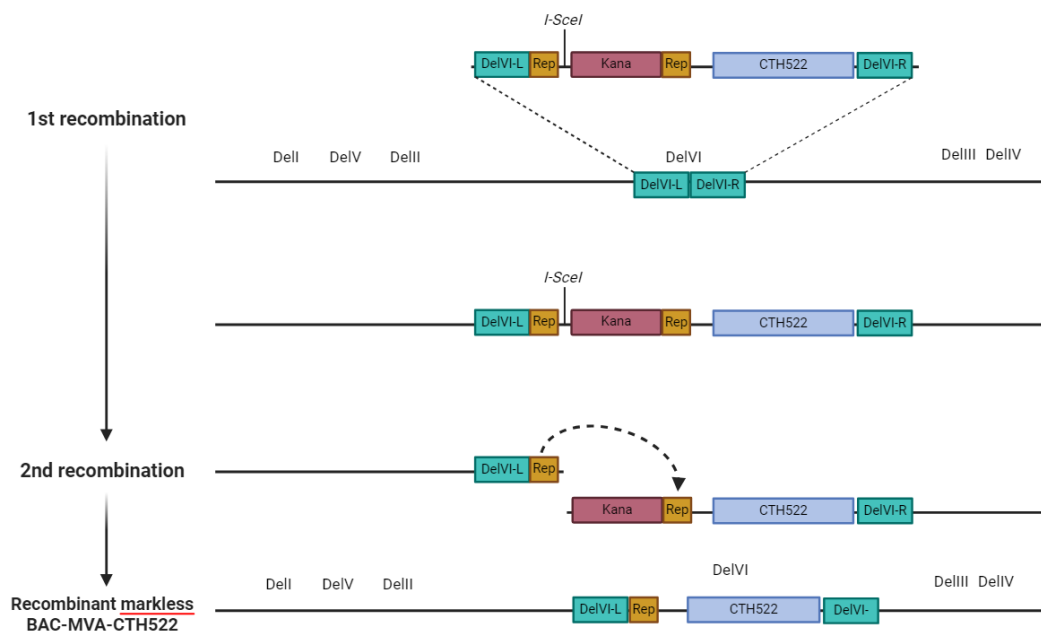


Figure 9. Schematic map showing the recombination steps for the integration of the expression cassette from pVI-PmH5-CTH522 into the BAC-MVA genome

In the first recombination step, the linearized shuttle vector containing both the kanamycin and CTH522 expression cassettes is inserted into the BAC-MVA genome using a heat-induced red recombination system. This process facilitates recombination of the DelVI-L and -R regions surrounding the shuttle vector with the corresponding DelVI regions in the MVA genome. Once the shuttle vector is integrated into the BAC-MVA genome, the bacteria are treated with L-arabinose to induce expression of the I-SceI restriction enzyme. The I-SceI enzyme then cleaves between the first REP sequence and the kanamycin cassette. Heat induction of the red recombination system then induces recombination of the two REP sequences flanking the kanamycin cassette, resulting in a recombinant BAC-MVA genome containing the CTH522 expression cassette without the kanamycin cassette.

In the second step, the recombinant BAC-MVA was used as a template to produce recombinant MVA. This was achieved by transfection of DF-1 chicken cells with the recombinant BAC and subsequent abortive infection of the cells with rabbit fibroma virus (RFV). RFV acted as a helper virus, providing the initial transcription machinery necessary to initiate DNA replication of the recombinant MVA genome contained in the BAC. DF-1 cells are susceptible to MVA but not to RFV, making this approach uniquely suited to recovering the recombinant MVA. The first-generation viral progeny of the recombinant MVA was propagated in DF-1 cells through multiple sub-passages to eliminate the GFP gene-containing BAC cassette, taking advantage of the self-excision property of the BAC cassette. After three passages in DF-1 cells, several rounds of limiting dilutions were performed to generate single viral clones. The integrity of these single viral clones was verified by PCR using specific primers targeting the CTH522 and spCTH522 cassettes, the GFP cassette (to confirm the correct excision of the BAC backbone) and the RFV genome (to demonstrate the correct removal of the helper virus during the successive sub-passages), as shown in Figure 10.

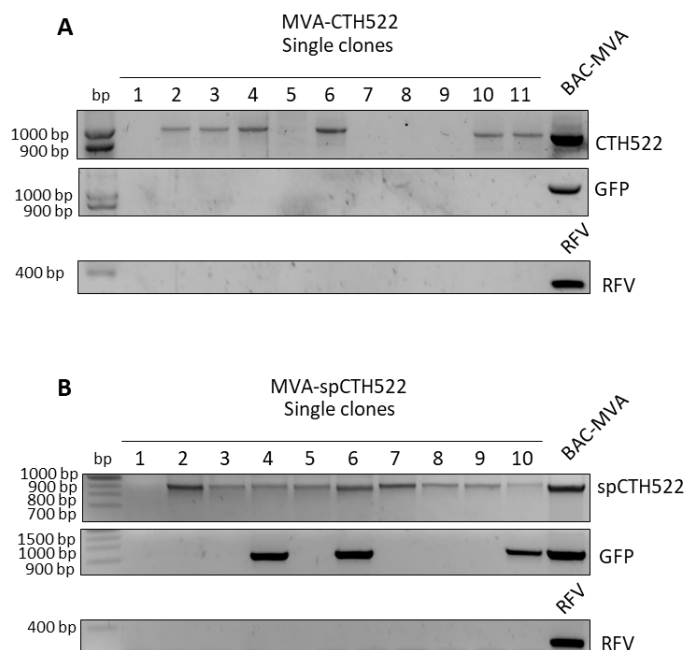


Figure 10. Screening of MVA-CTH522 and MVA-spCTH522 single clones derived from limiting dilution by PCR.

DNA was extracted from MVA-CTH522 (A) and MVA-spCTH522 (B) infected DF-1 cells seeded in a 96-well plate in several limiting dilutions (10^{-6} to 10^{-8}). Single clones were screened and selected for the presence of cytopathic effect. Total DNA was extracted and used as template for PCR using primers annealing within the GFP cassette, RFV genome or DelVI/CTH522.

After confirming the correct identity of each clone lacking GFP expression and helper virus DNA, MVA-CTH522 and MVA-spCTH522 were amplified, purified and titrated. To ensure that the virus preparations were free from contamination, various tests were carried out to certify that the stocks were free from bacteria, fungi and mycoplasma.

5.2. In vitro characterization of MVA-CTH522 and MVA-spCTH522

5.2.1. Analysis of the stability passage of MVA-CTH522 and MVA-spCTH522

The first approach to validate the efficacy of MVA-based vaccines is to investigate the genomic stability and the correct synthesis of the recombinant antigen. To ensure that MVA-CTH522 and MVA-spCTH522 remain stable and that the recombinant DNA is stably integrated into the viral genome without loss of the sequences encoding CTH522 and spCTH522, recombinant MVAs were passaged in DF-1 cells infected at an undefined MOI for 10 consecutive rounds. After approximately 48 hours post infection, DNA and total proteins were extracted from each passage and analyzed by PCR and western blot, respectively. PCR was performed using primers annealing within the deletion VI of the MVA genome and either the CTH522 or the spCTH522 sequence, and the results confirmed that both the CTH522 (Fig. 11A) and spCTH522 (Fig. 11B) genes are retained within the deletion VI in each of the 10 passages.

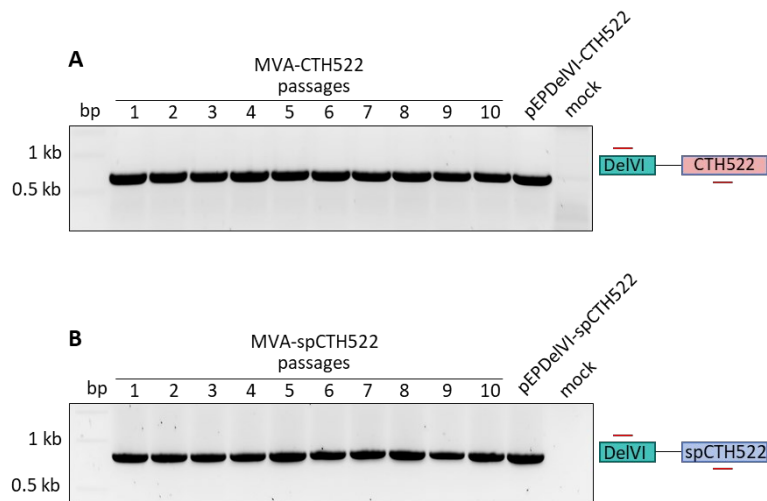


Figure 11. Genetic stability analysis of MVA-CTH522 and MVA-spCTH522 by PCR.

PCR analysis of the MVA deletion VI locus was performed for each of the 10 stability passages. DF-1 cells were sequentially infected with either MVA-CTH522 or MVA-spCTH522 for approximately 48 hours for ten rounds. At the end of each round, cells were lysed to extract DNA to assess the integrity of the recombinant expression cassette within the MVA genome. Primers targeting the deletion VI locus-CTH522 cassette (a) and the deletion VI locus-spCTH522 cassette (b) were used for PCR analysis of the CTH522 (690 bp) and spCTH522 (855 bp) expression cassettes integrated into the deletion VI locus of MVA-CTH522 and MVA-spCTH522, respectively.

To further assess whether the successive passages affected the stability of the CTH522 and spCTH522 constructs within the MVA genome, the synthesis of the antigens was examined. Specifically, the total cell lysate from each of the 10 passages was analyzed by western blot (Fig. 12). The synthesis of the *in silico* predicted 57.4 kDa spCTH522 protein, was stably maintained at each infection passage (Fig. 12A). Surprisingly, the *in silico* predicted 53.5 kDa CTH522 protein was not detected in any of the 10 passages (Fig. 12B) although MVA derived H3 protein was detected in each of the 10 passages of both MVA-CTH522 and MVA-spCTH522 infected DF1 cells, suggesting that the lack of detection of CTH522 is not due to *in vitro* infection defects.

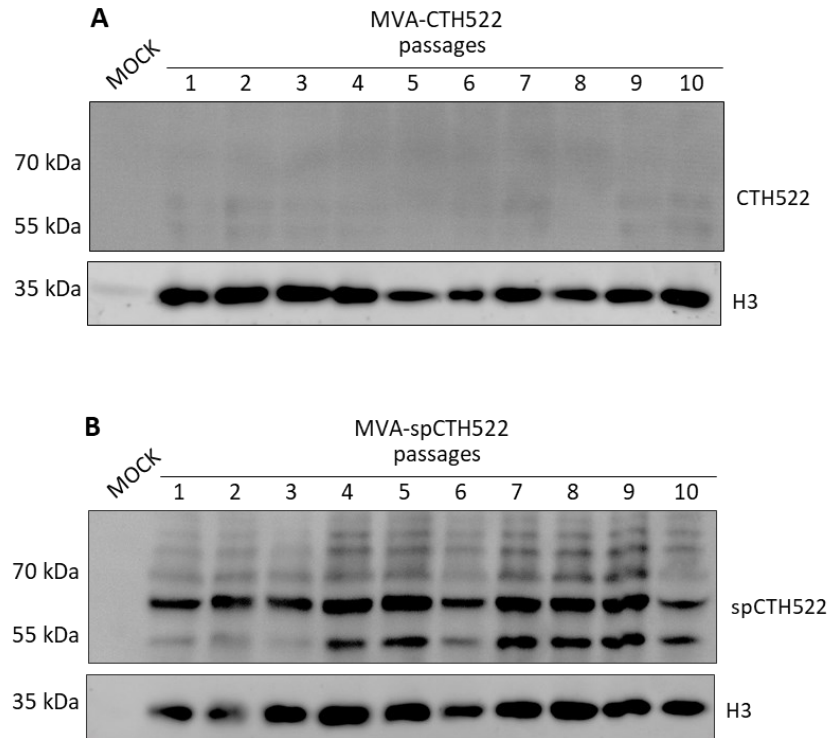


Figure 12. Analysis of antigen synthesis in MVA-CTH522 and MVA-spCTH522 infected DF1 cells.

The synthesis of ~53.5 kDa CTH522 (A) and ~57.4 kDa spCTH522 (B) proteins in each stability passage was determined by western blot analysis. DF-1 cells were sequentially infected with either MVA-CTH522 or MVA-spCTH522 for approximately 48 hours for all together ten rounds. At the end of each round, cells were harvested and lysed to extract total protein to assess the synthesis of the recombinant antigens using a mouse anti-MOMP protein antibody. Rabbit anti-VACV H3 protein antibody was used to detect viral H3 protein (~37.5 kDa) that served as infection control. Alkaline phosphatase-conjugated anti-mouse and anti-rabbit secondary antibodies were used to detect bound mouse anti-MOMP and rabbit anti-H3, respectively.

5.2.2. Kinetics of CTH522 and spCTH522 antigen synthesis

To further characterize the two vaccine candidates, CTH522 and spCTH522 antigens were analyzed regarding their kinetics for synthesis. To this end, monolayers of HeLa cells were infected with MVA-WT, MVA-CTH522, or MVA-spCTH522 at an MOI of 5. Infected cells were harvested at different time points post infection and cell lysates were used for western blot. For kinetic analysis of protein synthesis, cell lysates were collected at 0, 4, 8 and 24 hours post infection (Figure 13). A protein with a molecular weight in the range of 55 kDa to 70 kDa was identified in HeLa cells infected with MVA-spCTH522 at 4 hours post infection (h.p.i.) (Fig. 13A). This corresponds to the *in silico* predicted molecular weight of the antigen, which is approximately 59,596 kDa. western blot analysis showed a progressive increase in

spCTH522 protein levels as the infection progressed. The same trend was observed for the H3 viral protein. Furthermore, western blot analysis showed that the spCTH522 protein remained detectable for up to 72 hours post infection (Fig. 13B). In contrast, CTH522 protein was only weakly detectable at 4 h.p.i. and, unlike the viral H3 protein, there was no detectable increase in CTH522 protein levels at 8 and 24 h.p.i. In addition, CTH522 protein was not detectable at later time points of infection, despite the continued presence of the viral H3 protein.

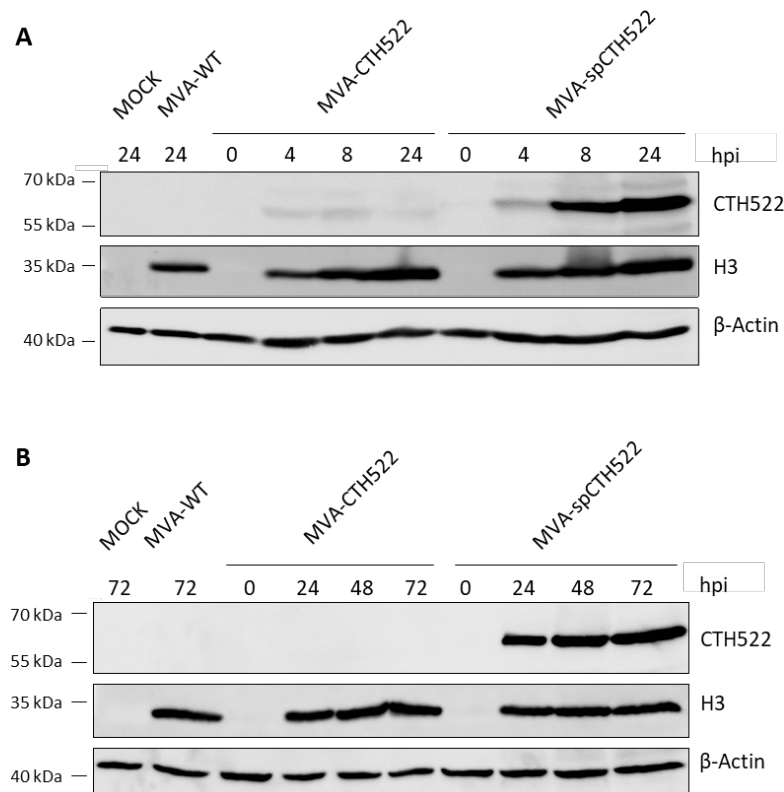


Figure 13. CTH522 and spCTH522 protein synthesis analysis.

HeLa cells were infected with MVA-WT, MVA-CTH522 or MVA-spCTH522 at an MOI of 5 and cell lysates were collected at 0, 4, 8, 24 (a) and at 0, 24, 48 and 72 (b) hours post infection. The kinetics of CTH522 (~53.5 kDa) and spCTH522 (~57.4 kDa) protein synthesis was determined by western blot analysis using a mouse anti-MOMP protein antibody. Rabbit anti-VACV H3 protein antibody was used to detect viral H3 protein (~37.5 kDa) that served as infection control.; mouse anti-β-actin protein antibody was used to detect β-actin (~42 kDa) that served as loading control. Alkaline phosphatase-conjugated anti-mouse was used to detect mouse anti-MOMP and anti-β-actin while alkaline phosphatase-conjugated anti rabbit was used to detect rabbit anti-H3.

Previous data showed that while spCTH522 was synthesized during infection, CTH522 was undetectable in western blot assays. To rule out the possibility that random mutations within the CTH522 open reading frame sequence were responsible for the lack of CTH522 detection, viral DNA was extracted from purified virus stocks and sequenced, focusing on the deletion VI site. The sequencing data showed no mutation in either the CTH522 open reading frame or the PmH5 promoter sequence, which regulates the transcription of the gene (data not

shown). Given that CTH522 is an engineered construct designed for bacterial production and purification, the antigen could be recognized as a foreign or misfolded protein when synthesized in mammalian cells through MVA vectors, and thus be rapidly degraded. To confirm this hypothesis, a proteasome-ubiquitin system inhibition assay was performed, followed by western blot detection of the proteins. Specifically, monolayers of HeLa cells were infected with MVA-WT, MVA-CTH522 and MVA-spCTH522 at an MOI of 5 for 24 hours. At 3 hours post infection, 2 μ M of irreversible proteasome inhibitor, epoxomicin or DMSO vehicle control was added to the infected cells and cell lysates were harvested at 24 hours post infection and analyzed by western blot (Fig. 14). The synthesis of spCTH522 was comparable between epoxomicin and DMSO treatment, whereas the CTH522 antigen was not detected under DMSO treatment. Interestingly, inhibition of the proteasome-ubiquitin system allowed the detection the CTH522 protein, albeit at a lower intensity compared to spCTH522.

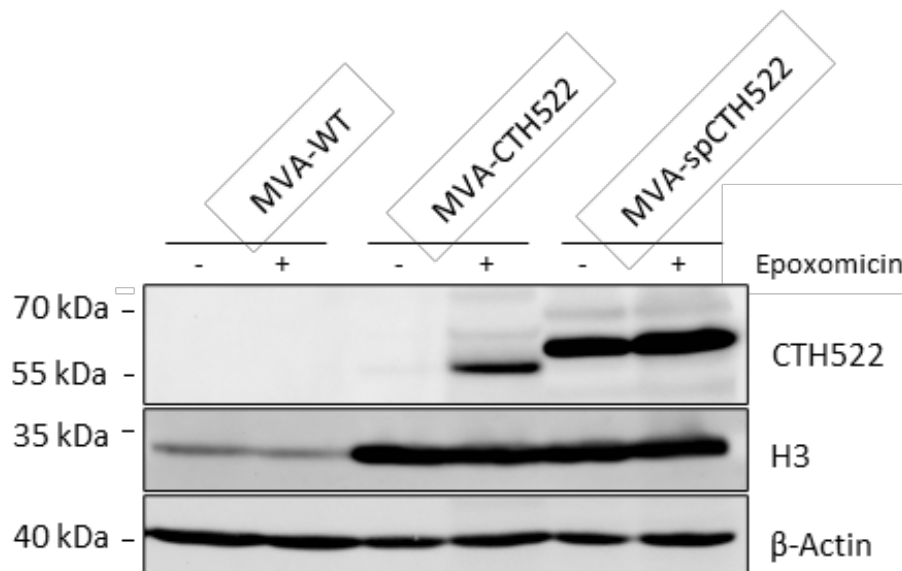


Figure 14. Proteasome-Ubiquitin system interferes with CTH522 protein stability in MVA-CTH522 infected cells.

HeLa cells were infected with MVA-WT, MVA-CTH522 or MVA-spCTH522 (MOI of 5). Proteasome inhibitor Epoxomicin (2 μ M) or DMSO was added at 3 hours post infection; cell lysates were collected at 24 hours post infection and the synthesis of CTH522 (~53.5 kDa) and spCTH522 (~57.4 kDa) protein was determined by western blot analysis using a mouse anti-MOMP protein antibody. Rabbit anti-VACV H3 protein antibody was used to detect viral H3 protein (~37.5 kDa) that served as infection control; mouse anti- β -actin protein antibody was used to detect β -actin (~42 kDa) as that served as loading control. Alkaline phosphatase-conjugated anti-mouse was used to detect mouse anti-MOMP and anti- β -actin while alkaline phosphatase-conjugated anti rabbit was used to detect rabbit anti-H3.

5.2.3. Growth kinetics analysis of MVA-CTH522 and MVA-spCTH522

One of the most important features of the MVA vector is the lack of replication in most mammalian cells, which determines the high safety of MVA as a vaccine platform. To determine whether the insertion of the CTH522 and spCTH522 expression cassettes into the MVA genome affects the replication behavior of the viruses, the replication kinetics of MVA-CTH522 and MVA-spCTH522 were investigated. Specifically, monolayers of HeLa and DF-1 cells were infected with MVA-WT, MVA-CTH522 and MVA-spCTH522 at an MOI of 0.01. Infected cells were harvested at 0, 24, 48, and 72 hours post infection. The viral content in every time point was determined by the tissue culture infectious dose (TCID₅₀) titration assay. The replication behavior and kinetics of MVA-WT, MVA-CTH522 and MVA-spCTH522 were comparable. Indeed, for the recombinant viruses, as well as for the non-recombinant MVA, viral titers increased from the range of 10²-10³ to 10⁶-10⁷ within 24 hours post infection in DF-1 cells. At 48 hours post infection the TCID₅₀ increased to the range of 10⁷-10⁸ for both not recombinant and recombinant viruses, while no further increase was observed at 72 hours post infection. As expected, there was no detectable increase in viral titers in HeLa cells for both non recombinant and recombinant MVAs, as the TCID₅₀ remained in the range of 10²-10³ in every time point of infection (Fig. 15A). No significant differences in viral growth were observed between MVA-WT, MVA-CTH522 and MVA-spCTH522 in DF-1 cells at 72 hours post infection. Similarly, no significant differences were observed in HeLa cells (Fig 15B).

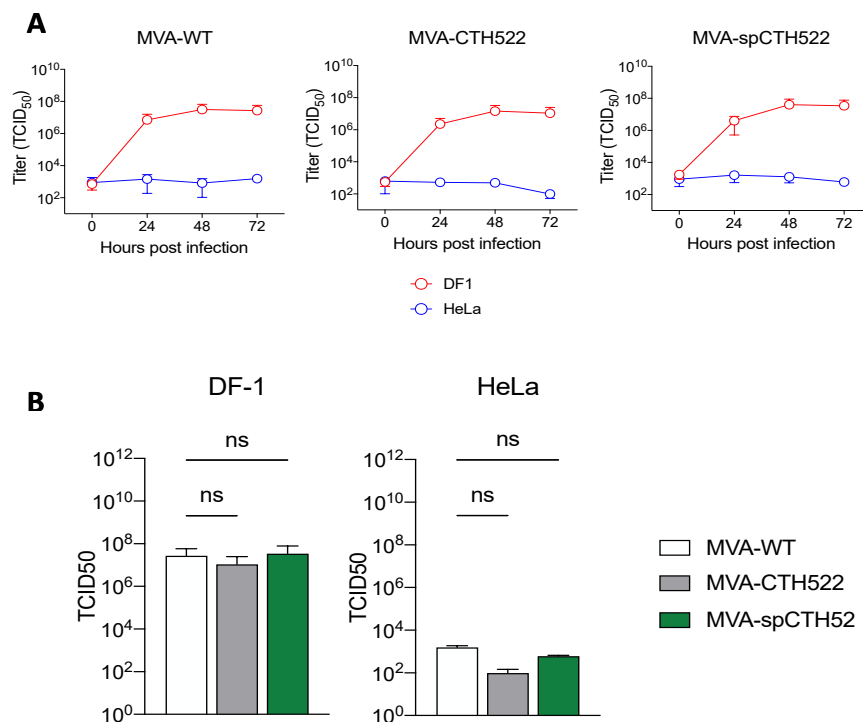


Figure 15. Viral growth kinetics of MVA-CTH522 and MVA-spCTH522.

Monolayers of semi-permissive HeLa or permissive DF-1 cells were infected at MOI 0,01 with MVA-WT, MVA-CTH522 or MVA-spCTH522. (A) At different time points post infection (0, 24, 48, and 72 h.p.i.) virus titers in cell lysates were quantified by median tissue culture infectious dose (TCID₅₀) assay. (B) Comparison of TCID₅₀ between MVA-WT, MVA-CTH522 and MVA-spCTH522 obtained after 72 hours post infection in DF-1 and HeLa cells (One-way ANOVA with Kruskal-Wallis's Multiple Comparison Test).

5.2.4. Localization of spCTH522

Chlamydia MOMP is known to be released from inclusion bodies and to be localized to mitochondria of infected cells¹⁹⁵. To investigate whether spCTH522 expressed by recombinant MVA also localizes to mitochondria, an analysis of antigen localization was performed by immunofluorescence microscopy. HeLa cells were infected with MVA-spCTH522 or MVA-WT at an MOI of 5 for 6 hours. At the end of the infection time, a potential colocalization of mitochondria and CTH522 was determined using Mito Tracker and anti-MOMP antibody for detection. Results from immunofluorescence microscopy showed that spCTH522 partially localized to the mitochondria of infected cells (Fig. 16A). To further understand the localization of spCTH522, HeLa cells were infected with MVA-spCTH522 or MVA-WT and subsequently stained with antibodies for MOMP and calnexin. Immunofluorescence microscopy showed that spCTH522 was also partially localized within the endoplasmic reticulum (ER) of infected cells (Fig. 16B).

Ms. Sara Moreno Mascaraque generated and characterized an additional virus, MVA-CTH522:B7. The CTH522:B7 construct represents a cell membrane-anchored form of CTH522. She showed that modifying the CTH522 antigen by adding the signal sequence of the murine IgG κ chain at the N-terminus and the transmembrane region together with the cytoplasmic domain of murine CD80 at the C-terminus enhances the cell surface localization of CTH522. To further evaluate whether spCTH522 protein could be also detected on the cell surface, HeLa cells were infected with MVA-WT, MVA-spCTH522, or MVA-CTH522:B7. Non-permeabilized infected cells were incubated with WGA probe to label the cell surface and stained with an anti-MOMP antibody. Cells were then analyzed by immunofluorescence microscopy. While the cell surface was clearly visible with the WGA probe, spCTH522 protein was only weakly detected on the surface of MVA-spCTH522-infected cells (Fig. 16C). In contrast, substantial localization of CTH522:B7 protein was observed on the surface of MVA-CTH522:B7-infected cells (Supplementary figure 1). These results demonstrate that

both spCTH522 and CTH522:B7 proteins are produced after MVA infection (Supplementary figure 3), and that CTH522:B7, but not spCTH522, is effectively targeted to the cell surface.

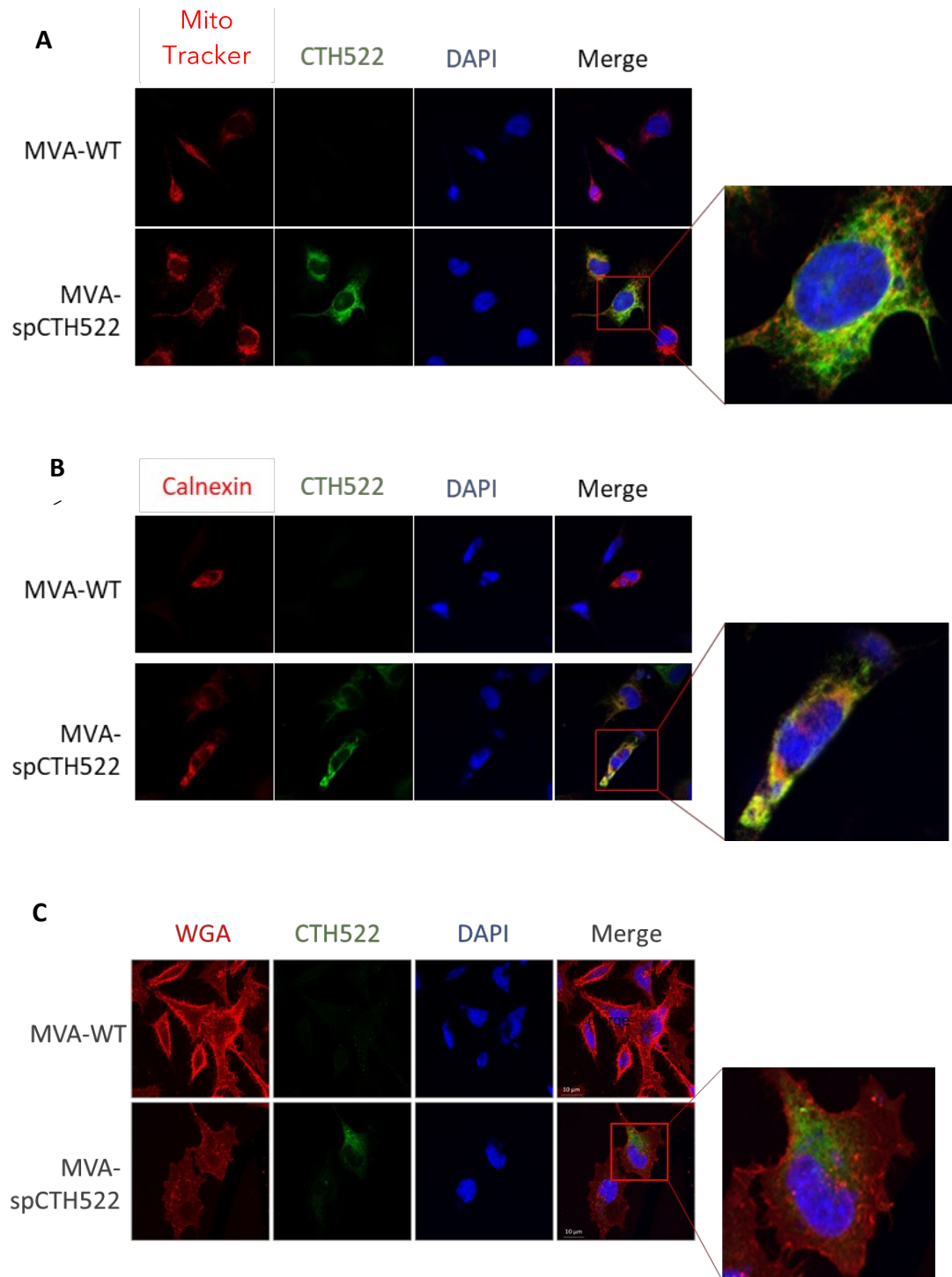


Figure 16. Localization of spCTH522 in infected cells.

HeLa cells were infected with MVA-WT or MVA-spCTH522 at MOI of 5 for 6 hours. A) Infected cells were washed and treated with MitoTracker™ Red CMXRos (red) for 30 min. Cells were then washed, fixed, and permeabilized. After permeabilization, cells were incubated with mouse monoclonal anti-MOMP. B) Infected cells were washed, fixed, and permeabilized. After permeabilization, cells were incubated with mouse anti-MOMP and Alexa Fluor 647 conjugated rabbit anti-calnexin (red). C) Non-permeabilized infected cells were fixed and stained

with WGA probe conjugated to Alexa Fluor 594 (red) and a mouse monoclonal anti-MOMP antibody. In all conditions, bound anti-MOMP was visualized using an anti-mouse secondary antibody conjugated to Alexa Fluor 488 (green). Nuclei were stained with DAPI (blue). Scale bars: 10 μ m.

5.3. Ex-vivo analysis of CTH522-specific immune response in C57BL/6J mice

5.3.1. MVA-spCTH522 and MVA-CTH522:B7 induced CD4⁺ but not CD8⁺ T-cell responses in C57BL/6J mice

In prime/boost vaccination regimens, the MVA booster dose has been well documented to enhance and sustain T cell memory responses in both homologous and heterologous vaccination strategies. By enhancing the immune system's ability to recognize and respond to the target antigen, this booster not only strengthens the initial immune activation, but also promotes the long-term persistence of memory T cells. These memory T cells play a critical role in ensuring a robust and durable immune response, providing enhanced protection against subsequent exposures to the pathogen¹⁹⁶. To evaluate the cellular immune response of recombinant MVAs, C57BL/6J mice were subjected to a homologous prime/boost vaccination regimen. In addition to the MVA-spCTH522, a further virus was included in this investigation, MVA-CTH522:B7. To evaluate the CD8⁺ T-cell response, the mice received an initial immunization dose of either MVA-WT, MVA-spCTH522, or MVA-CTH522:B7 followed by a second dose of the same vaccine vector on day 28. On day 56, the mice were euthanized and their spleens were harvested to isolate single cells (Fig. 17).

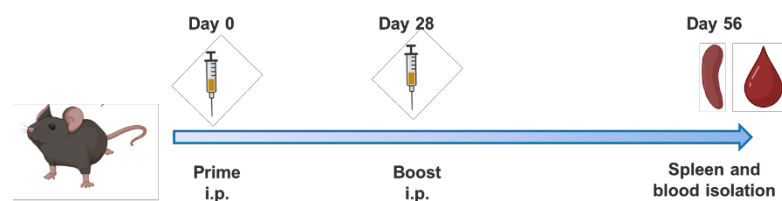


Figure 17. Schematic representation of the immunization scheme.

C57BL/6J mice were immunized intraperitoneally with MVA-WT, MVA-spCTH522 or MVA-CTH522:B7 on day 0 and boosted on day 28. Spleens and blood were collected on day 56.

Splenocytes were then cultured with a pool of overlapping peptides covering the entire protein sequence of spCTH522 ([Supplementary table 2](#)). These peptides, designed as 15-mers with an overlap of 11 amino acids, were used to encompass all possible MHC-I and MHC-II restricted epitopes. The pool consists of 127 peptides. Overlapping sequences from peptide 1 to peptide 14 cover the amino acid sequence of MOMP^D (aa 1-67), which is part of the spCTH522

antigen. While, overlapping sequences from peptide 16 to peptide 127 cover MOMP^D (aa 56-349) and the external VD4 domains of serovars E (aa 282-349), F (aa 283-351), and G (aa 283-351), which are present in both spCTH522 and CTH522:B7 antigens. Thus, the pool can be used to stimulate splenocytes from mice immunized with either MVA-spCTH522 or MVA-CTH522:B7. Hereafter, this pool will be referred to as the CTH522 pool. Splenocytes were incubated with the pool of overlapping peptides for 5-6 hours in the presence of Brefeldin A. The vaccinia virus-specific B8₂₀₋₂₇ peptide was used as a positive control, while OVA₂₅₇₋₂₆₄ peptide derived from chicken ovalbumin was used as a negative control. After incubation with the peptides, the splenocytes were washed and subjected to an intracellular cytokine staining (ICS) assay followed by flow cytometry analysis (Fig. 18).

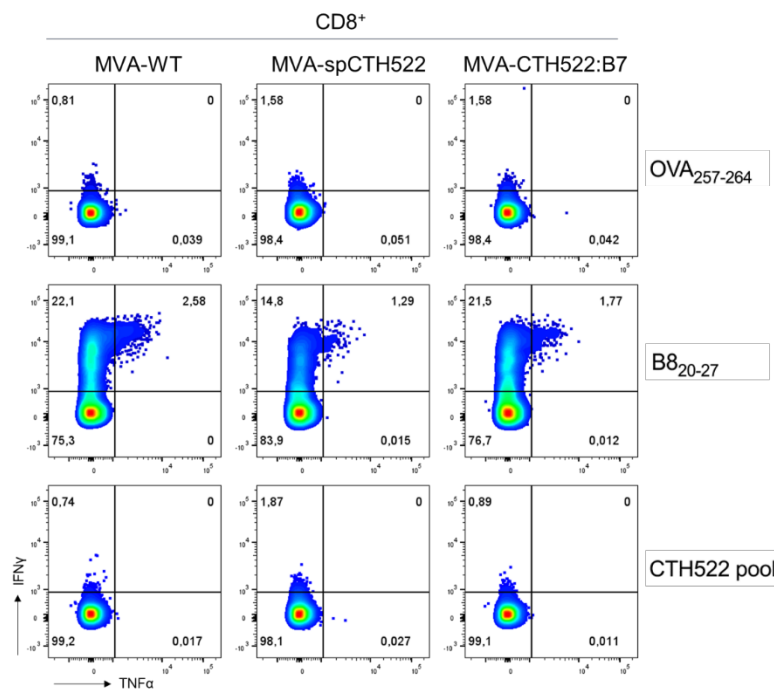


Figure 18. Representative flow cytometry plots showing IFN- γ and TNF- α -producing CD8⁺ T-cells from the spleens of MVA-WT, MVA-spCTH522 or MVA-CTH522:B7 immunized mice.

C57BL/6J mice were primed i.p. with 10⁷ TCID50 of either MVA-WT, MVA-spCTH522 or MVA-CTH522:B7 on days 0 and boosted with a dose of 10⁸ TCID50 on day 28, as shown in figure 17. Spleens were harvested on day 56 and splenocytes were restimulated with the pool of overlapping peptides spanning the full spCTH522 sequence in the presence of Brefeldin A. OVA-specific (OVA₂₅₇₋₂₆₄) and MVA-specific (B8₂₀₋₂₇) peptides were used as negative and positive controls, respectively. Frequencies of cytokine-producing CD8⁺ T-cells were determined by flow cytometry.

Surprisingly, there was no activation of CD8⁺ T-cells when splenocytes from mice immunized with MVA-spCTH522 and MVA-CTH522:B7 were pulsed with the overlapping peptides of spCTH522 (Fig. 19). However, it is worth noting that the same splenocytes showed reactivity to B8-derived peptide, with approximately 12% and 18% of CD8⁺ T-cells producing IFN- γ in

MVA-spCTH522 and MVA-CTH522:B7 immunized mice, respectively. This suggests that the lack of response was not due to an immunization failure.

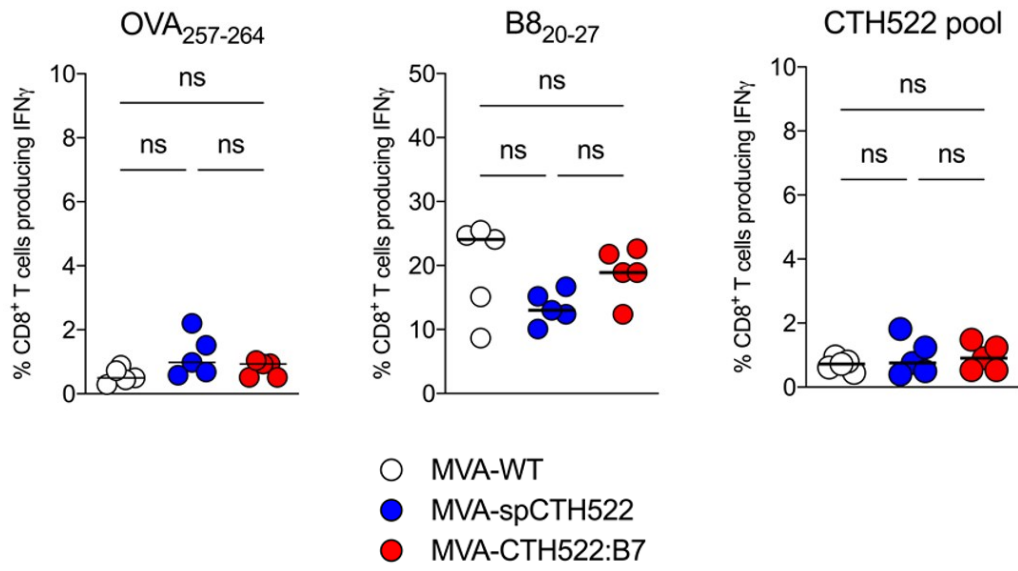


Figure 19. MVA-spCTH522 and MVA-CTH522:B7 failed to induce CTH522-specific CD8⁺ T-cell responses in mice.

C57BL/6J mice were primed i.p. with 10^7 TCID₅₀ of either MVA-WT, MVA-spCTH522 or MVA-CTH522:B7 (n=5 per group) on days 0 and boosted with a dose of 10^8 TCID₅₀ on day 28, as shown in figure 17. Spleens were harvested on day 56 and splenocytes were restimulated with a pool of overlapping peptides spanning the full spCTH522 sequence. OVA₂₅₇₋₂₆₄ and B8₂₀₋₂₇ peptides were used as negative and positive controls, respectively. Frequencies of IFN- γ -producing CD8⁺ T-cells were determined by flow cytometry. Each data point represents one mouse, and short horizontal lines geometrical mean of three independent experiments. Kruskal–Wallis test followed by Dunn’s multiple comparisons was used to compare groups (ns, non-significant).

Several are the studies that highlight the protective role of the CD4⁺ T-cell response in vaccine-induced immunity against *C. Trachomatis*. To evaluate the CD4⁺ T-cell response, the mice were immunized as mentioned above (5.3.1) with a priming (Day 0) and a subsequent booster (Day 28) dose of either MVA-WT, MVA-spCTH522, or MVA-CTH522:B7. On day 56, the mice were euthanized and their spleens were harvested to isolate single cells, as shown in figure 17. Splenocytes were then cultured with the pool of overlapping peptides covering the entire protein sequence of spCTH522 for 5-6 hours in the presence of Brefeldin A. The vaccinia virus-specific B5₄₆₋₆₀ peptide was used as a positive control, while OVA₃₂₃₋₃₃₉ peptide was used as a negative control. After incubation with the peptides, the splenocytes were washed and subjected to an ICS assay followed by flow cytometry analysis (Fig. 20).

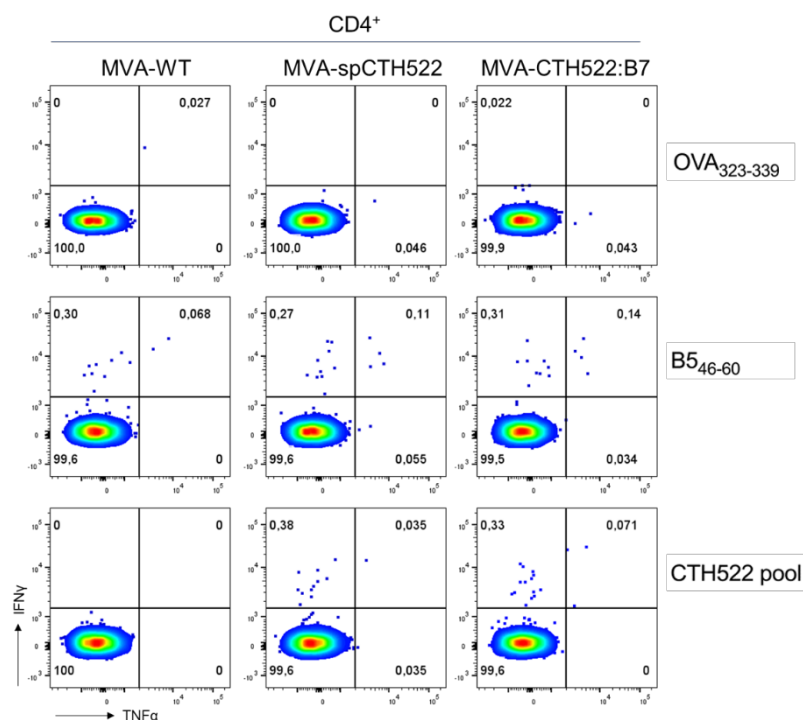


Figure 20. Representative flow cytometry plots showing IFN- γ and TNF- α -producing CD4⁺ T-cells from the spleen of MVA-WT, MVA-spCTH522 or MVA-CTH522:B7 immunized mice.

C57BL/6J mice were primed i.p. with 10^7 TCID50 of either MVA-WT, MVA-spCTH522 or MVA-CTH522:B7 on days 0 and boosted with a dose of 10^8 TCID50 on day 28, as shown in figure 17. Spleens were harvested on day 56 and splenocytes were restimulated with a pool of overlapping peptides spanning the full spCTH522 sequence in the presence of Golgi apparatus-transport-inhibitors (Brefeldin A). OVA-specific (OVA₃₂₃₋₃₃₉) and MVA-specific (B5₄₆₋₆₀) peptides were used as negative and positive controls, respectively. Frequencies of cytokine-producing CD4⁺ T-cells were determined by flow cytometry.

Both MVA-spCTH522 and MVA-CTH522:B7 induced comparable CD4⁺ T-cell responses against the B5 derived peptide and spCTH522 overlapping peptides, while MVA-WT showed CD4⁺ T-cell responses only against B5. Specifically, we observed approximately 0.2% of CTH522-specific CD4⁺ T-cells producing IFN- γ and less than 0.1% of CTH522-specific CD4⁺ T-cells producing TNF- α in both MVA-spCTH522 and MVA-CTH522:B7 immunized mice (Fig 21).

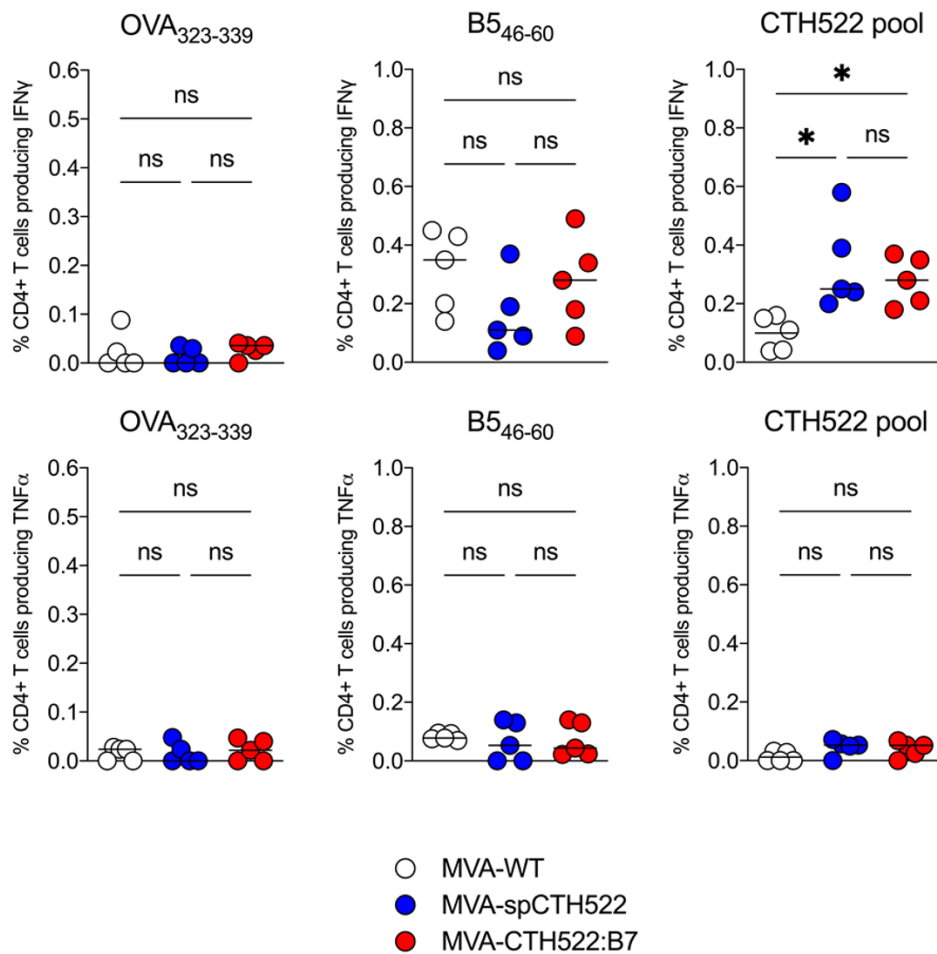


Figure 21. MVA-spCTH522 and MVA-CTH522:B7 induced CTH522-specific CD4⁺ T-cell responses in C57BL/6J mice.

C57BL/6J mice were primed i.p. with 10^7 TCID₅₀ of either MVA-WT, MVA-spCTH522 or MVA-CTH522:B7 (n=5 per group) on days 0 and boosted with a dose of 10^8 TCID₅₀ on day 28, as shown in figure 17. Spleens were harvested on day 56 and splenocytes were restimulated with a pool of overlapping peptides spanning the full spCTH522 sequence. OVA₃₂₃₋₃₃₉ and B5₄₆₋₆₀ peptides were used as negative and positive controls, respectively. Frequencies of IFN- γ and TNF- α -producing CD4⁺ T-cells were determined by flow cytometry. Each data point represents one mouse, and short horizontal lines geometrical mean of three independent experiments. Kruskal–Wallis test followed by Dunn’s multiple comparisons was used to compare groups (ns, non-significant, * p < 0.05).

5.3.1. MVA-CTH522:B7 but not MVA-spCTH522 induces antibody responses in C57BL/6J mice

The following results were obtained by Ms. Esma Özün during her four-month research stay at the laboratory of Prof. Dr. med. Ingo Drexler as part of her bachelor thesis. During her time in the laboratory, Esma was assigned a part of this project to be carried out under my direct supervision. Her specific focus was the analysis of the humoral immune response induced by

the vaccine candidates discussed in this thesis. The experiments were carried out collaboratively, with close supervision at each step. The results presented here are also detailed in Esma's bachelor thesis and have been included in the publication mentioned at the beginning of this thesis.

To evaluate the humoral immune response induced by MVA-spCTH522 and MVA-CTH522:B7 vaccine candidates, we measured the levels of CTH522-specific antibodies in C57BL/6J mice. These mice were immunized with MVA-WT, MVA-spCTH522, or MVA-CTH522:B7, followed by a booster dose 28 days later. Blood and vaginal wash samples were collected four weeks after boosting to assess antibody responses. The results showed that mice immunized with MVA-CTH522:B7 developed detectable humoral responses specific to CTH522. Specifically, we observed an OD405 of approximately 3.8 in serum samples diluted 1:50 from mice immunized with MVA-CTH522:B7. In addition, there was a clear correlation between increasing dilution factors and a corresponding decrease in OD405 values. However, no such response was observed in mice vaccinated with MVA-spCTH522. Importantly, the control group immunized with MVA-WT also failed to develop a CTH522-specific antibody response, as we observed an OD405 of approximately 0.3 in serum samples diluted 1:50 from mice immunized with MVA-WT, confirming the specificity of the ELISA assay and the absence of cross-reactivity between the antibody response to the MVA vector and the CTH522 antigen (Fig. 22A). Interestingly, all vaccinated groups, including those receiving MVA-WT, MVA-spCTH522 and MVA-CTH522:B7, generated an antibody response against antigens present in the MVA backbone (Fig. 22B). This observation rules out the possibility that the lack of CTH522-specific antibodies in mice vaccinated with MVA-spCTH522 was due to a failure in the immunization process itself.

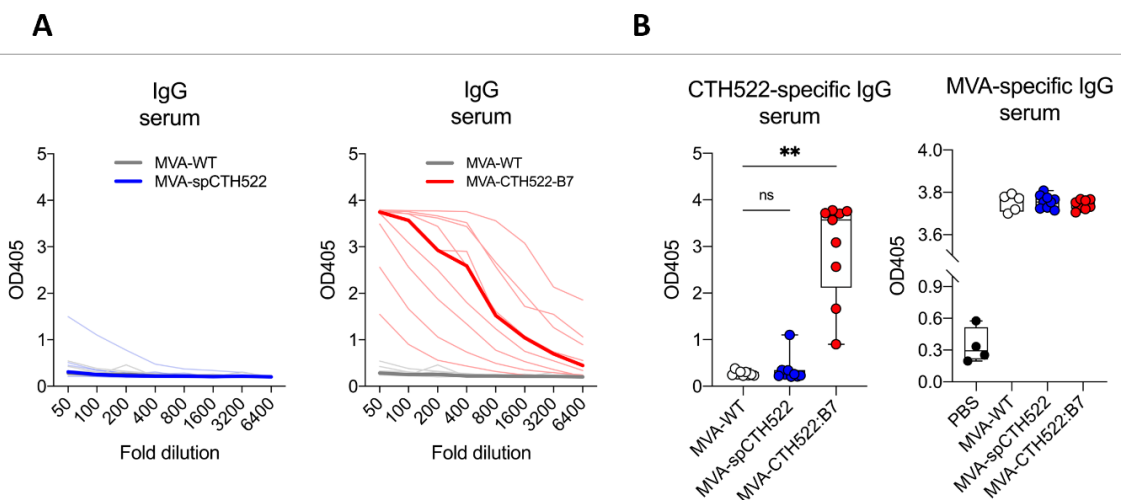


Figure 22. MVA-CTH522:B7, but not MVA-spCTH522, induced CTH522-specific antibody responses in C57BL/6J mice.

C57BL/6J mice (n=9 per group) were primed i.p. with 10^7 TCID₅₀ of either MVA-WT, MVA-spCTH522 or MVA-CTH522:B7 on days 0 and boosted with a dose of 10^8 TCID₅₀ on day 28, as shown in figure 17. PBS-injected mice were used as naive, unimmunized controls (n=3). Blood samples were taken on day 56 and serum was obtained by centrifugation of coagulated blood. (A) Serum samples were serially diluted and added to CTH522-coated plates. Antigen-specific total IgG levels were determined by enzyme-linked immunosorbent assay (ELISA). Thin lines represent data from individual mice, while thick lines represent the geometric mean optical density (OD) values for each dilution step. (B) Individual OD 405 values for IgG were analyzed at a serum dilution of 1:100 for CTH522-specific antibodies (left) and at a dilution of 1:500 for MVA-specific antibodies (right). Antibodies specific for MVA were evaluated by performing an ELISA using a plate coated with MVA virions (10^5 particles per well). Statistical comparisons of CTH522-specific antibody levels between groups of four independent experiments were performed using the Kruskal-Wallis test followed by Dunn's multiple comparisons (** $p < 0.005$; ns, not significant).

A more detailed analysis of the CTH522-specific antibody response in mice immunized with MVA-CTH522:B7 revealed a diverse profile of IgG subclasses. In particular, IgG2b and IgG2c were significantly elevated compared to IgG1 and IgG3, suggesting that the immunization primarily induced a Th1-polarised humoral immune response (Fig. 23A, B). In contrast, no CTH522-specific IgA antibodies were detected in the serum of immunized mice, indicating that the vaccine candidate did not induce detectable mucosal antibodies in the systemic circulation (Fig. 23C). To further evaluate the mucosal antibody response, the presence of antibodies in the genital tract was assessed by measurements in vaginal washings. However, neither IgG nor IgA antibodies specific to CTH522 were detected in these samples. This finding highlights a limited mucosal antibody response despite the systemic humoral response observed in serum after systemic MVA immunization.

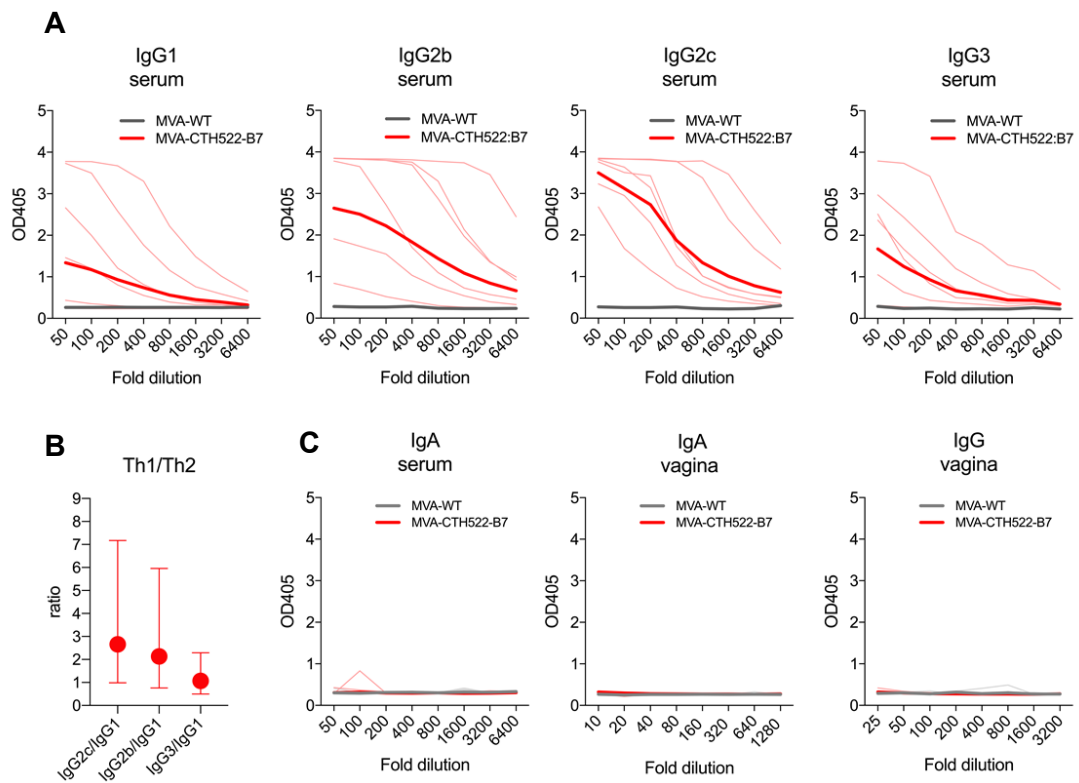


Figure 23. MVA-CTH522:B7 induced several IgG subtypes composing the CTH522-specific antibody response in C57BL/6J mice.

C57BL/6J mice (n=9 per group) were primed i.p. with 10^7 TCID₅₀ of either MVA-WT or MVA-CTH522:B7 on days 0 and boosted with a dose of 10^8 TCID₅₀ on day 28, as shown in figure 17. Blood samples and vaginal washes were taken on day 56. Serum was obtained by centrifugation of coagulated blood. (A) Serum levels of CTH522-specific IgG subtypes (IgG1, IgG2b, IgG2c and IgG3) were analyzed by ELISA in mice immunized with either MVA-CTH522:B7 or MVA-WT. Serum samples were serially diluted and added to CTH522 protein-coated plates. Thin lines represent data from individual mice of four independent experiments, while thick lines represent the geometric mean of OD405 values across serial dilution steps. (B) The ratio of OD405 values at a serum dilution of 1:100 was calculated for IgG2b, IgG2c and IgG3 relative to IgG1. The results are presented as geometric means with geometric standard deviations. (C) CTH522-specific IgG and IgA antibody levels were determined by ELISA in both serum and vaginal wash samples from mice immunized with MVA-CTH522:B7 or MVA-WT. Serum samples and vaginal washes were serially diluted and added to CTH522 protein-coated plates.

5.4. Ex-vivo analysis of CTH522-specific immune responses in HLA-A2.DR1 mice

5.4.1. Single dose of MVA-spCTH522 and MVA-CTH522:B7 induces T-cell responses in HLA-A2.DR1 mice

Since our goal was to develop a human vaccine with a specific focus on the T-cell response, we chose to use a transgenic mouse model, the HLA-A2.DR1 mice, to study vaccine-induced T-cell responses in an HLA-restricted manner. These mice lack endogenous major histocompatibility complexes (MHC) I and II and are transgenic for HLA-A*02:01/Db and HLA-DR1, which serve as the sole sources of MHC-I and MHC-II, respectively. To investigate the T-cell specific immune response elicited by MVA-spCTH522 and MVA-CTH522:B7, the activation of spleen-derived T-cells from immunized HLA-A2.DR1 mice was analyzed. HLA-A2.DR1 mice received a single immunization dose with 10^7 TCID₅₀ of either MVA-WT, MVA-spCTH522, or MVA-CTH522:B7. On day 7, the mice were euthanized and their spleens were harvested to isolate single cells (Fig. 24).



Figure 24. Schematic representation of the immunization scheme.

HLA-A2.DR1 mice were immunized intraperitoneally with MVA-WT, MVA-spCTH522 or MVA-CTH522:B7 on days 0. Spleens were collected on day 7.

Splenocytes were incubated with the pool of CTH522 overlapping peptides for 5-6 hours in the presence of Brefeldin A. The MVA-specific A10₂₀₋₂₇ peptide was used as a CD4⁺ T cell peptide positive control, while Influenza-specific peptide (M1₂₅₇₋₂₆₄) peptide was used as a CD4⁺ T cell peptide negative control (Supplementary figure 4). After incubation with the peptides, the splenocytes were washed and subjected to ICS assay followed by flow cytometry analysis. CD4⁺ T-cells from mice immunized with MVA-WT showed no reactivity to the CTH522 pool of overlapping peptides (Fig. 25). This suggests that there is no cross-reactivity of the HLA-DR1 restricted CD4⁺ T-cell response between the recombinant antigens and the MVA backbone. On the other hand, immunization with MVA-spCTH522 and MVA-CTH522:B7 resulted in a Th1-directed CD4⁺ T-cell response. Indeed, approximately 0,15-

0,20 % of CD4⁺ T-cells specific to the CTH522 overlapping peptide pool produced IFN- γ in MVA-spCTH522 and MVA-CTH522:B7 immunized mice. However, only about 0,10 % of CD4⁺ T-cells produced TNF- α in both MVA-spCTH522 and MVA-CTH522:B7 immunized mice (Fig. 25).

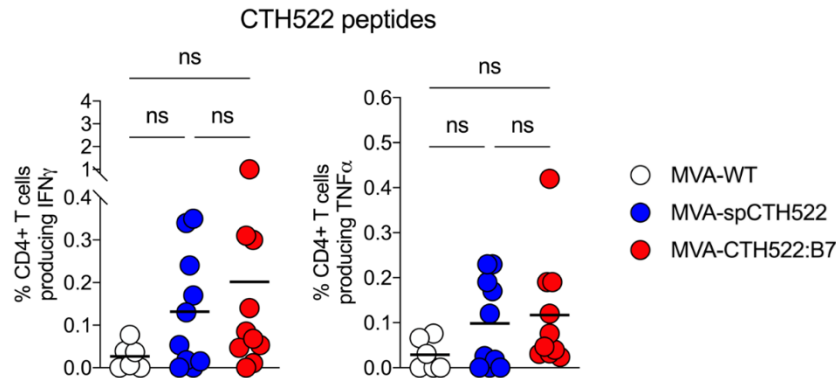


Figure 25. MVA-spCTH522 and MVA-CTH522:B7 failed to stably induce CTH522-specific CD4⁺ T-cell responses in HLA-A2.DR1 mice.

HLA-A2.DR1 mice were immunized i.p. with 10^7 TCID₅₀ of either MVA-WT (n = 6), MVA-spCTH522 (n = 10), or MVA-CTH522:B7 (n = 11) on day 0. Spleens were harvested on day 7 and splenocytes were restimulated with a pool of overlapping peptides spanning the full spCTH522 sequence to determine CD4⁺ T-cell responses. Total percentage of CTH522-specific CD4⁺ T cells producing IFN- γ or TNF- α . Each data point represents one mouse, and short horizontal lines geometrical mean. Kruskal–Wallis test followed by Dunn’s multiple comparisons was used to compare groups of four independent experiments (ns, non-significant).

To investigate and characterize the CD8⁺ T-cell responses in immunized HLA-A2.DR1 mice, the overlapping peptides covering the full sequence of spCTH522 were divided into several groups to identify specific HLA-A*02:01 restricted epitopes. Specifically, HLA-A2.DR1 mice were immunized as mentioned above (Fig. 17) with a priming (Day 0) and booster (Day 28) dose of either MVA-WT or MVA-spCTH522, since the CTH522:B7 antigen contains the same MOMP sequences from serovars D, E, F, and G as the spCTH522 antigen. In addition, the different pools help to assess the presence of a CD8⁺ T cell epitope potentially present in the sequence of MOMP^D (aa 1-55), which is not included in the CTH522:B7 antigen. On day 56, the mice were euthanized and their spleens were harvested to isolate single cells. Splenocytes were then cultured with fourteen pools of ten overlapping peptides each for 5-6 hours in the presence of Brefeldin A. The MVA-specific B8₂₀₋₂₇ peptide was used as a CD8⁺ T cell peptide positive control, while Influenza-specific peptide M1₅₇₋₆₆ peptide was used as a CD8⁺ T cell peptide negative control (Supplementary fig. 4). CD8⁺ T-cells from mice immunized with MVA-WT showed no reactivity to any of the peptide pools. This suggests that there is no cross-reactivity of the HLA-A*02:01 restricted CD8⁺ T-cell response between

the recombinant antigens and the MVA backbone. On the other hand, immunization with MVA-spCTH522 resulted in CD8⁺ T-cell response when splenocytes were pulsed with pools 1, 4, 7, 8, 9, 10 and 11 (Fig. 26).

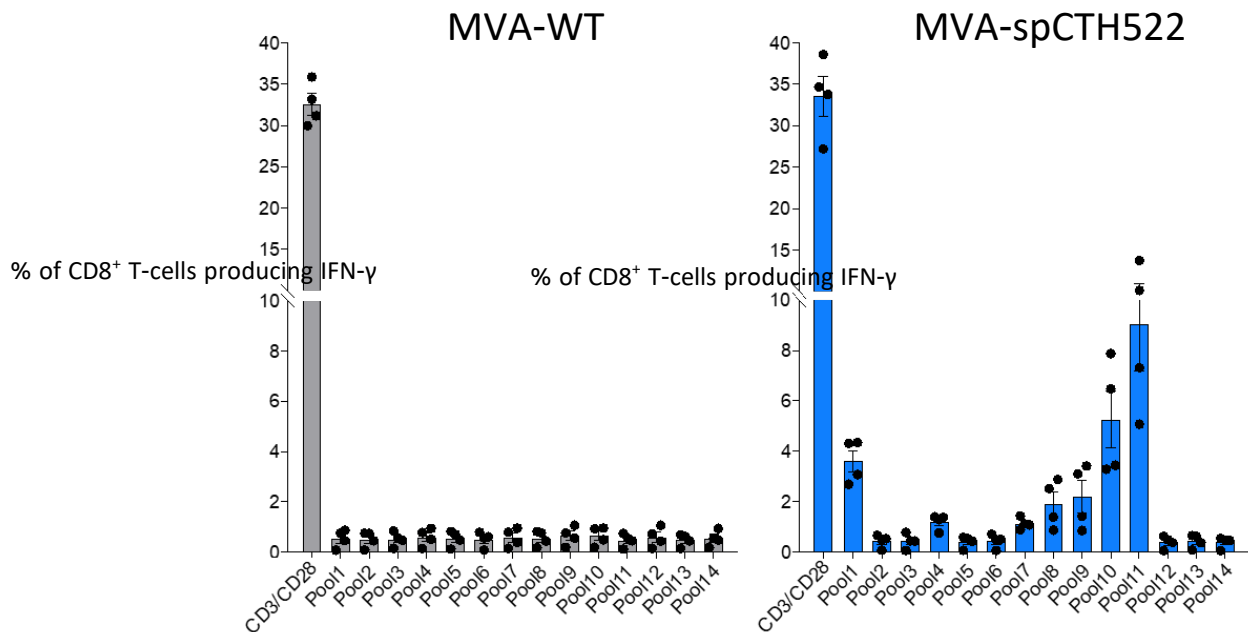


Figure 26. MVA-spCTH522 induced CTH522-specific CD8⁺ T-cell responses in HLA-A2.DR1 mice.

HLA-A2.DR1 mice (n=4 per group) were immunized i.p. with 10⁷ TCID₅₀ of either MVA-WT or MVA-spCTH522 on days 0 and boosted with a dose of 10⁸ TCID₅₀ on day 28. Spleens were harvested on day 56 and splenocytes were restimulated with fourteen pools of overlapping peptides spanning the full spCTH522 sequence. IFN-γ -producing CD8⁺ T-cells were measured by flow cytometry and frequencies were calculated using FlowJo software. Data are represented as bars and SEM of two independent experiments, and each data point represents one mouse.

To identify the CD8⁺ restricted epitopes within the spCTH522 protein sequence, the peptide pools shown in figure 26 that elicited CD8⁺ T cell responses were selected for further analysis. Specifically, individual peptides from pools 1, 4, 7, 8, 9, 10, and 11 were used to stimulate splenocytes from HLA-A2.DR1 mice, which had been primed and boosted with MVA-spCTH522 as in Fig. 17. Splenocytes were pulsed with the single peptides for 5-6 hours in the presence of Brefeldin A. After incubation with the peptides, the splenocytes were washed and subjected to ICS assay followed by flow cytometry analysis. Among all the peptides screened, only eight peptides were able to reactivate CTH522-specific CD8⁺ T-cells. These correspond to Peptide 51, Peptide 52, Peptide 72, Peptide 89, Peptide 123, Peptide 124, Peptide 142 and Peptide 146 (Fig 27).

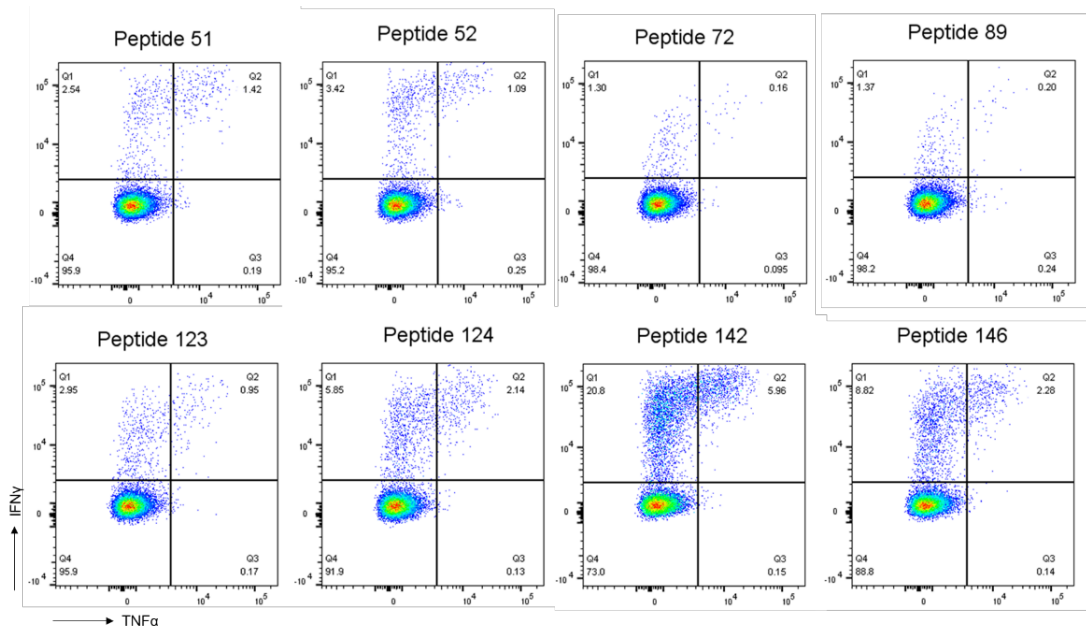


Figure 27. Representative flow cytometry plots of epitope-specific CD8⁺ T-cells producing IFN- γ and TNF- α from the spleen of MVA-spCTH522 immunized HLA-A2.DR1 mice.

HLA-A2.DR1 mice were immunized i.p. with 10^7 TCID₅₀ of MVA-spCTH522 and boosted with a dose of 10^8 TCID₅₀ on day 28. Spleens were harvested on day 56 and splenocytes were restimulated with single overlapping peptides from the positive-tested pools (Fig. 26) in the presence of Brefeldin A. Cytokines-producing CD8⁺ T-cells were measured by flow cytometry and frequencies were calculated using FlowJo software.

The sequences of these peptides were subsequently analyzed and aligned to pinpoint common shared sequences, which might be core epitope sequences. We identified two common core epitopes within the peptide pools tested. In overlapping peptides 72, 89, 123 and 124 we found the 9-mer NMFTPYIGV, which corresponds to MOMP₂₈₂₋₂₉₀. This epitope was previously described as a dominant CD8⁺ T-cell-specific epitope in PBMCs of a cohort of *C. trachomatis* positive patients¹⁹⁷. In addition, we identified a second common core epitope in peptides 51 and 52, the 10-mer ALWECGCATL which corresponds to MOMP₂₀₀₋₂₀₉ (Table 9).

Peptide 72	YRL <u>NMFTPYIGV</u> KWS
Peptide 89	QLN <u>NMFTPYIGV</u> KWS
Peptide 123	LQLN <u>NMFTPYIGV</u> KW
Peptide 124	<u>NMFTPYIGV</u> KWSRAS
Peptide 51	GARA <u>ALWECGCATL</u> G
Peptide 52	<u>ALWECGCATL</u> GASFQ

Table 9. Sequences of peptides containing CD8⁺ T-cell epitopes recognized by CTL in the spleens of MVA-spCTH522 immunized HLA-A2.DR1 mice.

To confirm that these two sequences are the core epitopes within the peptides that induced CD8⁺ T-cell responses, HLA-A2.DR1 mice were immunized with a single immunization dose of either MVA-WT, MVA-spCTH522, or MVA-CTH522:B7. On day 7, the mice were euthanized and their spleens were harvested to isolate single cells (Fig. 24) Splenocytes were pulsed with MOMP₂₈₂₋₂₉₀ and MOMP₂₀₀₋₂₀₉ peptides for 5-6 hours in the presence of Brefeldin A. After incubation with the peptides, the splenocytes were washed and subjected to ICS assay followed by flow cytometry analysis. Both peptides were able to recall CD8⁺ T-cell responses, with approximately 15% of CD8⁺ T-cells specific to MOMP₂₈₂₋₂₉₀ producing IFN- γ in MVA-spCTH522 and approximately 5% in MVA-CTH522:B7 immunized mice. In both MVA-spCTH522 and MVA-CTH522:B7 immunized mice, less than 2% of CD8⁺ T-cells specific to MOMP₂₈₂₋₂₉₀ produced TNF- α . On the other hand, about 4% and 3% of CD8⁺ T-cells specific to MOMP₂₀₀₋₂₀₉ peptide produced IFN- γ in MVA-spCTH522 and MVA-CTH522:B7 immunized mice, respectively, while less than 1% of CD8⁺ T-cells specific to MOMP₂₀₀₋₂₀₉ peptide produced TNF- α in both MVA-spCTH522 and MVA-CTH522:B7 immunized mice (Fig. 28). This suggest an immunodominance of the MOMP₂₈₂₋₂₉₀ epitope and an immuno-subdominance of the MOMP₂₀₀₋₂₀₉ epitope.

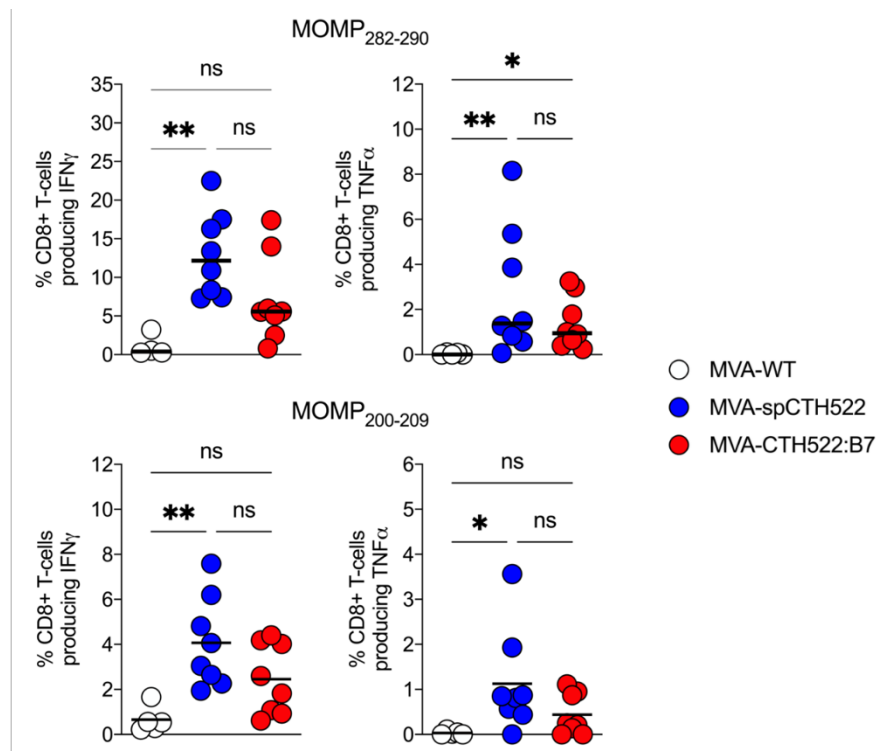


Figure 28. MVA-spCTH522 and MVA-CTH522:B7 induced epitope-specific CD8⁺ T-cell responses in HLA-A2.DR1 mice.

HLA-A2.DR1 mice were immunized i.p. with 10^7 TCID₅₀ of either MVA-WT (n = 6), MVA-spCTH522 (n = 10), or MVA-CTH522:B7 (n = 11) on day 0. Spleens were harvested on day 7 and splenocytes were restimulated with MOMP₂₈₂₋₂₉₀ or MOMP₂₀₀₋₂₀₉ peptides to determine CD8⁺ T-cell responses by ICS followed by FACS analysis.

Total percentage of MOMP₂₈₂₋₂₉₀- (upper graphs) and MOMP₂₀₀₋₂₀₉- (lower graphs) specific CD8⁺ T-cells producing IFN- γ or TNF- α . Each data point represents one mouse, and short horizontal lines geometrical mean of four independent experiments. Kruskal–Wallis test followed by Dunn’s multiple comparisons was used to compare groups (ns, non-significant, * $p < 0.05$, ** $p < 0.005$).

5.4.1. A booster dose of MVA-spCTH522 and MVA-CTH522:B7 increased T-cell responses in HLA-A2.DR1 mice

To evaluate whether a second dose of MVA-spCTH522 and MVA-CTH522:B7 would increase the CD4⁺ T-cell response, HLA-A2.DR1 mice were immunized with a prime (Day 0) and boost (Day 28) dose of either MVA-WT, MVA-spCTH522, or MVA-CTH522:B7. On day 56, the mice were euthanized and their spleens were harvested to isolate single cells (Fig. 17). Splenocytes were then cultured with the pool of overlapping peptides covering the entire protein sequence of spCTH522 for 5-6 hours in the presence of Brefeldin A. The MVA-specific A10₂₀₋₂₇ peptide was used as a CD4⁺ T-cell peptide positive control, while Influenza-specific peptide (M1₂₅₇₋₂₆₄) peptide was used as a CD4⁺ T-cell peptide negative control (Supplementary fig. 4). After incubation with the peptides, the splenocytes were washed and subjected to ICS assay followed by flow cytometry analysis (Fig. 29)

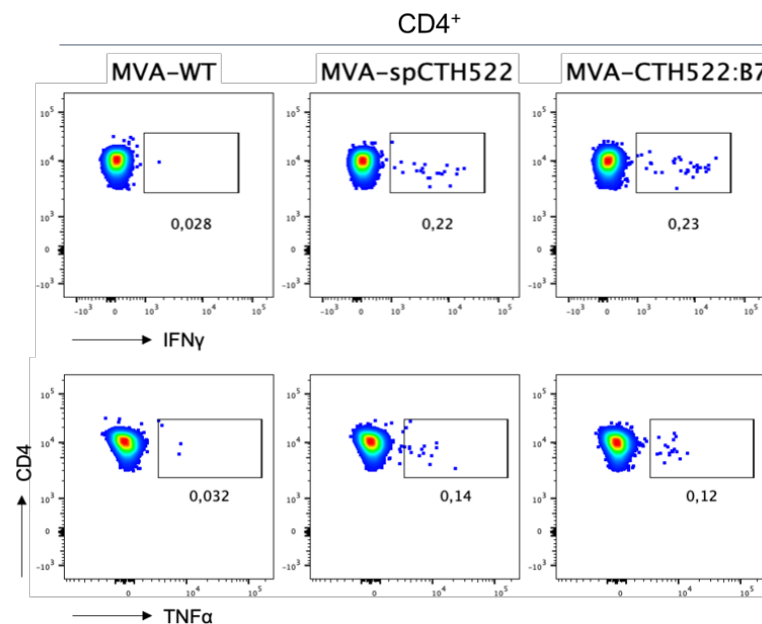


Figure 29. Representative flow cytometry plots showing IFN- γ and TNF- α -producing CD4⁺ T-cells from the spleen of MVA-WT, MVA-spCTH522 or MVA-CTH522:B7 immunized HLA-A2.DR1 mice.

HLA-A2.DR1 mice were immunized i.p. with 10^7 TCID₅₀ of either MVA-WT, MVA-spCTH522 or MVA-CTH522:B7 on days 0 and boosted with a dose of 10^8 TCID₅₀ on day 28. Spleens were harvested on day 56 and splenocytes were restimulated with a pool of overlapping peptides spanning the full spCTH522 sequence in the

presence of Brefeldin A. Cytokines-producing CD4⁺ T-cells were measured by flow cytometry and frequencies were calculated using FlowJo software.

The booster of both MVA-spCTH522 and MVA-CTH522:B7 immunized mice induced comparable CD4⁺ T-cell responses against spCTH522 overlapping peptides, while MVA-WT showed no spCTH522-specific CD4⁺ T-cell responses. Specifically, approximately 0.25% of spCTH522-specific CD4⁺ T-cells producing IFN- γ and less than 0.2% of spCTH522-specific CD4⁺ T-cells producing TNF- α were observed in both MVA-spCTH522 and MVA-CTH522:B7 immunized mice (Fig. 28).

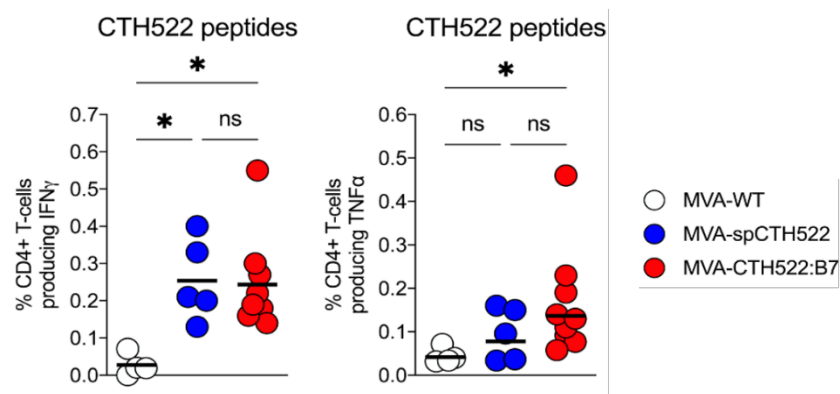


Figure 30. A booster dose of MVA-spCTH522 and MVA-CTH522:B7 induced reliable CTH522-specific CD4⁺ T-cell responses in HLA-A2.DR1 mice.

HLA-A2.DR1 mice were immunized i.p. with 10⁷ TCID50 of either MVA-WT (n = 4), MVA-spCTH522 (n = 5) or MVA-CTH522:B7 (n = 8) on days 0 and boosted with a dose of 10⁸ TCID50 on day 28. Splens were harvested on day 56 and splenocytes were restimulated with a pool of overlapping peptides spanning the full spCTH522 sequence. Activation of CD4⁺ T-cells was measured by ICS assay followed by flow cytometry analysis. Overall percentage of CTH522-specific CD4⁺ T-cells producing IFN- γ or TNF- α after stimulation with the peptide pool. Each data point represents one mouse, and short horizontal lines geometrical mean of four independent experiments. For statistical analysis, Kruskal–Wallis test followed by Dunn’s multiple comparisons was used to compare groups (ns, non-significant, * p < 0.05).

The same prime/boost approach was used to assess whether the booster dose would enhance the CD8⁺ T-cell response. As for the evaluation of the CD4⁺ T-cell response, HLA-A2.DR1 mice were immunized with a prime (day 0) and boost (day 28) dose of either MVA-WT, MVA-spCTH522 or MVA-CTH522:B7. On day 56, the mice were euthanized and their spleens were harvested to isolate single cells. Splenocytes were then were pulsed with MOMP₂₈₂₋₂₉₀ and MOMP₂₀₀₋₂₀₉ peptides for 5-6 hours in the presence of Brefeldin A. The MVA-specific B8₂₀₋₂₇ peptide was used as a CD8⁺ T-cell peptide positive control, while Influenza-specific peptide M1₅₇₋₆₆ peptide was used as a CD8⁺ T-cell peptide negative control

(Supplementary fig. 4). After incubation with the peptides, the splenocytes were washed and subjected to ICS assay followed by flow cytometry analysis (Fig. 31).

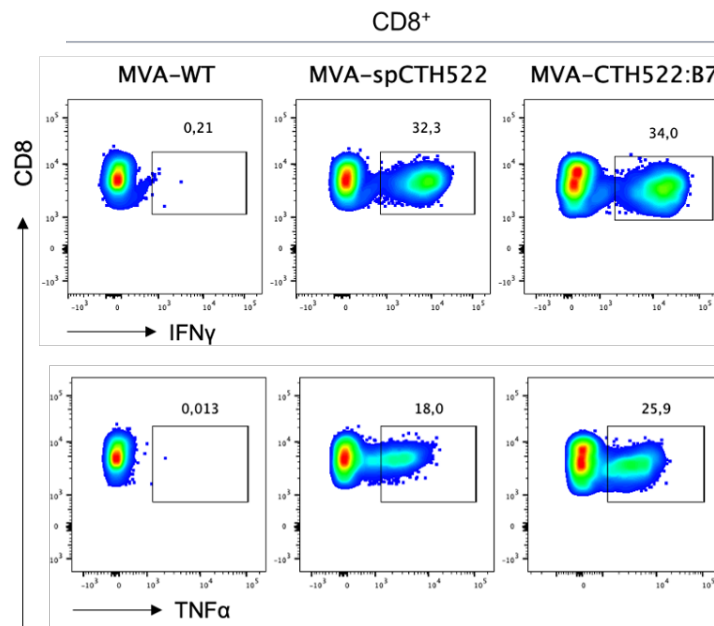


Figure 31. Representative flow cytometry plots showing IFN- γ and TNF- α -producing CD8⁺ T-cells from the spleen of MVA-WT, MVA-spCTH522 or MVA-CTH522:B7 immunized HLA-A2.DR1 mice.

HLA-A2.DR1 mice were immunized i.p. with 10⁷ TCID50 of either MVA-WT, MVA-spCTH522 or MVA-CTH522:B7 on days 0 and boosted with a dose of 10⁸ TCID50 on day 28. Spleens were harvested on day 56 and splenocytes were restimulated with MOMP₂₈₂₋₂₉₀ peptide in the presence of Golgi apparatus-transport-inhibitors (Brefeldin A). Frequencies of cytokine-producing CD8⁺ T-cells were determined by flow cytometry.

The booster dose in both MVA-spCTH522 and MVA-CTH522:B7 immunized mice induced comparable CD8⁺ T-cell responses against both MOMP₂₈₂₋₂₉₀ and MOMP₂₀₀₋₂₀₉ peptides, while MVA-WT showed no CTH522-specific CD8⁺ T-cell responses. Specifically, in both MVA-spCTH522 and MVA-CTH522:B7 immunized mice, we observed approximately 20% of MOMP₂₈₂₋₂₉₀ -specific CD8⁺ T-cells producing cytokines and approximately 2,5% of MOMP₂₀₀₋₂₀₉-specific CD8⁺ T-cells producing cytokines (Fig 32).

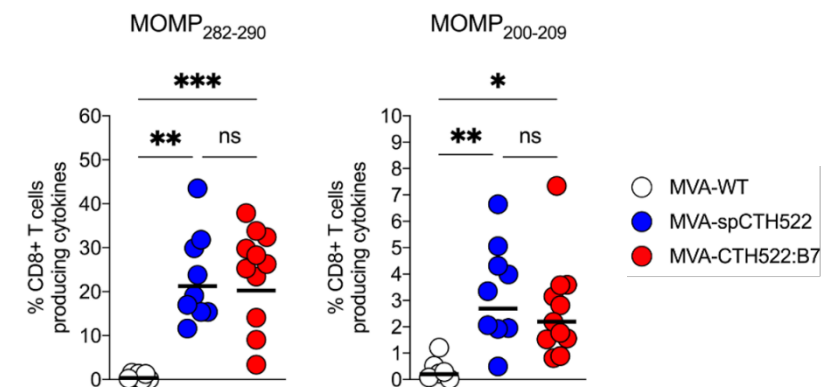


Figure 32. A booster dose of MVA-spCTH522 and MVA-CTH522:B7 only increased MOMP₂₈₂₋₂₉₀ epitope-specific CD8⁺ T-cell responses in HLA-A2.DR1 mice.

HLA-A2.DR1 mice were immunized i.p. with 10^7 TCID₅₀ of either MVA-WT (n = 5), MVA-spCTH522 (n = 9) or MVA-CTH522:B7 (n = 11) on days 0 and boosted with a dose of 10^8 TCID₅₀ on day 28. Splens were harvested on day 56 and splenocytes were restimulated MOMP₂₈₂₋₂₉₀ or MOMP₂₀₀₋₂₀₉ peptides to determine CD8⁺ T-cell responses by ICS followed by flow cytometry analysis. Overall percentage of MOMP₂₈₂₋₂₉₀- or MOMP₂₀₀₋₂₀₉-specific CD8⁺ T-cells producing IFN- γ and TNF- α , here referred as cytokines (calculated by summing the percentages of CD8⁺ T cells positive for IFN γ only, TNF α only, and double positive for both IFN γ and TNF α). These populations were determined by using Boolean combination of gates, as shown in supplementary fig. 4) after stimulation with the peptides. Each data point represents one mouse, and short horizontal lines geometrical mean of four independent experiments. Kruskal–Wallis test followed by Dunn’s multiple comparisons was used to compare groups (ns, non-significant, * p < 0.05, ** p < 0.005, *** p < 0.0005).

To evaluate whether the booster dose significantly increased both CD8⁺ and CD4⁺ T-cells compared to single vaccination regimen, the magnitudes of MOMP₂₈₂₋₂₉₀- and MOMP₂₀₀₋₂₀₉-specific CD8⁺ T-cells and CTH522-specific CD4⁺ T-cells were compared between the single-dose and two-dose vaccination regimens. These comparisons were analyzed using an unpaired *t*-test with Welch's correction. Notably, a significant increase in the magnitude of MOMP₂₈₂₋₂₉₀-specific CD8⁺ T-cells was observed 28 days after the booster dose compared to 7 days after the single dose vaccination. However, there was no statistical difference in the level of MOMP₂₀₀₋₂₀₉-specific CD8⁺ T-cells between the two regimens. Interestingly, while there was a trend toward an increase in the magnitude of CTH522-specific CD4⁺ T-cells following the booster dose, this difference was not statistically significant compared to the single-dose regimen (Fig 33).

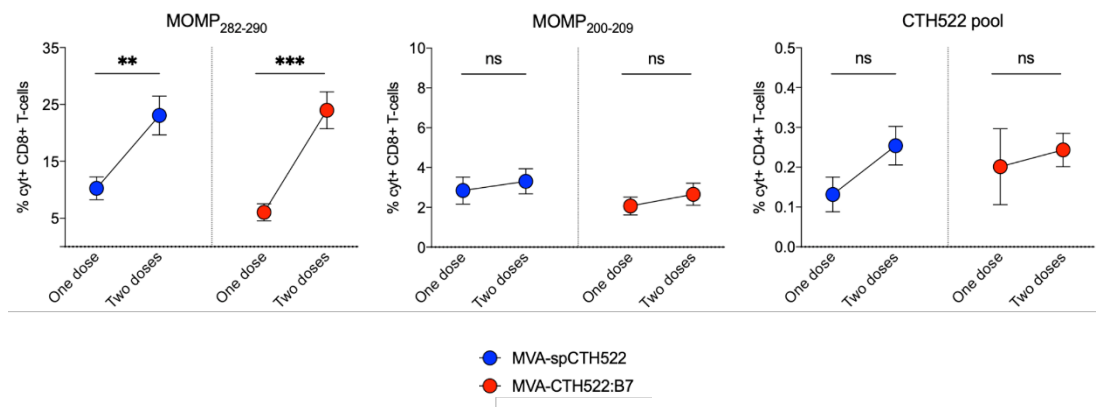


Figure 33. A booster dose of MVA-spCTH522 and MVA-CTH522:B7 increased MOMP₂₈₂₋₂₉₀-specific CD8⁺ T-cell responses in HLA-A2.DR1 mice.

Comparison of antigen-specific CD8⁺ and CD4⁺ T-cells at 7 days after prime (see Figure 28 and Figure 25) or 28 days after boost (see Figure 32 and Figure 30) with MVA-spCTH522 or MVA-CTH522:B7. Statistical analysis was performed using unpaired *t* test with Welch’s correction (ns, non-significant, ** p < 0.005, *** p < 0.0005).

To further evaluate the quality of the CD8⁺ T-cell response elicited by MVA-spCTH522 and MVA-CTH522:B7, phenotypic characterization was performed to assess the multifunctionality of the CD8⁺ T-cells. For this purpose, splenocytes from mice immunized with either MVA-spCTH522 or MVA-CTH522:B7 in the prime/boost regimen were incubated with MOMP₂₈₂₋₂₉₀ and MOMP₂₀₀₋₂₀₉ peptides for 5-6 hours in the presence of Brefeldin A. After the incubation, splenocytes were washed, subjected to ICS assay and flow cytometry analysis. To characterize the multifunctional phenotype of the T-cells, a Boolean combination of gates was employed to determine the single and combined expression of cytokines (IFN- γ , TNF- α , IL-2) and degranulation marker (CD107) (Supplementary Fig. 3). In both MVA-spCTH522 and MVA-CTH522:B7 immunized mice, the majority of MOMP₂₈₂₋₂₉₀-specific CD8⁺ T-cells expressed a combination of two cytokines, with approximately 9% showing positivity for both IFN- γ and TNF- α , and approximately 1.5% showing positivity for both IFN- γ and CD107. The second most prevalent group of MOMP₂₈₂₋₂₉₀-specific CD8⁺ T-cells showed single cytokine expression, with ~2% expressing IFN- γ and ~1% expressing CD107. Lastly, a third functional group of CD8⁺ T-cells was observed, with around 10% co-expressing IFN- γ , TNF- α , and CD107, while approximately 0.5% co-expressed IFN- γ , TNF- α , and IL-2 (Fig. 34, left graph). A similar pattern of multifunctional phenotype was observed for MOMP₂₀₀₋₂₀₉-specific CD8⁺ T-cells, with around 1% expressing both IFN- γ and TNF- α , approximately 0.4% expressing IFN- γ and CD107, about 0.7% expressing IFN- γ alone, roughly 0.6% expressing CD107 alone, and around 0.4% expressing IFN- γ , TNF- α , and CD107 (Fig. 34, right graph).

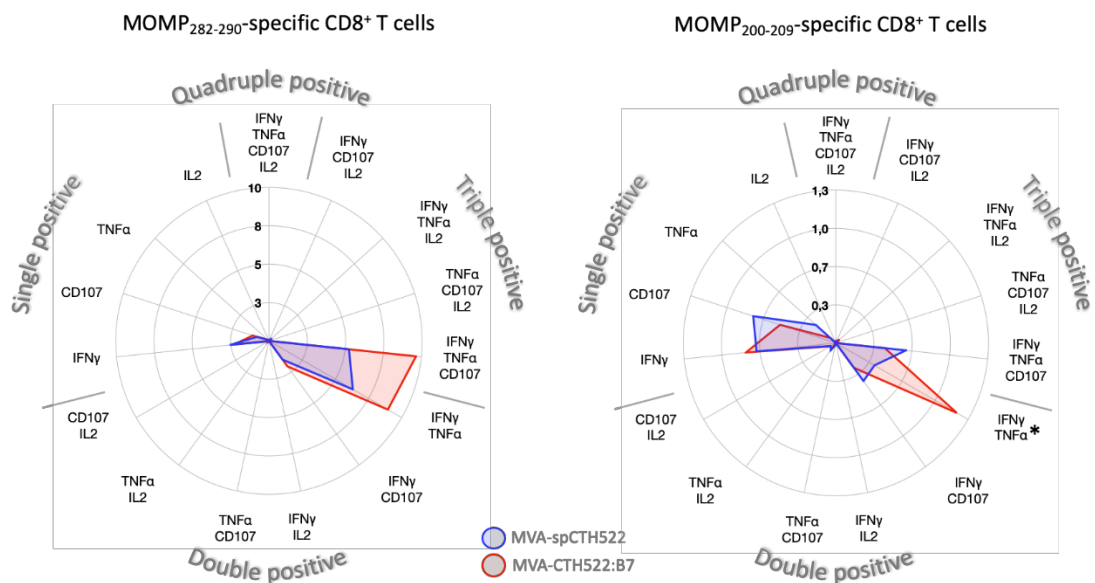


Figure 34. Multifunctional CD8⁺ T-cells induced by MVA-spCTH522 and MVA-CTH522:B7 in HLA-A2.DR1 mice.

HLA-A2.DR1 mice were immunized i.p. with 10^7 TCID₅₀ of either MVA-spCTH522 or MVA-CTH522:B7 (as shown in Fig. 17) on days 0 and boosted with a dose of 10^8 TCID₅₀ on day 28. Spleens were harvested on day 56 and splenocytes were restimulated MOMP₂₈₂₋₂₉₀ or MOMP₂₀₀₋₂₀₉ peptides to determine the polyfunctional profiles of epitope-specific CD8⁺ T-cells. Radar plots showing the geometric mean of the percentage of MOMP₂₈₂₋₂₉₀ (left) and MOMP₂₀₀₋₂₀₉ (right) specific CD8⁺ T-cells in mice immunized with either MVA-spCTH522 (blue) or MVA-CTH522:B7 (red). The axes represent all possible combinations of 3 cytokines (IFN γ , TNF α , IL-2) and 1 degranulation marker (CD107) tested, categorized into functional responses of single, double, triple and quadruple positive markers. The concentric scales indicate the percentage of CD8⁺ T cells expressing each combination of cytokines and degranulation marker. For statistical analysis, Mann–Whitney test was used for comparing the multifunctional CD8⁺ T-cell populations between MVA-spCTH522 and MVA-CTH522:B7 immunized mice in four independent experiments (* $p < 0.05$).

5.4.2. MVA-CTH522:B7 but not MVA-spCTH522 induce antibody responses in HLA-A2.DR1 mice

To assess the humoral immune response elicited by the vaccine candidates MVA-spCTH522 and MVA-CTH522:B7, we measured the levels of CTH522-specific antibodies in HLA-A2.DR1 mice. These mice were immunized with MVA-WT, MVA-spCTH522 or MVA-CTH522:B7 followed by a booster dose 28 days after immunization. Blood samples were collected four weeks after the booster to evaluate antibody responses. The results showed that mice immunized with MVA-CTH522:B7 developed detectable CTH522-specific IgG responses, with a mean of the OD₄₀₅ of approximately 1.3 observed in serum samples diluted 1:100. In contrast, no CTH522-specific antibody response was detected in mice vaccinated with MVA-spCTH522. This response was consistent with that observed in C57BL/6J mice. Similarly, the control group immunized with MVA-WT failed to produce CTH522-specific antibodies, as we observed a mean of the OD₄₀₅ of 0.3, confirming the specificity of the ELISA assay and the absence of cross-reactivity between the antibody response to the MVA vector and the CTH522 antigen in HLA-A2.DR1 mice. Importantly, all immunized groups, including those receiving MVA-WT, MVA-spCTH522, and MVA-CTH522:B7, generated antibodies against antigens present in the MVA backbone. This finding confirms the efficacy of MVA immunization and suggests that the absence of CTH522-specific antibodies in MVA-spCTH522-vaccinated mice is not due to immunization failure (Fig. 35).

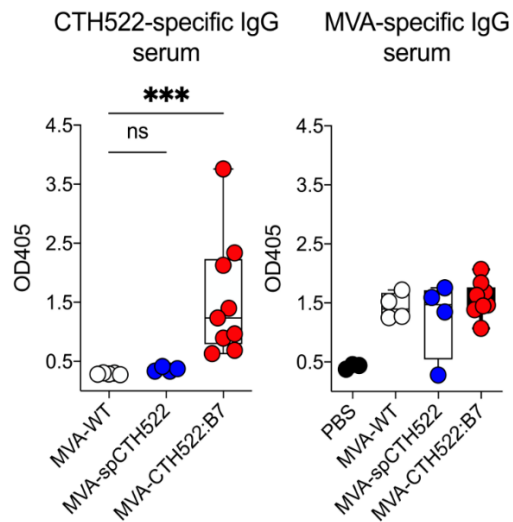


Figure 35. MVA-CTH522:B7, but not MVA-spCTH522, induced CTH522-specific antibody responses in HLA-A2.DR1 mice.

HLA-A2.DR1 mice were immunized i.p. with 10^7 TCID₅₀ of MVA-WT (n = 4), MVA-spCTH522 (n = 4) or MVA-CTH522:B7 (n = 9) on days 0 and boosted with a dose of 10^8 TCID₅₀ on day 28. PBS-injected mice were used as naïve, unimmunized controls (n = 3). Blood samples were taken on day 56 and serum was obtained by centrifugation of coagulated blood. Individual OD 405 values for IgG were analyzed at a serum dilution of 1:100 for CTH522-specific antibodies (left) and MVA-specific antibodies (right). For statistical analysis, Kruskal–Wallis test followed by Dunn’s multiple comparisons was used to compare CTH522-specific antibodies between groups of three independent experiments (ns, non-significant, *** p < 0.0005).

6. Discussion

C. trachomatis is the most common sexually transmitted bacterial pathogen worldwide. In 2020, an estimated 128.5 million new cases were reported worldwide, with a prevalence of approximately 4% in women and 2.5% in men aged 15-49 years¹⁹⁸. The bacterium targets epithelial cells in the urogenital, respiratory and gastrointestinal tracts, as well as the conjunctiva of the eye. In women, acute and recurrent infections can lead to serious long-term complications, including pelvic inflammatory disease, chronic abdominal pain, ectopic pregnancy and infertility. A significant proportion of infections, particularly among young sexually active individuals, remain asymptomatic, occurring in approximately 50% of men and 80% of women, contributing to its silent spread¹¹⁵. Despite public health initiatives focusing on diagnostic screening and antibiotic treatment, efforts to control both urogenital and ocular infections have been largely unsuccessful. These factors highlight the urgent need to understand the natural immune response to *C. trachomatis* and to prioritize the development of an effective vaccine¹⁸³.

In humans, cellular immunity plays a crucial role in recovery from *C. trachomatis* infection, with T-cellular Th1 responses and IFN- γ production being key factors associated with protection against reinfection¹⁹⁹. Humoral responses are also associated with a clinical correlate of protection²⁰⁰. However, other studies showed that cervical anti-chlamydia IgG and IgA are ineffective in preventing bacterial ascension, and elevated levels of anti-chlamydia IgG are associated with a higher risk of new infections²⁰¹. In addition, resistance to chlamydia infection and prevention of bacterial ascent to the upper genital tract have been associated with a higher median frequency (approximately +4.3%) of CD8⁺ T-cell responses in women with lower genital tract infections²⁰².

Mouse models have been instrumental in studying the immune response to chlamydia infection, particularly those using *C. muridarum*²⁰³. These studies show that CD4⁺ T-cells are essential for protective immunity, with Th1 response-associated cytokines, particularly IFN- γ , being crucial for defense against *C. trachomatis*¹³³. Conversely, the Th2 response-associated cytokine IL-10 is correlated with pathological reactions²⁰⁴. Antibodies, in addition to CD4⁺ T-cells, have been shown to provide protection against reinfection²⁰⁵. Following primary genital infection with *C. muridarum*, mice are resistant to rechallenge in the presence of CD4⁺ T-cells and/or antibodies²⁰⁶. Passive immunization with a neutralizing IgA monoclonal antibody has also been shown to protect mice from vaginal shedding and infertility following genital infection with *C. muridarum*²⁰⁷. The role of CD8⁺ T-cells in mice during chlamydial infection

remains controversial. Chlamydia infection in mice impairs the development of memory CD8⁺ T-cell responses, likely due to excessive production of pro-inflammatory cytokines and disruption of the PD-1/PD-L1 immunomodulatory pathway. PD-L1 expression increases in uterine epithelial cells and DCs within draining lymph nodes during both primary and secondary infections^{168,169}. This increased PD-L1 expression drives chlamydia-specific CD8⁺ T-cells towards a central memory phenotype, which primarily migrates through secondary lymphoid organs and lymphatic vessels, but lacks the capacity for effective homing to or for exerting effector functions in peripheral tissues. These findings suggest that local memory CD8⁺ T-cells may play a critical role in protection against chlamydia.

Further studies have suggested a potential role for CD8⁺ T-cells in genital tract tissue damage during chlamydia infection, as observed in the OT-I mouse model. In OT-I mice, the majority of CD8⁺ T-cell receptors are genetically engineered to recognize only the H-2Kb-restricted ovalbumin-derived peptide SIINFEKL, preventing recognition of chlamydial antigens and resulting in the absence of chlamydial-specific CD8⁺ T-cells²⁰⁸. Notably, OT-I mice did not develop hydrosalpinx following intravaginal chlamydial infection. Furthermore, adoptive transfer of spleen- or mesenteric lymph node-derived CD8⁺ T-cells from chlamydia-infected C57BL/6J mice to infected OT-I mice exacerbated tissue damage in the latter¹⁷¹. However, given the impaired protective function of CD8⁺ T-cells during chlamydial infection, this approach may underestimate their protective role against chlamydia. Interestingly, further studies have shown that bystander, non-protective CD8⁺ and CD4⁺ T-cells recruited to the site of infection via CXCR3 contribute significantly to chlamydial immunopathology²⁰⁹. Nevertheless, the absence of CXCR3 and CCR5 increases susceptibility to *C. trachomatis* infection. In knockout mice lacking these chemokine receptors, chlamydia-specific CD4⁺ T-cells failed to migrate and remain in genital tract tissues, resulting in reduced clearance of infection compared to wild-type mice¹⁷³.

Overall, the precise role of CD8⁺ T-cells in the immunopathology of *C. trachomatis* infection remains unclear. It is also uncertain whether a vaccine can successfully induce protective CD8⁺ T-cell responses against chlamydia. In the 1950s, both live and inactivated whole-organism chlamydial vaccines were tested in humans and non-human primates to prevent trachoma^{175–177,183}. While some vaccination protocols successfully induced protective immunity, the protection was typically short-lived, serovar or subgroup specific and lasted only two to three years. In addition, some vaccinated individuals experienced adverse effects, including hypersensitivity reactions or increased susceptibility to reinfection upon exposure to *C. trachomatis*²¹⁰. Increased susceptibility was demonstrated in mice when inactivated *C. trachomatis* was introduced directly into the uterus. This phenomenon was associated with the

induction of tolerogenic *C. trachomatis*-specific regulatory T-cells, driven by the ingestion of dead bacteria by IL-10-producing CD103⁺ DCs²¹¹. Although the precise mechanism behind these hypersensitivity reactions remains to be elucidated, it is thought to involve a component of the whole organism. This has led to a shift in focus towards the development of subunit vaccines, such as those based on the MOMP.

MOMP is the most studied protein in the development of vaccines against *C. trachomatis*. The chlamydial MOMP consists of five genetically conserved domains and four variable domains used for serovar identification within different species. These domains contain several T-cell and B-cell epitopes relevant to human immunity¹⁸². The first MOMP-based vaccine to demonstrate potent protection was a denatured trimer of native MOMP (nMOMP) combined with Freund's adjuvant. Mice vaccinated with this formulation were subsequently challenged with *C. muridarum* in the ovarian bursa. The vaccine significantly protected the mice, as evidenced by a reduction in the number of mice that resulted positive for chlamydia in vaginal secretions and in the duration of bacterial shedding, the decrease of number of infectious units recovered and the increase in the number of pregnant mice and embryos¹⁸⁴. However, the purification of nMOMP directly from chlamydia cells significantly hinders the practicality of large-scale antigen production. The high costs of culturing large quantities of chlamydia, the steps required to extract, purify and refold MOMP significantly increase the costs of vaccine production. In addition, the entire process carries the potential risk of contamination by harmful agents in the tissue culture system²¹². These challenges led to research into alternative antigen production and vaccine delivery methods.

Currently, the most common approach for the development of subunit vaccines is recombinant protein production in bacterial, yeast, plant, or mammalian cells and subsequent purification²¹³. The recombinant MOMP (rMOMP) of *C. muridarum*, combined with both mucosal and systemic immunization routes, was the first to demonstrate protection by providing long-term protection against vaginal shedding, upper genital tract pathology and infertility in mice^{214,215}. However, mice vaccinated with rMOMP from *C. trachomatis* serovar D (UW-3/Cx) showed significant protection against vaginal shedding and infertility when challenged with the same serovars D (UW-3/Cx), a different isolate of serovar D (UCI-96/Cx) or serovar E (IOL-43) in the ovarian bursa, but not with serovar F (N.I.1)²¹⁶. These findings suggest that a multivalent vaccine containing rMOMP from the four major immune groups (D, E, F, and G) should provide protection against all genital *C. trachomatis* serovars.

In 2019, a multivalent protein vaccine, called CTH522, containing the MOMP sequences of the most prevalent *C. trachomatis* serovars became the first vaccine candidate to be tested in

humans since the 1970s¹⁹¹. Clinical trials showed the vaccine could induce neutralizing IgG and IgA in serum and in the female reproductive tract. In the B6C3F1/OlaHsd (H-2b, -2k) mouse model, immunization with CTH522 induced CD4⁺ T-cell response and antibody production, conferring protection against *C. trachomatis* infection¹⁸⁷. However, the role of the CD8⁺ T-cell response has not been thoroughly investigated. Traditionally, viral constructs and DNA-based vaccines have been preferred for stimulating CD8⁺ T-cells in experimental vaccination models^{217,218}. Indeed, DNA-based vaccines are internalized by APCs that subsequently present peptide fragments directly on MHC class I molecules. Recombinant live attenuated virus-based and nucleic acid-based vaccines provide APCs with both the recombinant antigen and pathogen-associated molecular patterns (PAMPs), which activate APCs through pattern recognition receptors (PRRs). In contrast, highly purified antigens used in subunit vaccines generally do not sufficiently activate APCs, making them less immunogenic²¹⁹. Among the live attenuated viruses used as vaccine vectors, MVA is notable for its significantly reduced virulence and inability to replicate in most mammalian cells. This poxvirus has been extensively studied in both preclinical and clinical trials for a variety of infectious and non-infectious diseases. MVA is considered to be safe, cost-effective and highly immunogenic, as recombinant MVA vaccines can induce strong humoral and cellular immune responses against a wide range of pathogens⁸⁵.

This led to the investigation of MVA as a promising vaccine platform to induce both cellular and humoral immunity against chlamydia infection. The results of this work showed that MVA vectors expressing modified versions of CTH522, specifically MVA-spCTH522 and MVA-CTH522:B7, elicited distinct immune responses in two different mouse models. Both vaccine candidates induced IFN- γ -producing CD4⁺ T-cells in C57BL/6J and HLA-A2.DR1 mice, suggesting that *C. trachomatis* MOMP contains both I-Ab and HLA-DR1 restricted epitopes. As discussed above, MOMP-specific CD4⁺ T-cells play a protective role against chlamydia infection. However, neither vaccine was able to induce CTH522-specific CD8⁺ T-cell responses in C57BL/6J mice, in contrast to HLA-A2.DR1 mice in which both MVA-spCTH522 and MVA-CTH522:B7 successfully induced strong CD8⁺ T-cell responses. This suggests that MOMP contains HLA-A*02:01 restricted epitopes but it may lack H2-Kb/Db restricted epitopes. In C57BL/6J mice, only a limited number of chlamydia antigens, such as the cysteine-rich protein antigen CrpA, have been identified as containing MHC-I-restricted immunodominant epitopes. This suggests that MOMP may be less immunogenic in C57BL/6J mice compared to the CrpA antigen¹⁶³, and such limitation may affect the efficacy of a MOMP-based vaccine in stimulating a strong CD8⁺ T-cell response in this mouse model. Interestingly, a vaccinia virus-based vaccine has been shown to induce CrpA-specific effector memory CD8⁺ T-cells in C57BL/6J mice¹⁶⁹.

While this demonstrates the ability of MVA-based vaccines to elicit T-cell responses against recombinant antigens, including CTH522, the results of this work highlight a significant barrier to the CD8⁺ T-cell immunogenicity of the MOMP antigen in C57BL/6J mice. This raises the possibility that previous preclinical studies using C57BL/6J mice to evaluate MOMP-based vaccines, whether native, recombinant protein or contained in other vaccine platforms such as DNA plasmids, viral vectors, nanoparticles and extracellular vesicles, may have underestimated the efficacy of the vaccines in inducing chlamydial MOMP-specific CD8⁺ T-cells. For example, a study found that depletion of CD8⁺ T cells in mice immunized with Hirep1, a recombinant protein containing partial MOMP sequences from *C. trachomatis* serovars D, E, and F, did not affect protection against chlamydial infection. In contrast, depletion of CD4⁺ T cells significantly reduced protection, suggesting that CD4⁺ T cells play a predominant role in vaccine-induced immunity. However, the study did not evaluate whether the vaccine effectively induced CD8⁺ T cell responses¹⁸⁶. If the vaccine failed to generate a robust population of MOMP-specific CD8⁺ T cells, as observed with our MVA-based vaccines in C57BL/6J mice, the lack of an observed effect from CD8⁺ T cell depletion could be misleading. Indeed, these results would not necessarily indicate that CD8⁺ T cells are unimportant for protection but rather that they may not have been sufficiently induced by the vaccine. This distinction is crucial for understanding the true contribution of CD8⁺ T cells to protective anti-chlamydial immunity. Future research should include direct assessment of vaccine-induced CD8⁺ T cell responses to clarify whether CD8⁺ T cells play a protective role when effectively induced and whether alternative vaccine strategies, such as viral vectors or adjuvants that enhance CD8⁺ T cell activation, could improve protective immunity against chlamydia.

On the other hand, our results highlight the potential of MVA-based vaccines to induce effective chlamydial MOMP-specific CD8⁺ T-cells in other mouse models, such as the HLA-A2.DR1 model, which partially recapitulate the CD8⁺ T-cell response in humans. The HLA-A2.DR1 mouse model, which uses HLA-A*02:01/Db for MHC-I and HLA-DR1 for MHC-II, has proven to be a valuable tool for identifying HLA-restricted epitopes in both viral and bacterial diseases and has been crucial in evaluating vaccine-induced T-cell-specific immunogenicity¹⁴⁷. The results of this thesis showed that recombinant MVA expressing engineered CTH522 antigens can induce both Th1-biased CD4⁺ T-cells and multifunctional CD8⁺ T-cells in this model, allowing us to explore the role of MHC-dependent T-cells in clearing infection and/or shaping the immunopathology caused by chlamydia infection.

In this work we have identified two primary HLA-A*02:01 restricted epitopes induced by vaccination with both MVA-spCTH522 and MVA-CTH522:B7. The first epitope that showed immunodominance corresponds to MOMP₂₈₂₋₂₉₀. This epitope has been previously described as a dominant CD8⁺ T-cell-specific epitope in PBMCs of a cohort of *C. trachomatis*-positive patients¹⁹⁷. The second epitopes identified corresponds to MOMP₂₀₀₋₂₀₉ and the results of this thesis suggest that this HLA-A*02:01-restricted epitope within the *C. trachomatis* MOMP is immunosubdominant compared to MOMP₂₈₂₋₂₉₀. Further clinical trials investigating the immune response in *C. trachomatis*-positive subjects would determine whether this epitope is recognized by human CD8⁺ T-cells. These findings not only validate the utility of the HLA-A2.DR1 mouse model for studying HLA-restricted CD8⁺ T-cell responses, but also highlight its potential for the discovery of novel pathogen-associated epitopes, both of which are important for antigen design and vaccine development.

Sequence analysis of MOMP (Supplementary table 3) across different *Chlamydia* species revealed that the MOMP₂₀₀₋₂₀₉ and MOMP₂₈₂₋₂₉₀ epitopes are not only present in different serovars of *C. trachomatis*, but also in other species such as *Chlamydia suis* and *Chlamydia muridarum*. In addition, the MOMP₂₈₂₋₂₉₀ epitope is found in *Chlamydia abortus*, *Chlamydia gallinacea*, *Chlamydia pecorum* and *Chlamydia psittaci*. Among *C. trachomatis* serovars, these epitopes are found in serovars A, B, Ba and C, which are the major causes of ocular trachoma. Trachoma is a leading cause of blindness and visual impairment, with 0.4 million and 1.6 million cases reported in 2015, respectively²²⁰. Efforts are underway to develop a vaccine to prevent ocular trachoma^{192,221}. In addition, these epitopes are present in the MOMP of *C. trachomatis* serovars L1, L2 and L3, which belong to the *lymphogranuloma venereum* (LGV) biovar. LGV serovars are responsible for invasive urogenital and anorectal infections, with the ability to invade and replicate in regional lymph nodes. LGV may present with genital ulcers, swollen inguinal lymph nodes or proctitis²²². *C. abortus* primarily infects ruminants, but poses a potential risk to humans. *C. abortus* infections can have serious consequences, including pelvic inflammatory disease, placental dysfunction and fetal death in pregnant women who test positive for *C. abortus*^{223,224}. The presence of these epitopes in different *Chlamydia* strains highlights the potential for cross-protective immunity induced by MVA-spCTH522 and MVA-CTH522:B7.

The epitopes identified in this study are also present in the MOMP of *C. muridarum*, a strain of chlamydia that infects mice. In mice, vaginal inoculation of *C. muridarum* typically results in hydrosalpinx, fibrosis and infertility, which are similar to the post-infection complications commonly seen in women infected with *C. trachomatis*²²⁵. In contrast, intravaginal inoculation of *C. trachomatis* in mice usually results in a mild genital tract infection that resolves relatively

quickly, without the severe symptoms seen in *C. muridarum* infections. However, post-infection complications with *C. trachomatis* in mice only occur when high doses of the bacterium are inoculated directly into specific sites such as the uterus, uterine horns or ovarian bursa²²⁶. This artificial inoculation method does not accurately mimic the natural course of infection, making it difficult to assess the effectiveness of a *C. trachomatis* vaccine in protecting mice from vaginal infection. Given this challenge, one potential solution lies in the role of CD8⁺ T-cells, which are able to recognize short, conserved epitopes shared by different chlamydia species. This recognition could provide cross-species protection. The presence of these conserved epitopes therefore provides an opportunity to explore the protective capacity of MVA-spCTH522 and MVA-CTH522:B7 vaccine candidates in the context of natural vaginal infection with *C. muridarum* in HLA-A2.DR1 mice. This might provide insights into the potential of MVA-spCTH522 and MVA-CTH522:B7 in conferring broader protection against chlamydia infections.

The epitope sequence of MOMP₂₀₀₋₂₀₉ (ALWECGCATL) includes two cysteines at positions 5 and 7 within the decamer peptide. This highlights the advantages of MVA-based vaccines encoding CTH522 antigens, which allow the native amino acid sequence of the recombinant antigen to be preserved. In contrast, the production of recombinant proteins for subunit vaccines, such as the CTH522/CAF01 vaccine, often requires the substitution of cysteines with serines to increase expression levels and solubility, reduce misfolding and aggregation, and improve stability²²⁷. While cysteine-to-serine substitutions may not significantly affect the recognition of vaccine-induced antibodies to native pathogen-associated antigens, they may affect CD8⁺ T-cell-mediated immune responses^{228,229}. Even a single amino acid mutation within a CD8⁺ T-cell-restricted epitope can disrupt T-cell recognition through several mechanisms²³⁰. One key mechanism involves mutation of anchor residues that are essential for tight binding to the MHC class I molecule. Suboptimal binding weakens the stability of the MHC class I/peptide complex, leading to loss of the epitope and CD8⁺ T-cell immune escape²³¹. This mechanism is a common form of immune escape in HIV, with most substitutions occurring at critical anchor residues²³². In addition, amino acid changes outside of T-cell recognition or MHC anchor residues can still affect vaccine-induced T-cell responses²³³.

Moreover, amino acid substitutions can affect CD8⁺ T-cell epitope processing. Many steps of antigen presentation, including proteasomal degradation of viral and recombinant proteins, and stabilization of the MHC class I/peptide complex are sequence dependent and variations within or near the epitope can disrupt the process²³⁴. For example, substitutions within the epitope can lead to preferential proteasomal cleavage within the epitope itself, preventing its

proper endogenous processing²³⁵. Therefore, MVA serves as an optimal vaccine vector for the expression of recombinant antigens specifically designed to induce conserved epitopes of pathogens such as *C. trachomatis*. In addition, the MVA vector is exceptionally easy to genetically manipulate, allowing the production of large quantities of recombinant antigens depending on the promoter controlling their expression²³⁶. In this study, the expression cassettes for spCTH522 and CTH522:B7 were regulated by the potent modified H5 promoter, which allows antigen expression during both the early and late phases of the viral replication cycle²³⁷. This ensured prolonged antigen production in infected cells, with synthesis of spCTH522 and CTH522:B7 detected as early as 4 hours post-infection, corresponding to the early phase of viral gene expression, and continuing up to 72 hours post-infection.

A brief exposure to an antigen during a viral infection *in vivo* is sufficient to initiate the proliferation and differentiation of antigen-specific T-cells and to induce antibody production. However, the strength and duration of antigen presentation, as well as costimulatory signals, play a critical role in shaping this process and determining the functional properties of both effector and particularly memory T-cells²³⁸. Consequently, most vaccines require multiple doses to achieve robust and long-lived immune protection at both the individual and population levels. Preclinical studies of various vaccine platforms, including subunit vaccines and DNA vaccines, using chlamydia MOMP as the antigen formulation, have also required multiple immunizations, typically consisting of three doses given at two-week intervals^{187,239–242}. The results presented in this thesis demonstrate that in HLA-A2.DR1 mice, a single vaccination is sufficient to activate MOMP-specific CD8⁺ T-cells. Furthermore, a single booster immunization significantly increased the magnitude of the CD8⁺ T-cell response to the dominant epitope, MOMP₂₈₂₋₂₉₀, while having no significant effect on the response to the MOMP₂₀₀₋₂₀₉ epitope. This confirms the dominance of the HLA-A*02:01-restricted epitope MOMP₂₈₂₋₂₉₀ over MOMP₂₀₀₋₂₀₉. These findings are consistent with previous research suggesting that after booster vaccination with MVA-based vaccines, the expansion of both virus-specific and recombinant antigen-specific CD8⁺ T-cells is regulated by T-cell cross-competition, prioritizing those that rapidly recognize dominant epitopes on infected cells²⁴³. From this perspective, future studies should explore strategies to expand CD8⁺ T-cell populations that recognize subdominant epitopes. One potential approach is booster vaccination with MOMP₂₀₀₋₂₀₉ peptide-based vaccines to selectively expand MOMP₂₀₀₋₂₀₉-specific T cells²⁴⁴. Alternatively, the development of recombinant MVA-based vaccines carrying single MOMP-derived epitopes could be explored in a vaccine-mixture immunization model. Notably, previous elegant research has demonstrated that cross-competition among resident tissue CD8⁺ T cells occurs between those recognizing antigens presented by a common APC. The use of different MVA vectors has been shown to promote the presentation

of both immunodominant and subdominant epitopes, resulting in a balanced expansion of T cell populations targeting both dominant and subdominant epitopes²⁴⁵.

Our data indicate that two doses of the recombinant MVA vaccine expressing CTH522 antigens are sufficient to elicit a strong immunodominant epitope-specific T-cell response. Similarly, Sara Moreno Mascaraque, whose PhD research focused on characterizing CD4⁺ T-cell and antibody responses to the MVA-CTH522:B7 vaccine in C57BL/6J mice, demonstrated that a prime/boost vaccination regimen significantly increased the CTH522-specific CD4⁺ T-cell and antibody responses compared to a single dose regimen. This suggests that a prime/boost vaccination regimen with MVA-based vaccines expressing CTH522 antigens is sufficient and necessary to induce a strong humoral and cellular response.

While evaluating different vaccination regimens is crucial to determine the most effective approach for eliciting optimal humoral and cellular responses, it is equally important to assess the antigen stability as well as the accessibility of specific epitopes on the antigenic surface when developing vaccine candidates. For example, subunit vaccines effectively induce strong humoral responses because the recombinant antigen is synthesized *in vitro*, ensuring that antigenic epitopes are readily accessible to the BCRs upon immunization²¹⁷. In contrast, MVA-based vaccines rely on host cells to produce the recombinant antigen after administration, so the design of recombinant antigens expressed by MVA-based vaccines must be carefully optimized to ensure that the antigen is stable and accessible to BCRs for antibody production¹⁹⁶. This work highlighted the critical importance of evaluating the synthesis and stability of recombinant antigens when developing recombinant MVA-based vaccines. In fact, in the initial phase of this project, our efforts to develop an MVA-based vaccine against *C. trachomatis* began with the generation of a recombinant MVA engineered to carry an expression cassette for the original CTH522 antigen. This approach was designed to evaluate the feasibility of expressing the antigen in its native form within the MVA vector system. However, detailed analysis of the kinetics of CTH522 protein synthesis during *in vitro* infection revealed an unexpected outcome: the CTH522 protein was rapidly targeted and degraded by the proteasome system. This finding highlighted the inherent instability of the unmodified antigen when synthesized by MVA in mammalian cells and underscored the need for further optimization to improve antigen stability and ensure proper presentation for an effective immune response. Without a thorough *in vitro* analysis of protein synthesis following MVA infection, the impact of this rapid degradation on the immune response to CTH522 upon *in vivo* immunization may have been underestimated.

In addition to assessing antigen stability, this work emphasized the critical importance of evaluating the localization of the recombinant antigen in the cell after infection. Indeed, while both MVA-spCTH522 and MVA-CTH522:B7 induced comparable T-cell responses, as both antigens were endogenously synthesized and accessible for MHC presentation, only MVA-CTH522:B7 elicited a strong antibody response. This was due to the fact that the CTH522:B7 construct was specifically designed to anchor the antigen to the surface of infected cells, whereas the spCTH522 construct lacked this modification. This suggests that other MVA-based chlamydia vaccines utilizing the unmodified MOMP amino acid sequence, without modification for cell surface localization, may have underestimated their potential to induce strong antibody responses. These findings suggest that in order to achieve robust humoral and cellular responses against recombinant antigens expressed by MVA-based vaccines, the antigen sequence must be strategically designed. For the CTH522 antigen, incorporation of an extracellular targeting signal sequence at the N-terminus ensures antigen export within the cell to the cell surface, while a transmembrane domain, such as the CD80 (B7.1) antigen TM domain, anchors the antigen on the cell surface. Therefore, when characterizing vaccine candidates, it is essential to verify that the modified recombinant antigen is correctly localized e.g., at the surface of infected cells.

In C57BL/6J mice, the humoral immune response elicited by MVA-CTH522:B7 was notably dominated by a greater prevalence of IgG2b and IgG2c antibodies relative to IgG1. This antibody profile is particularly relevant because previous research has shown that the immune response induced by CpG plus Montanide ISA 720-adjuvanted MOMP-based vaccines, characterized by predominantly IgG2b and IgG2c antibodies, was associated with protective efficacy against *C. trachomatis* infection²⁴⁶. The predominance of IgG2b and IgG2c is often associated with a Th1-skewed cellular immune response, which plays a critical role in combating intracellular pathogens such as *C. trachomatis*. This confirms that the MVA-CTH522:B7 vaccine induced both humoral and cellular immune responses tailored to the requirements for effective protection against *C. trachomatis* infection. These results confirm the potential of MVA-based vaccines to induce protective humoral responses and further support their utility for the development of *C. trachomatis* vaccines.

Notably, the immunogenicity of MVA-spCTH522 and MVA-CTH522:B7 vaccine candidates was evaluated exclusively by intraperitoneal injection. This systemic vaccination approach demonstrated that our MVA-based vaccine candidates are capable of inducing *C. trachomatis*-specific T-cell responses in the spleen and antibody responses in the serum. However, it is critical to emphasize the important role of tissue-resident T-cells and mucosal antibodies in

providing protection against mucosal pathogens, including *C. trachomatis*. Over the past decades, numerous immunological studies have highlighted the interconnected nature of mucosal sites such as the respiratory and genital tracts, demonstrating that these sites function as a system-wide organ²⁴⁷. Several studies have demonstrated that specific mucosal immunization approaches can induce immune responses at distant mucosal sites. Intranasal vaccination effectively induces immune responses in the respiratory, gastrointestinal and genital tracts. Oral vaccination stimulates immune responses primarily in the gut and mammary glands. Rectal vaccination induces immune responses in the colon and rectum, while intravaginal vaccination induces immune responses specifically in the genital tract²⁴⁸.

In the context of *C. trachomatis* infection, intranasal inoculation with *C. trachomatis* has been shown to induce a robust immune response in the genital tract that protects mice for at least 180 days against the long-term consequences of intrabursal challenge with *C. trachomatis*²⁴⁹. In this view, several studies have been conducted to assess whether mucosal vaccination strategies could effectively protect against *C. trachomatis* infection. Indeed, intranasal vaccination of mice with UV-inactivated *C. trachomatis* has been shown to successfully induce tissue-resident CD4⁺ T-cells, which provided protection against intravaginal challenge with *C. trachomatis*²¹¹. Nevertheless, parenteral vaccination using the CTH522/CAF01 formulation has also been demonstrated to generate tissue-resident CD4⁺ T-cells that protected against *C. trachomatis* infection²⁵⁰. Interestingly, three intranasal immunizations at two-week intervals using bacterial outer membrane vesicles (OMVs) decorated with CTH522 elicited a robust immune response in the genital tract, characterized by CTH522-specific Th1/Th17 CD4⁺ T-cells and CTH522-specific IgG, though not IgA²⁴². Conversely, a simultaneous subcutaneous/intrauterine immunization strategy with CTH522/CAF01, administered in three doses at two-week intervals, induced strong systemic and mucosal chlamydia-specific Th1/Th17 cell responses and IgA production²⁵¹.

These findings suggest that distinct vaccination routes can lead to the induction of heterogeneous immune responses, highlighting the versatility of different immunization strategies. At the same time, they underscore the need for further investigations to fully understand the role of mucosal vaccination in achieving protective efficacy against *C. trachomatis*. Additionally, it is plausible that different vaccine platforms and/or adjuvants exhibit varying capacities to induce distinct local immune responses. MVA-based vaccines are widely recognized for their ability to induce robust tissue-resident T-cell responses in addition to the production of mucosal IgG and IgA antibodies against recombinant antigens^{112,113,245,252,253}. This work provides an important basis for evaluating whether MVA-spCTH522 and MVA-CTH522:B7 can effectively generate MOMP-specific tissue-resident

CD4⁺ T-cells and mucosal antibody responses in C57BL/6J mice upon mucosal vaccination. To achieve this goal, it is essential to explore different routes of vaccination, although previous studies suggest that systemic priming followed by mucosal boosting is the most effective strategy to elicit a strong and broad immune response²⁵⁴⁻²⁵⁶. In addition, the role of tissue-resident CD8⁺ T-cells in combating chlamydia infection remains unknown. Understanding their contribution could further improve vaccine efficacy. The results presented here highlight the potential of the HLA-A2.DR1 mouse model as a valuable experimental tool for studying HLA-restricted MOMP-specific tissue-resident CD8⁺ T-cell responses. This model provides a unique opportunity to study how MVA-based vaccines modulate both systemic and local immune mechanisms to confer protection against *C. trachomatis*. These findings could significantly advance the development of more effective vaccination strategies that target both systemic and mucosal immunity to combat chlamydia infections.

7. Conclusion

In summary, this research represents a significant advance in addressing the global challenge of preventing *C. trachomatis* infection and disease. It underscores the complexities involved in developing an effective vaccine, particularly the critical role of antigen design and the strategic selection of animal models in vaccine research. The study highlights the need to comprehensively investigate vaccine-induced immune responses to understand their protective mechanisms against Chlamydia infection. Using innovative methods, we analyzed the contributions of different immune components induced by our MVA-based vaccine candidates in the C57BL/6J and HLA-A2.DR1 mouse models. In the C57BL/6J model, the MVA-spCTH522 vaccine would provide insight into the protective role of CD4⁺ T-cells alone, while the MVA-CTH522:B7 vaccine would elucidate the combined effects of CD4⁺ T-cells and antibody responses against chlamydia infection. Similarly, in the HLA-A2.DR1 model, the MVA-spCTH522 vaccine would elucidate the role of both CD4⁺ and CD8⁺ T-cells, while the MVA-CTH522:B7 vaccine would elucidate the interplay of CD4⁺ T-cells, CD8⁺ T-cells, and antibody responses against chlamydia infection. These findings would provide a valuable foundation for the design of effective vaccines capable of optimally eliciting robust and targeted immune responses to protect against *C. trachomatis*. This study also highlighted the limitations of systemic immunization routes and emphasized the need to explore alternative approaches, such as mucosal vaccination or combined intramuscular and mucosal immunization strategies, to achieve more targeted and effective immune responses. These strategies may enhance the ability of MVA-based vaccines to induce mucosal antibodies and tissue-resident T-cells, which are critical for comprehensive immune protection against chlamydia. Despite these promising findings, translating results from mouse models to humans remains a significant challenge. While mouse models are invaluable for understanding immune mechanisms, they do not fully recapitulate the progression of human chlamydia infection, such as ascending infection and tubal pathology. This limitation highlights the need for further testing alternative models, such as non-human primates, that more closely mimic human immune responses and disease progression. Such studies are essential to validate the immunological findings and to assess the protective efficacy of MVA-based vaccines in humans. Finally, our research highlights the need for a multifaceted approach that integrates precise antigen design, advanced vaccine platforms and optimized immunization strategies. These efforts are crucial for the development of effective vaccines not only against *C. trachomatis*, but also against other related pathogens. By addressing these challenges, we are moving closer to reducing the global burden of chlamydia infection and advancing public health initiatives worldwide.

References

1. Chi, H., Pepper, M. & Thomas, P. G. Principles and therapeutic applications of adaptive immunity. *Cell* **187**, 2052–2078 (2024).
2. Sebina, I. & Pepper, M. Humoral immune responses to infection: Common mechanisms and unique strategies to combat pathogen immune evasion tactics. *Curr Opin Immunol* **51**, 46 (2018).
3. Cyster, J. G. & Allen, C. D. C. B Cell Responses: Cell Interaction Dynamics and Decisions. *Cell* **177**, 524–540 (2019).
4. MacLennan, I. C. M. *et al.* Extrafollicular antibody responses. *Immunol Rev* **194**, 8–18 (2003).
5. Gatto, D. & Brink, R. The germinal center reaction. *Journal of Allergy and Clinical Immunology* **126**, 898–907 (2010).
6. Victora, G. D. & Nussenzweig, M. C. Germinal Centers. *Annu Rev Immunol* **40**, 413–442 (2022).
7. Shlomchik, M. J. & Weisel, F. Germinal center selection and the development of memory B and plasma cells. *Immunol Rev* **247**, 52–63 (2012).
8. Chiu, M. L., Goulet, D. R., Teplyakov, A. & Gilliland, G. L. Antibody Structure and Function: The Basis for Engineering Therapeutics. *Antibodies* **8**, 55 (2019).
9. Schroeder, H. W. & Cavacini, L. Structure and Function of Immunoglobulins. *J Allergy Clin Immunol* **125**, S41 (2010).
10. Sikorav, J. L., Auffray, C. & Rougeon, F. Structure of the constant and 3' untranslated regions of the murine balb/c γ 2a heavy chain messenger RNA. *Nucleic Acids Res* **8**, 3143–3156 (1980).
11. Yamawaki-Kataoka, Y., Miyata, T. & Honjo, T. The complete nucleotide sequence of mouse immunoglobulin γ 2a gene and evolution of heavy chain genes: Further evidence for intervening sequence-mediated domain transfer. *Nucleic Acids Res* **9**, 1365–1382 (1981).
12. Zhang, Z., Goldschmidt, T. & Salter, H. Possible allelic structure of IgG2a and IgG2c in mice. *Mol Immunol* **50**, 169–171 (2012).
13. O'Kennedy, R., Murphy, C. & Devine, T. Technology advancements in antibody purification. *Antibody Technology Journal Volume 6*, 17–32 (2016).
14. Cragg, M. S., Berthelot, L., Van Egmond, M. & Breedveld, A. IgA and Fc α RI: Pathological Roles and Therapeutic Opportunities. *Front Immunol* **10**, 553 (2019).
15. Lu, L. L., Suscovich, T. J., Fortune, S. M. & Alter, G. Beyond binding: antibody effector functions in infectious diseases. *Nature Reviews Immunology 2017 18:1* **18**, 46–61 (2017).
16. Pollard, A. J. & Bijker, E. M. A guide to vaccinology: from basic principles to new developments. *Nature Reviews Immunology 2020 21:2* **21**, 83–100 (2020).
17. Chaplin, D. D. Overview of the Immune Response. *J Allergy Clin Immunol* **125**, S3 (2010).
18. Lebien, T. W. & Tedder, T. F. B lymphocytes: how they develop and function. *Blood* **112**, 1570 (2008).
19. Kumar, B. V., Connors, T. J. & Farber, D. L. Human T cell development, localization, and function throughout life. *Immunity* **48**, 202 (2018).
20. Bassing, C. H., Swat, W. & Alt, F. W. The mechanism and regulation of chromosomal V(D)J recombination. *Cell* **109**, S45–S55 (2002).
21. Netea, M. G., Schlitzer, A., Placek, K., Joosten, L. A. B. & Schultze, J. L. Innate and Adaptive Immune Memory: an Evolutionary Continuum in the Host's Response to Pathogens. *Cell Host Microbe* **25**, 13–26 (2019).
22. Danilova, N. The Evolution of Adaptive Immunity. *Adv Exp Med Biol* **738**, 218–235 (2012).
23. Avalos, A. M. & Ploegh, H. L. Early BCR events and antigen capture, processing, and loading on MHC class II on B cells. *Front Immunol* **5**, 72915 (2014).
24. Shah, K., Al-Haidari, A., Sun, J. & Kazi, J. U. T cell receptor (TCR) signaling in health and disease. *Signal Transduction and Targeted Therapy 2021 6:1* **6**, 1–26 (2021).
25. Seder, R. A. & Ahmed, R. Similarities and differences in CD4⁺ and CD8⁺ effector and memory T cell generation. *Nature Immunology 2003 4:9* **4**, 835–842 (2003).
26. Neeffjes, J., Jongasma, M. L. M., Paul, P. & Bakke, O. Towards a systems understanding of MHC class I and MHC class II antigen presentation. *Nature Reviews Immunology 2011 11:12* **11**, 823–836 (2011).

27. Hansen, T. H. & Bouvier, M. MHC class I antigen presentation: learning from viral evasion strategies. *Nature Reviews Immunology* 2009 9:7 **9**, 503–513 (2009).
28. Barry, M. & Bleackley, R. C. Cytotoxic T lymphocytes: all roads lead to death. *Nature Reviews Immunology* 2002 2:6 **2**, 401–409 (2002).
29. Andersen, M. H., Schrama, D., Thor Straten, P. & Becker, J. C. Cytotoxic T Cells. *Journal of Investigative Dermatology* **126**, 32–41 (2006).
30. Ting, J. P. Y. & Trowsdale, J. Genetic Control of MHC Class II Expression. *Cell* **109**, S21–S33 (2002).
31. Roche, P. A. & Furuta, K. The ins and outs of MHC class II-mediated antigen processing and presentation. *Nat Rev Immunol* **15**, 203–216 (2015).
32. Colbert, J. D., Cruz, F. M. & Rock, K. L. Cross-presentation of exogenous antigens on MHC I molecules. *Curr Opin Immunol* **64**, 1–8 (2020).
33. Münz, C. Autophagy Beyond Intracellular MHC Class II Antigen Presentation. *Trends Immunol* **37**, 755–763 (2016).
34. Roche, P. A. & Cresswell, P. Antigen Processing and Presentation Mechanisms in Myeloid Cells. *Microbiol Spectr* **4**, (2016).
35. Hwang, J. R., Byeon, Y., Kim, D. & Park, S. G. Recent insights of T cell receptor-mediated signaling pathways for T cell activation and development. *Experimental & Molecular Medicine* 2020 52:5 **52**, 750–761 (2020).
36. Lanzavecchia, A., Iezzi, G. & Viola, A. From TCR Engagement to T Cell Activation. *Cell* **96**, 1–4 (1999).
37. Sharpe, A. H. Mechanisms of Costimulation. *Immunol Rev* **229**, 5 (2009).
38. Linsley, P. S. *et al.* Human B7-1 (CD80) and B7-2 (CD86) bind with similar avidities but distinct kinetics to CD28 and CTLA-4 receptors. *Immunity* **1**, 793–801 (1994).
39. Grewal, I. S. & Flavell, R. A. The role of CD40 ligand in costimulation and T-cell activation. *Immunol Rev* **153**, 85–106 (1996).
40. Laidlaw, B. J., Craft, J. E. & Kaech, S. M. The multifaceted role of CD4⁺ T cells in CD8⁺ T cell memory. *Nature Reviews Immunology* 2016 16:2 **16**, 102–111 (2016).
41. SR Bennett, F. C. F. K. J. M. W. H. Induction of a CD8⁺ cytotoxic T lymphocyte response by cross-priming requires cognate CD4⁺ T cell help. *J. Exp. Med.* **186**, 65–70 (1997).
42. SP Schoenberger, R. T. E. van der V. R. O. C. M. T-cell help for cytotoxic T lymphocytes is mediated by CD40-CD40L interactions. *Nature* **393**, 480–483 (1998).
43. Castellino, F. Chemokines enhance immunity by guiding naive CD8⁺ T cells to sites of CD4⁺ T cell-dendritic cell interaction. *Nature* **440**, 890–895 (2006).
44. Eickhoff, S. Robust anti-viral Immunity requires multiple distinct T cell-dendritic cell interactions. *Cell* **162**, 1322–1337 (2015).
45. Hor, J. Spatiotemporally distinct interactions with dendritic cell subsets facilitates CD4⁺ and CD8⁺ T cell activation to localized viral infection. *Immunity* **43**, 554–565 (2015).
46. Laidlaw, B. J., Craft, J. E. & Kaech, S. M. The multifaceted role of CD4⁺ T cells in CD8⁺ T cell memory. *Nature Reviews Immunology* 2016 16:2 **16**, 102–111 (2016).
47. Kumar, B. V., Connors, T. J. & Farber, D. L. Human T cell development, localization, and function throughout life. *Immunity* **48**, 202 (2018).
48. Chatzileontiadou, D. S. M., Sloane, H., Nguyen, A. T., Gras, S. & Grant, E. J. The Many Faces of CD4⁺ T Cells: Immunological and Structural Characteristics. *Int J Mol Sci* **22**, 73 (2020).
49. Zhang, N. & Bevan, M. J. CD8⁺ T Cells: Foot Soldiers of the Immune System. *Immunity* **35**, 161–168 (2011).
50. Koh, C. H., Lee, S., Kwak, M., Kim, B. S. & Chung, Y. CD8 T-cell subsets: heterogeneity, functions, and therapeutic potential. *Experimental & Molecular Medicine* 2023 55:11 **55**, 2287–2299 (2023).
51. Trinchieri, G. Interleukin-12: A Cytokine Produced by Antigen-Presenting Cells With Immunoregulatory Functions in the Generation of T-Helper Cells Type 1 and Cytotoxic Lymphocytes. *Blood* **84**, 4008–4027 (1994).
52. Mitrücker, H. W., Visekruna, A. & Huber, M. Heterogeneity in the differentiation and function of CD8⁺ T cells. *Arch Immunol Ther Exp (Warsz)* **62**, 449–458 (2014).
53. Basu, R. *et al.* Cytotoxic T Cells Use Mechanical Force to Potentiate Target Cell Killing. *Cell* **165**, 100–110 (2016).
54. Gordy, C. & He, Y. W. Endocytosis by target cells: an essential means for perforin- and granzyme-mediated killing. *Cell Mol Immunol* **9**, 5–6 (2012).
55. Fu, Q. *et al.* Structural Basis and Functional Role of Intramembrane Trimerization of the Fas/CD95 Death Receptor. *Mol Cell* **61**, 602–613 (2016).

56. Restifo, N. P. & Gattinoni, L. Lineage relationship of effector and memory T cells. *Curr Opin Immunol* **25**, 556–563 (2013).
57. Jameson, S. C. & Masopust, D. Understanding subset diversity in T cell memory. *Immunity* **48**, 214 (2018).
58. Farber, D. L., Yudanin, N. A. & Restifo, N. P. Human memory T cells: generation, compartmentalization and homeostasis. *Nat Rev Immunol* **14**, 24 (2013).
59. Kaech, S. M., Wherry, E. J. & Ahmed, R. Effector and memory T-cell differentiation: implications for vaccine development. *Nat Rev Immunol* **2**, 251–262 (2002).
60. Jenner, E. An Inquiry into the Causes and Effects of the Variolae Vaccinae. *Scientific and Medical Knowledge Production, 1796-1918* 40–50 (2023) doi:10.4324/9781003009337-8/INQUIRY-CAUSES-EFFECTS-VARIOLAE-VACCINAE-EDWARD-JENNER.
61. Riedel, S. Edward Jenner and the history of smallpox and vaccination. *Proc (Bayl Univ Med Cent)* **18**, 21 (2005).
62. (1829-1971), P. V.-R.-R. des D. M. & 1935, undefined. La première vaccination contre la rage. *JSTORP Vallery-RadotRevue des Deux Mondes (1829-1971), 1935•JSTOR*.
63. Montero, D. A. *et al.* Two centuries of vaccination: historical and conceptual approach and future perspectives. *Front Public Health* **11**, 1326154 (2024).
64. Bouazzaoui, A. & Abdellatif, A. A. H. Vaccine delivery systems and administration routes: Advanced biotechnological techniques to improve the immunization efficacy. *Vaccine X* **19**, 100500 (2024).
65. Falahi, S. & Kenarkoohi, A. Host factors and vaccine efficacy: Implications for COVID-19 vaccines. *J Med Virol* **94**, 1330–1335 (2022).
66. Siegrist, C.-A. The Challenges of Vaccine Responses in Early Life: Selected Examples. *J Comp Pathol* **137**, S4–S9 (2007).
67. Dhakal, S. & Klein, S. L. Host Factors Impact Vaccine Efficacy: Implications for Seasonal and Universal Influenza Vaccine Programs. *J Virol* **93**, (2019).
68. Zimmermann, P. & Curtis, N. Factors That Influence the Immune Response to Vaccination. *Clin Microbiol Rev* **32**, (2019).
69. Pollard, A. J. & Bijker, E. M. A guide to vaccinology: from basic principles to new developments. *Nat Rev Immunol* **21**, 83–100 (2021).
70. Ura, T. *et al.* Current Vaccine Platforms in Enhancing T-Cell Response. *Vaccines (Basel)* **10**, 1367 (2022).
71. Gilbert, S. C. T-cell-inducing vaccines – what’s the future. *Immunology* **135**, 19–26 (2012).
72. Sánchez-Sampedro, L. *et al.* The Evolution of Poxvirus Vaccines. *Viruses* **7**, 1726–1803 (2015).
73. Mackett, M., Smith, G. L. & Moss, B. Vaccinia virus: a selectable eukaryotic cloning and expression vector. *Proc Natl Acad Sci U S A* **79**, 7415–7419 (1982).
74. Smith, G. L., MacKett, M. & Moss, B. Infectious vaccinia virus recombinants that express hepatitis B virus surface antigen. *Nature* **1983** 302:5908 **302**, 490–495 (1983).
75. Cairns, J. The initiation of vaccinia infection. *Virology* **11**, 603–623 (1960).
76. Hillen, H. S. *et al.* Structural Basis of Poxvirus Transcription: Transcribing and Capping Vaccinia Complexes. *Cell* **179**, 1525-1536.e12 (2019).
77. Meade, N., DiGiuseppe, S. & Walsh, D. Translational Control during Poxvirus Infection. *Wiley Interdiscip Rev RNA* **10**, e1515 (2018).
78. Draper, S. J., Cottingham, M. G. & Gilbert, S. C. Utilizing poxviral vectored vaccines for antibody induction—Progress and prospects. *Vaccine* **31**, 4223–4230 (2013).
79. García-Arriaza, J. & Esteban, M. Enhancing poxvirus vectors vaccine immunogenicity. *Hum Vaccin Immunother* **10**, 2235–2244 (2014).
80. Cono, J., Casey, C. G., Bell, D. M. & Centers for Disease Control and Prevention. Smallpox vaccination and adverse reactions. Guidance for clinicians. *MMWR Recomm Rep* **52**, 1–28 (2003).
81. Centers for Disease Control and Prevention (CDC). Progressive vaccinia in a military smallpox vaccinee - United States, 2009. *MMWR Morb Mortal Wkly Rep* **58**, 532–6 (2009).
82. Redfield, R. R. *et al.* Disseminated Vaccinia in a Military Recruit with Human Immunodeficiency Virus (HIV) Disease. *New England Journal of Medicine* **316**, 673–676 (1987).
83. Lane, J. M., Ruben, F. L., Neff, J. M. & Millar, J. D. Complications of Smallpox Vaccination, 1968. *New England Journal of Medicine* **281**, 1201–1208 (1969).
84. Sutter, G. & Moss, B. Nonreplicating vaccinia vector efficiently expresses recombinant genes. *Proceedings of the National Academy of Sciences* **89**, 10847–10851 (1992).

85. Volz, A. & Sutter, G. Modified Vaccinia Virus Ankara. in 187–243 (2017). doi:10.1016/bs.aivir.2016.07.001.
86. Stickl, H. *et al.* MVA-Stufenimpfung gegen Pocken. *DMW - Deutsche Medizinische Wochenschrift* **99**, 2386–2392 (1974).
87. Sutter, G. & Staib, C. Vaccinia Vectors as Candidate Vaccines: The Development of Modified Vaccinia Virus Ankara for Antigen Delivery. *Current Drug Target -Infectious Disorders* **3**, 263–271 (2003).
88. Meyer, H., Sutter, G. & Mayr, A. Mapping of deletions in the genome of the highly attenuated vaccinia virus MVA and their influence on virulence. *J Gen Virol* **72 (Pt 5)**, 1031–1038 (1991).
89. Meisinger-Henschel, C. *et al.* Genomic sequence of chorioallantois vaccinia virus Ankara, the ancestor of modified vaccinia virus Ankara. *Journal of General Virology* **88**, 3249–3259 (2007).
90. Antoine, G., Scheiflinger, F., Dorner, F. & Falkner, F. G. The Complete Genomic Sequence of the Modified Vaccinia Ankara Strain: Comparison with Other Orthopoxviruses. *Virology* **244**, 365–396 (1998).
91. Verheust, C., Goossens, M., Pauwels, K. & Breyer, D. Biosafety aspects of modified vaccinia virus Ankara (MVA)-based vectors used for gene therapy or vaccination. *Vaccine* **30**, 2623–2632 (2012).
92. McFadden, G. Poxvirus tropism. *Nature Reviews Microbiology* **2005 3:3 3**, 201–213 (2005).
93. Okeke, M. I., Nilssen, Ø. & Traavik, T. Modified vaccinia virus Ankara multiplies in rat IEC-6 cells and limited production of mature virions occurs in other mammalian cell lines. *J Gen Virol* **87**, 21–27 (2006).
94. Drexler, I., Heller, K., Wahren, B., Erfle, V. & Sutter, G. Highly attenuated modified vaccinia virus Ankara replicates in baby hamster kidney cells, a potential host for virus propagation, but not in various human transformed and primary cells. *J Gen Virol* **79 (Pt 2)**, 347–352 (1998).
95. Drexler, I., Staib, C. & Sutter, G. Modified vaccinia virus Ankara as antigen delivery system: how can we best use its potential? *Curr Opin Biotechnol* **15**, 506–512 (2004).
96. Assarsson, E. *et al.* Kinetic analysis of a complete poxvirus transcriptome reveals an immediate-early class of genes. *Proc Natl Acad Sci U S A* **105**, 2140–2145 (2008).
97. Yang, Z., Bruno, D. P., Martens, C. A., Porcella, S. F. & Moss, B. Simultaneous high-resolution analysis of vaccinia virus and host cell transcriptomes by deep RNA sequencing. *Proc Natl Acad Sci U S A* **107**, 11513–11518 (2010).
98. Yang, Z., Bruno, D. P., Martens, C. A., Porcella, S. F. & Moss, B. Genome-Wide Analysis of the 5' and 3' Ends of Vaccinia Virus Early mRNAs Delineates Regulatory Sequences of Annotated and Anomalous Transcripts. *J Virol* **85**, 5897–5909 (2011).
99. Sutter, G. A vital gene for modified vaccinia virus Ankara replication in human cells. *Proc Natl Acad Sci U S A* **117**, 6289–6291 (2020).
100. Tolonen, N., Doglio, L., Schleich, S. & Krijnse Locker, J. Vaccinia virus DNA replication occurs in endoplasmic reticulum-enclosed cytoplasmic mini-nuclei. *Mol Biol Cell* **12**, 2031–2046 (2001).
101. Tao, S. *et al.* Sequestration of Late Antigens Within Viral Factories Impairs MVA Vector-Induced Protective Memory CTL Responses. *Front Immunol* **10**, 500216 (2019).
102. Pittman, P. R. *et al.* Phase 3 Efficacy Trial of Modified Vaccinia Ankara as a Vaccine against Smallpox. *New England Journal of Medicine* **381**, 1897–1908 (2019).
103. Cosma, A. *et al.* Therapeutic vaccination with MVA-HIV-1 nef elicits Nef-specific T-helper cell responses in chronically HIV-1 infected individuals. *Vaccine* **22**, 21–29 (2003).
104. Milligan, I. D. *et al.* Safety and Immunogenicity of Novel Adenovirus Type 26- and Modified Vaccinia Ankara-Vectored Ebola Vaccines: A Randomized Clinical Trial. *JAMA* **315**, 1610–1623 (2016).
105. Larivière, Y. *et al.* Ad26.ZEBOV, MVA-BN-Filo Ebola virus disease vaccine regimen plus Ad26.ZEBOV booster at 1 year versus 2 years in health-care and front-line workers in the Democratic Republic of the Congo: secondary and exploratory outcomes of an open-label, randomised, phase 2 trial. *Lancet Infect Dis* **24**, 746–759 (2024).
106. Milligan, I. D. *et al.* Safety and Immunogenicity of Novel Adenovirus Type 26- and Modified Vaccinia Ankara-Vectored Ebola Vaccines: A Randomized Clinical Trial. *JAMA* **315**, 1610–1623 (2016).
107. Ishola, D. *et al.* Safety and long-term immunogenicity of the two-dose heterologous Ad26.ZEBOV and MVA-BN-Filo Ebola vaccine regimen in adults in Sierra Leone: a combined open-label, non-randomised stage 1, and a randomised, double-blind, controlled stage 2 trial. *Lancet Infect Dis* **22**, 97–109 (2022).

108. Mutua, G. *et al.* Safety and immunogenicity of 2-dose heterologous Ad26.ZEBOV, MVA-BN-Filo Ebola vaccination in healthy and HIV-infected adults: A randomised, placebo-controlled Phase II clinical trial in Africa. *PLoS Med* **18**, e1003813 (2021).
109. Anywaine, Z. *et al.* Safety and Immunogenicity of a 2-Dose Heterologous Vaccination Regimen With Ad26.ZEBOV and MVA-BN-Filo Ebola Vaccines: 12-Month Data From a Phase I Randomized Clinical Trial in Uganda and Tanzania. *J Infect Dis* **220**, 46–56 (2019).
110. Tscherne, A. *et al.* Immunogenicity and efficacy of the COVID-19 candidate vector vaccine MVA-SARS-2-S in preclinical vaccination. *Proc. Natl Acad. Sci. USA* **118**, e2026207118 (2021).
111. zu Natrup, C. M. *et al.* Stabilized recombinant SARS-CoV-2 spike antigen enhances vaccine immunogenicity and protective capacity. *J. Clin. Investig.* **132**, e159895 (2022).
112. Americo, J. L., Cotter, C. A., Earl, P. L., Liu, R. & Moss, B. Intranasal inoculation of an MVA-based vaccine induces IgA and protects the respiratory tract of hACE2 mice from SARS-CoV-2 infection. *Proc Natl Acad Sci U S A* **119**, (2022).
113. Pérez, P. *et al.* Intranasal administration of a single dose of MVA-based vaccine candidates against COVID-19 induced local and systemic immune responses and protects mice from a lethal SARS-CoV-2 infection. *Front Immunol* **13**, 995235 (2022).
114. Niu, S., Huang, S. & Liu, B. Chlamydia trachomatis. *Molecular Medical Microbiology, Third Edition* 1343–1356 (2023) doi:10.1016/B978-0-12-818619-0.00049-6.
115. Murray, S. M. & McKay, P. F. Chlamydia trachomatis: Cell biology, immunology and vaccination. *Vaccine* **39**, 2965–2975 (2021).
116. Elwell, C., Mirrashidi, K. & Engel, J. Chlamydia cell biology and pathogenesis. *Nat Rev Microbiol* **14**, 385 (2016).
117. Stephens, R. S. *et al.* Genome sequence of an obligate intracellular pathogen of humans: Chlamydia trachomatis. *Science (1979)* **282**, 754–759 (1998).
118. Hatch, T. P., Miceli, M. & Sublett, J. E. Synthesis of disulfide-bonded outer membrane proteins during the developmental cycle of Chlamydia psittaci and Chlamydia trachomatis. *J Bacteriol* **165**, 379 (1986).
119. Bastidas, R. J., Elwell, C. A., Engel, J. N. & Valdivia, R. H. Chlamydial intracellular survival strategies. *Cold Spring Harb Perspect Med* **3**, (2013).
120. Omsland, A., Sixt, B. S., Horn, M. & Hackstadt, T. Chlamydial metabolism revisited: Interspecies metabolic variability and developmental stage-specific physiologic activities. *FEMS Microbiol Rev* **38**, 779–801 (2014).
121. Schoborg, R. V. Chlamydia persistence - a tool to dissect chlamydia-host interactions. *Microbes Infect* **13**, 649–662 (2011).
122. Panzetta, M. E., Valdivia, R. H. & Saka, H. A. Chlamydia Persistence: A Survival Strategy to Evade Antimicrobial Effects in-vitro and in-vivo. *Front Microbiol* **9**, 3101 (2018).
123. Potroz, M. G. & Cho, N. J. Natural Products for the Treatment of Trachoma and Chlamydia trachomatis. *Molecules* 2015, Vol. 20, Pages 4180-4203 **20**, 4180–4203 (2015).
124. Chlamydia. <https://www.who.int/news-room/fact-sheets/detail/chlamydia>.
125. Tjahyadi, D. *et al.* Female urogenital chlamydia: Epidemiology, chlamydia on pregnancy, current diagnosis, and treatment. *Annals of Medicine and Surgery* **75**, 103448 (2022).
126. Joffe, G. P. *et al.* Multiple partners and partner choice as risk factors for sexually transmitted disease among female college students. *Sex Transm Dis* **19**, 272–278 (1992).
127. Wilson Chialepeh, N. & Sathiyasuman, A. Associated Risk Factors of STIs and Multiple Sexual Relationships among Youths in Malawi. *PLoS One* **10**, e0134286 (2015).
128. Althaus, C. L. *et al.* Transmission of Chlamydia trachomatis through sexual partnerships: a comparison between three individual-based models and empirical data. *J R Soc Interface* **9**, 136 (2011).
129. De Clercq, E., Kalmar, I. & Vanrompay, D. Animal Models for Studying Female Genital Tract Infection with Chlamydia trachomatis. *Infect Immun* **81**, 3060 (2013).
130. Nigg, C. An unidentified virus which produces pneumonia and systemic infection in mice. *Science (1979)* **95**, 49–50 (1942).
131. Barron, A. L., White, H. J., Rank, R. G., Soloff, B. L. & Moses, E. B. A New Animal Model for the Study of Chlamydia trachomatis Genital Infections: Infection of Mice with the Agent of Mouse Pneumonitis. *Journal of Infectious Diseases* **143**, 63–66 (1981).
132. De la Maza, L. M., Pal, S., Khamesipour, A. & Peterson, E. M. Intravaginal inoculation of mice with the Chlamydia trachomatis mouse pneumonitis biovar results in infertility. *Infect Immun* **62**, 2094–2097 (1994).

133. Gondek, D. C., Olive, A. J., Stary, G. & Starnbach, M. N. CD4⁺ T cells are necessary and sufficient to confer protection against Chlamydia trachomatis infection in the murine upper genital tract. *J Immunol* **189**, 2441–2449 (2012).
134. Darville, T. *et al.* Mouse strain-dependent variation in the course and outcome of chlamydial genital tract infection is associated with differences in host response. *Infect Immun* **65**, 3065–3073 (1997).
135. Bernstein-Hanley, I. *et al.* Genetic analysis of susceptibility to Chlamydia trachomatis in mouse. *Genes Immun* **7**, 122–129 (2006).
136. De la Maza, L. M., Pal, S., Khamesipour, A. & Peterson, E. M. Intravaginal inoculation of mice with the Chlamydia trachomatis mouse pneumonitis biovar results in infertility. *Infect Immun* **62**, 2094–2097 (1994).
137. Pal, S., Hui, W., Peterson, E. M. & De La Maza, L. M. Factors influencing the induction of infertility in a mouse model of Chlamydia trachomatis ascending genital tract infection. *J Med Microbiol* **47**, 599–605 (1998).
138. Tuffrey, M., Lett, D. T.-R.-F. M. & 1981, undefined. Progesterone as a key factor in the development of a mouse model for genital-tract infection with Chlamydia trachomatis. *academia.eduM Tuffrey, D Taylor-RobinsonFEMS Microbiol Lett, 1981•academia.edu.*
139. Gravitte, A. *et al.* The hormonal environment and estrogen receptor signaling alters Chlamydia muridarum infection in vivo. *Front Cell Infect Microbiol* **12**, 939944 (2022).
140. Su, S. *et al.* Modulation of innate immune response to viruses including SARS-CoV-2 by progesterone. *Signal Transduct Target Ther* **7**, 137 (2022).
141. Davis, S. M., Sweet, L. M., Oppenheimer, K. H., Suratt, B. T. & Phillippe, M. Estradiol and Progesterone Influence on Influenza Infection and Immune Response in a Mouse Model. *Am J Reprod Immunol* **78**, 10.1111/aji.12695 (2017).
142. Tuffrey, M., Lett, D. T.-R.-F. M. & 1981, undefined. Progesterone as a key factor in the development of a mouse model for genital-tract infection with Chlamydia trachomatis. *academia.eduM Tuffrey, D Taylor-RobinsonFEMS Microbiol Lett, 1981•academia.edu.*
143. Yu, H. *et al.* Chlamydia muridarum Induces Pathology in the Female Upper Genital Tract via Distinct Mechanisms. *Infect Immun* **87**, (2019).
144. Morrison, S. G., Farris, C. M., Sturdevant, G. L., Whitmire, W. M. & Morrison, R. P. Murine Chlamydia trachomatis Genital Infection Is Unaltered by Depletion of CD4⁺ T cells and Diminished Adaptive Immunity. *J Infect Dis* **203**, 1120 (2011).
145. Coers, J. *et al.* Compensatory T Cell Responses in IRG-Deficient Mice Prevent Sustained Chlamydia trachomatis Infections. *PLoS Pathog* **7**, e1001346 (2011).
146. Lyons, J. M., Ito, J. I., Peña, A. S. & Morré, S. A. Differences in growth characteristics and elementary body associated cytotoxicity between Chlamydia trachomatis oculogenital serovars D and H and Chlamydia muridarum. *J Clin Pathol* **58**, 397 (2005).
147. Pajot, A. *et al.* A mouse model of human adaptive immune functions: HLA-A2.1-/HLA-DR1-transgenic H-2 class I-/class II-knockout mice. *Eur J Immunol* **34**, 3060–9 (2004).
148. Drexler, I. *et al.* Identification of vaccinia virus epitope-specific HLA-A*0201-restricted T cells and comparative analysis of smallpox vaccines. *Proceedings of the National Academy of Sciences* **100**, 217–222 (2003).
149. Schumacher, T. *et al.* A vaccine targeting mutant IDH1 induces antitumour immunity. *Nature* **512**, 324–327 (2014).
150. Liu, H., Shen, W., Shu, J., Kou, Z. & Jin, X. A novel polyepitope vaccine elicited HIV peptide specific CD4⁺ T cell responses in HLA-A2/DRB1 transgenic mice. *PLoS One* **12**, e0184207 (2017).
151. Kruse, S. *et al.* Therapeutic vaccination using minimal HPV16 epitopes in a novel MHC-humanized murine HPV tumor model. *Oncimmunology* **8**, (2019).
152. Vu, P. Le *et al.* A Mutated Prostatic Acid Phosphatase (PAP) Peptide-Based Vaccine Induces PAP-Specific CD8⁺ T Cells with Ex Vivo Cytotoxic Capacities in HHDII/DR1 Transgenic Mice. *Cancers (Basel)* **14**, 1970 (2022).
153. Peng, S. *et al.* Identification of human MHC-I HPV18 E6/E7-specific CD8⁺ T cell epitopes and generation of an HPV18 E6/E7-expressing adenosquamous carcinoma in HLA-A2 transgenic mice. *J Biomed Sci* **29**, 80 (2022).
154. Conforti, A. *et al.* A Novel Mouse Model for Evaluation and Prediction of HLA-A2-restricted CEA Cancer Vaccine Responses. *Journal of Immunotherapy* **32**, 744–754 (2009).
155. Tammiruusu, A. *et al.* Clearance of Chlamydia pneumoniae infection in H-2 class I human leucocyte antigen-A2.1 monochain transgenic mice. *Scand J Immunol* **62**, 131–139 (2005).

156. Brunham, R. C. & Rey-Ladino, J. Immunology of Chlamydia infection: implications for a Chlamydia trachomatis vaccine. *Nature Reviews Immunology* 2005 5:2 **5**, 149–161 (2005).
157. Matyszak, M. K., Young, J. L. & Gaston, J. S. H. Uptake and processing of Chlamydia trachomatis by human dendritic cells. *Eur J Immunol* **32**, 742 (2002).
158. Shaw, J. H., Grund, V. R., Durling, L. & Caldwell, H. D. Expression of genes encoding Th1 cell-activating cytokines and lymphoid homing chemokines by chlamydia-pulsed dendritic cells correlates with protective immunizing efficacy. *Infect Immun* **69**, 4667–4672 (2001).
159. Labuda, J. C. & McSorley, S. J. Diversity in the T cell response to Chlamydia-sum are better than one. *Immunol Lett* **202**, 59–64 (2018).
160. Rey-Ladino, J., Koochesfahani, K. M., Zaharik, M. L., Shen, C. & Brunham, R. C. A live and inactivated Chlamydia trachomatis mouse pneumonitis strain induces the maturation of dendritic cells that are phenotypically and immunologically distinct. *Infect Immun* **73**, 1568–1577 (2005).
161. Stone, L. T cell response to C. trachomatis. *Nature Reviews Urology* 2016 13:12 **13**, 692–692 (2016).
162. Wizel, B., Nyström-Asklin, J., Cortes, C. & Tvinnereim, A. Role of CD8+ T cells in the host response to Chlamydia. *Microbes and infection / Institut Pasteur* **10**, 1420 (2008).
163. Starnbach, M. N. *et al.* An Inclusion Membrane Protein from *Chlamydia trachomatis* Enters the MHC Class I Pathway and Stimulates a CD8+ T Cell Response. *The Journal of Immunology* **171**, 4742–4749 (2003).
164. Grotenbreg, G. M. *et al.* Discovery of CD8 + T cell epitopes in *Chlamydia trachomatis* infection through use of caged class I MHC tetramers. *Proceedings of the National Academy of Sciences* **105**, 3831–3836 (2008).
165. Roan, N. R. & Starnbach, M. N. Antigen-Specific CD8+ T Cells Respond to Chlamydia trachomatis in the Genital Mucosa . *The Journal of Immunology* **177**, 7974–7979 (2006).
166. Martin, M. D. & Badovinac, V. P. Defining memory CD8 T cell. *Front Immunol* **9**, 416271 (2018).
167. Loomis, W. P. & Starnbach, M. N. Chlamydia trachomatis Infection Alters the Development of Memory CD8+ T Cells. *The Journal of Immunology* **177**, 4021–4027 (2006).
168. Zhang, X. & Starnbach, M. N. An Excess of the Proinflammatory Cytokines IFN-γ and IL-12 Impairs the Development of the Memory CD8+ T Cell Response to *Chlamydia trachomatis*. *The Journal of Immunology* **195**, 1665–1675 (2015).
169. Fankhauser, S. C. & Starnbach, M. N. PD-L1 Limits the Mucosal CD8+ T Cell Response to *Chlamydia trachomatis*. *The Journal of Immunology* **192**, 1079–1090 (2014).
170. Peng, B. *et al.* Enhanced upper genital tract pathologies by blocking Tim-3 and PD-L1 signaling pathways in mice intravaginally infected with Chlamydia muridarum. *BMC Infect Dis* **11**, (2011).
171. Vlcek, K. R. *et al.* The Contribution of Chlamydia-Specific CD8+ T Cells to Upper Genital Tract Pathology. *Immunol Cell Biol* **94**, 208 (2015).
172. Zhou, Z. *et al.* Characterization of Pathogenic CD8 + T cells in Chlamydia-Infected OT1 Mice. *Infect Immun* **90**, (2022).
173. Olive, A. J., Gondek, D. C. & Starnbach, M. N. CXCR3 and CCR5 are both required for T cell-mediated protection against C. trachomatis infection in the murine genital mucosa. *Mucosal Immunol* **4**, 208–216 (2011).
174. Nicolle: Etude expérimentale du trachome: conjonctivite... - Google Scholar. https://scholar.google.com/scholar_lookup?journal=Arch%20Inst%20Pasteur%20Tunis&title=Etude%20experimentale%20du%20trachome&author=C%20Nicolle&author=A%20Cuend&author=L%20Baizot&volume=4&publication_year=1913&pages=157-182&
175. Grayston, J. T., Woolridge, R. L. & Wang, S. -p. TRACHOMA VACCINE STUDIES ON TAIWAN*. *Ann N Y Acad Sci* **98**, 352–367 (1962).
176. Collier, L. H. & Blyth, W. A. Immunogenicity of experimental trachoma vaccines in baboons. I. Experimental methods, and preliminary tests with vaccines prepared in chick embryos and in HeLa cells. *J Hyg (Lond)* **64**, 513 (1966).
177. BELL, S. D., NICHOLS, R. L. & HADDAD, N. A. THE IMMUNOLOGY OF THE TRACHOMA AGENT WITH A PRELIMINARY REPORT ON FIELD TRIALS ON VACCINE. *Invest Ophthalmol* **2**, 471–81 (1963).
178. Pal, S., Theodor, I., Peterson, E. M. & De la Maza, L. M. Immunization with an acellular vaccine consisting of the outer membrane complex of Chlamydia trachomatis induces protection against a genital challenge. *Infect Immun* **65**, 3361 (1997).

179. de la Maza, L. M., Darville, T. L. & Pal, S. Chlamydia vaccines: where are we and how far is there to go? *Expert Rev Vaccines* **20**, 421 (2021).
180. Baehr, W. *et al.* Mapping antigenic domains expressed by Chlamydia trachomatis major outer membrane protein genes. *Proc Natl Acad Sci U S A* **85**, 4000–4004 (1988).
181. Salari, S. H. & Ward, M. E. Polypeptide composition of Chlamydia trachomatis. *J Gen Microbiol* **123**, 197–207 (1981).
182. Yuan, Y., Zhang, Y. X., Watkins, N. G. & Caldwell, H. D. Nucleotide and deduced amino acid sequences for the four variable domains of the major outer membrane proteins of the 15 Chlamydia trachomatis serovars. *Infect Immun* **57**, 1040–1049 (1989).
183. Phillips, S., Quigley, B. L. & Timms, P. Seventy years of Chlamydia vaccine research - Limitations of the past and directions for the future. *Front Microbiol* **10**, 70 (2019).
184. Pal, S., Theodor, I., Peterson, E. M. & De la Maza, L. M. Immunization with the Chlamydia trachomatis mouse pneumonitis major outer membrane protein can elicit a protective immune response against a genital challenge. *Infect Immun* **69**, 6240–6247 (2001).
185. Hansen, J. *et al.* Liposome Delivery of Chlamydia muridarum Major Outer Membrane Protein Primes a Th1 Response That Protects against Genital Chlamydial Infection in a Mouse Model. *J Infect Dis* **198**, 758–767 (2008).
186. Olsen, A. W., Follmann, F., Erneholm, K., Rosenkrands, I. & Andersen, P. Protection Against Chlamydia trachomatis Infection and Upper Genital Tract Pathological Changes by Vaccine-Promoted Neutralizing Antibodies Directed to the VD4 of the Major Outer Membrane Protein. *Journal of Infectious Diseases* **212**, 978–989 (2015).
187. Olsen, A. W. *et al.* Immune signature of Chlamydia vaccine CTH522/CAF®01 translates from mouse-to-human and induces durable protection in mice. *Nat Commun* **15**, 1665 (2024).
188. Singh, V., Salhan, S., Das, B. C. & Mittal, A. Predominance of Chlamydia trachomatis Serovars Associated with Urogenital Infections in Females in New Delhi, India. *J Clin Microbiol* **41**, 2700 (2003).
189. Yang, B. *et al.* The Prevalence and Distribution of Chlamydia trachomatis Genotypes among Sexually Transmitted Disease Clinic Patients in Guangzhou, China, 2005–2008. *Jpn. J. Infect. Dis* **63**, 342–345 (2010).
190. Lesiak-Markowicz, I., Schötta, A.-M., Stockinger, H., Stanek, G. & Markowicz, M. Chlamydia trachomatis serovars in urogenital and ocular samples collected 2014–2017 from Austrian patients. *Sci Rep* **9**, 18327 (2019).
191. Abraham, S. *et al.* Safety and immunogenicity of the chlamydia vaccine candidate CTH522 adjuvanted with CAF01 liposomes or aluminium hydroxide: a first-in-human, randomised, double-blind, placebo-controlled, phase 1 trial. *Lancet Infect Dis* **19**, 1091–1100 (2019).
192. Pollock, K. M. *et al.* An investigation of trachoma vaccine regimens by the chlamydia vaccine CTH522 administered with cationic liposomes in healthy adults (CHLM-02): a phase 1, double-blind trial. *Lancet Infect Dis* (2024) doi:10.1016/S1473-3099(24)00147-6.
193. Cottingham, M. G. & Gilbert, S. C. Rapid generation of markerless recombinant MVA vaccines by en passant recombineering of a self-excising bacterial artificial chromosome. *J Virol Methods* **168**, 233–236 (2010).
194. Kugler, F., Drexler, I., Protzer, U., Hoffmann, D. & Moeini, H. Generation of recombinant MVA-norovirus: a comparison study of bacterial artificial chromosome- and marker-based systems. *Virol J* **16**, 100 (2019).
195. Waguia Kontchou, C. *et al.* Chlamydia trachomatis inhibits apoptosis in infected cells by targeting the pro-apoptotic proteins Bax and Bak. *Cell Death Differ* **29**, 2046 (2022).
196. Orlova, O. V., Glazkova, D. V., Bogoslovskaya, E. V., Shipulin, G. A. & Yudin, S. M. Development of Modified Vaccinia Virus Ankara-Based Vaccines: Advantages and Applications. *Vaccines (Basel)* **10**, 1516 (2022).
197. Kim, S. K. *et al.* Induction of HLA class I-restricted CD8+ CTLs specific for the major outer membrane protein of Chlamydia trachomatis in human genital tract infections. *J Immunol* **162**, 6855–66 (1999).
198. *Global Progress Report on HIV, Viral Hepatitis and Sexually Transmitted Infections, 2021. Accountability for the Global Health Sector Strategies 2016–2021: Actions for Impact. Geneva: World Health Organization; 2021. Licence: CC BY-NC-SA 3.0 IGO.*
199. Rey-Ladino, J., Ross, A. G. P. & Cripps, A. W. Immunity, immunopathology, and human vaccine development against sexually transmitted Chlamydia trachomatis. *Hum Vaccin Immunother* **10**, 2664 (2014).
200. Yu, H. *et al.* Neutralizing Antibody Responses to Chlamydia trachomatis in Women and Associations With Chlamydia Outcomes. *J Infect Dis* (2024) doi:10.1093/INFDIS/JIAE519.

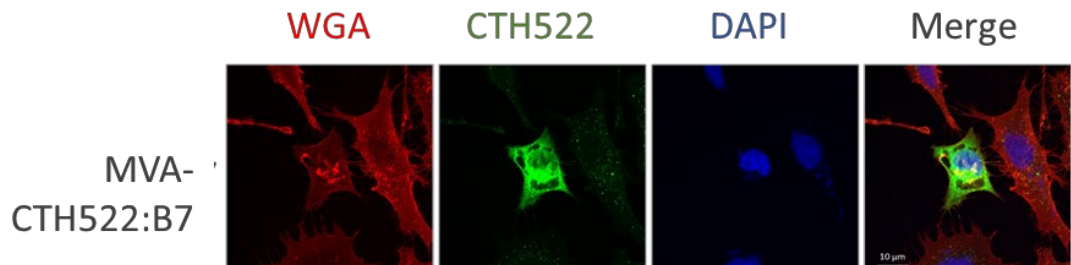
201. Darville, T. *et al.* Anti-chlamydia IgG and IgA are insufficient to prevent endometrial Chlamydia infection in women and increased anti-chlamydia IgG is associated with enhanced risk for incident infection. *Am J Reprod Immunol* **81**, e13103 (2019).
202. Russell, A. N. *et al.* Identification of *Chlamydia trachomatis* Antigens Recognized by T Cells From Highly Exposed Women Who Limit or Resist Genital Tract Infection. *Journal of Infectious Diseases* **214**, 1884–1892 (2016).
203. De Clercq, E., Kalmar, I. & Vanrompay, D. Animal Models for Studying Female Genital Tract Infection with *Chlamydia trachomatis*. *Infect Immun* **81**, 3060–3067 (2013).
204. Yang, X., Gartner, J., Zhu, L., Wang, S. & Brunham, R. C. IL-10 Gene Knockout Mice Show Enhanced Th1-Like Protective Immunity and Absent Granuloma Formation Following *Chlamydia trachomatis* Lung Infection. *The Journal of Immunology* **162**, 1010–1017 (1999).
205. Morrison, S. G. & Morrison, R. P. A Predominant Role for Antibody in Acquired Immunity to Chlamydial Genital Tract Reinfection. *J Immunol* **175**, 7536 (2005).
206. Farris, C. M. & Morrison, R. P. Vaccination against Chlamydia Genital Infection Utilizing the Murine *C. muridarum* Model. *Infect Immun* **79**, 986 (2010).
207. Pal, S., Theodor, I., Peterson, E. M. & De la Maza, L. M. Monoclonal immunoglobulin A antibody to the major outer membrane protein of the *Chlamydia trachomatis* mouse pneumonitis biovar protects mice against a chlamydial genital challenge. *Vaccine* **15**, 575–582 (1997).
208. Manam, S., Nicholson, B. J. & Murthy, A. K. OT-1 mice display minimal upper genital tract pathology following primary intravaginal *Chlamydia muridarum* infection. *Pathog Dis* **67**, 221–224 (2013).
209. Lijek, R. S., Helble, J. D., Olive, A. J., Seiger, K. W. & Starnbach, M. N. Pathology after chlamydia trachomatis infection is driven by nonprotective immune cells that are distinct from protective populations. *Proc Natl Acad Sci U S A* **115**, 2216–2221 (2018).
210. Morrison, R. P., Belland, R. J., Lyng, K. & Caldwell, H. D. Chlamydial disease pathogenesis. The 57-kD chlamydial hypersensitivity antigen is a stress response protein. *J Exp Med* **170**, 1271 (1989).
211. Stry, G. *et al.* A mucosal vaccine against *Chlamydia trachomatis* generates two waves of protective memory T cells. *Science* (1979) **348**, (2015).
212. Geraghty, R. J. *et al.* Guidelines for the use of cell lines in biomedical research. *British Journal of Cancer* *2014* **111**:6 **111**, 1021–1046 (2014).
213. Puetz, J. & Wurm, F. M. Recombinant Proteins for Industrial versus Pharmaceutical Purposes: A Review of Process and Pricing. *Processes* *2019*, *Vol. 7*, *Page 476* **7**, 476 (2019).
214. Sun, G., Pal, S., Weiland, J., Peterson, E. M. & de la Maza, L. M. Protection against an intranasal challenge by vaccines formulated with native and recombinant preparations of the *Chlamydia trachomatis* major outer membrane protein. *Vaccine* **27**, 5020–5025 (2009).
215. Ralli-Jain, P., Tifrea, D., Cheng, C., Pal, S. & de la Maza, L. M. Enhancement of the protective efficacy of a *Chlamydia trachomatis* recombinant vaccine by combining systemic and mucosal routes for immunization. *Vaccine* **28**, 7659–7666 (2010).
216. Tifrea, D. F., Pal, S. & de la Maza, L. M. A Recombinant *Chlamydia trachomatis* MOMP Vaccine Elicits Cross-serogroup Protection in Mice Against Vaginal Shedding and Infertility. *J Infect Dis* **221**, 191–200 (2020).
217. Pollard, A. J. & Bijker, E. M. A guide to vaccinology: from basic principles to new developments. *Nature Reviews Immunology* *2020* **21**:2 **21**, 83–100 (2020).
218. Vishweshwaraiah, Y. L. & Dokholyan, N. V. Toward rational vaccine engineering. *Adv Drug Deliv Rev* **183**, 114142 (2022).
219. Coffman, R. L., Sher, A. & Seder, R. A. Vaccine Adjuvants: Putting Innate Immunity to Work. *Immunity* **33**, 492 (2010).
220. Flaxman, S. R. *et al.* Global causes of blindness and distance vision impairment 1990–2020: a systematic review and meta-analysis. *Lancet Glob Health* **5**, e1221–e1234 (2017).
221. Mabey, D. C. W., Hu, V., Bailey, R. L., Burton, M. J. & Holland, M. J. Towards a safe and effective chlamydial vaccine: Lessons from the eye. *Vaccine* **32**, 1572–1578 (2014).
222. de Vrieze, N. H. N. & de Vries, H. J. C. Lymphogranuloma venereum among men who have sex with men. An epidemiological and clinical review. *Expert Rev Anti Infect Ther* **12**, 697–704 (2014).
223. Burgener, A.-V. *et al.* A Case Study of Zoonotic *Chlamydia abortus* Infection: Diagnostic Challenges From Clinical and Microbiological Perspectives. *Open Forum Infect Dis* **9**, (2022).
224. Pichon, N. *et al.* *Chlamydia abortus* in Pregnant Woman with Acute Respiratory Distress Syndrome. *Emerg Infect Dis* **26**, 628–629 (2020).

225. Ramsey, K. H., DeWolfe, J. L. & Salyer, R. D. Disease Outcome Subsequent to Primary and Secondary Urogenital Infection with Murine or Human Biovars of *Chlamydia trachomatis*. *Infect Immun* **68**, 7186–7189 (2000).
226. Carmichael, J. R., Tifrea, D., Pal, S. & de la Maza, L. M. Differences in infectivity and induction of infertility: a comparative study of *Chlamydia trachomatis* strains in the murine model. *Microbes Infect* **15**, 219–229 (2013).
227. Zhang, Z. X. *et al.* Strategies for efficient production of recombinant proteins in *Escherichia coli*: alleviating the host burden and enhancing protein activity. *Microbial Cell Factories* **2022** *21:1* **21**, 1–18 (2022).
228. Seid, C. A. *et al.* Cysteine mutagenesis improves the production without abrogating antigenicity of a recombinant protein vaccine candidate for human chagas disease. *Hum Vaccin Immunother* **13**, 621 (2016).
229. Chen, W., Yewdell, J. W., Levine, R. L. & Bennink, J. R. Modification of Cysteine Residues In Vitro and In Vivo Affects the Immunogenicity and Antigenicity of Major Histocompatibility Complex Class I-restricted Viral Determinants. *J Exp Med* **189**, 1757 (1999).
230. Zhang, C., Anderson, A. & DeLisi, C. Structural principles that govern the peptide-binding motifs of class I MHC molecules. *J Mol Biol* **281**, 929–947 (1998).
231. Agerer, B. *et al.* SARS-CoV-2 mutations in MHC-I-restricted epitopes evade CD8⁺ T cell responses. *Sci Immunol* **6**, eabg6461 (2021).
232. Carlson, J. M. *et al.* Correlates of Protective Cellular Immunity Revealed by Analysis of Population-Level Immune Escape Pathways in HIV-1. *J Virol* **86**, 13202 (2012).
233. Wilson, K. L., Xiang, S. D. & Plebanski, M. Functional Recognition by CD8⁺ T Cells of Epitopes with Amino Acid Variations Outside Known MHC Anchor or T Cell Receptor Recognition Residues. *Int J Mol Sci* **21**, 4700 (2020).
234. Ossendorp, F. *et al.* A single residue exchange within a viral CTL epitope alters proteasome-mediated degradation resulting in lack of antigen presentation. *Immunity* **5**, 115–124 (1996).
235. Kimura, Y., Gushima, T., Rawale, S., Kaumaya, P. & Walker, C. M. Escape Mutations Alter Proteasome Processing of Major Histocompatibility Complex Class I-Restricted Epitopes in Persistent Hepatitis C Virus Infection. *J Virol* **79**, 4870 (2005).
236. Kaynarcalidan, O., Moreno Mascaraque, S. & Drexler, I. Vaccinia virus: From crude smallpox vaccines to elaborate viral vector vaccine design. *Biomedicines* vol. 9 Preprint at <https://doi.org/10.3390/biomedicines9121780> (2021).
237. Becker, P. *et al.* Gene Expression Driven by a Strong Viral Promoter in MVA Increases Vaccination Efficiency by Enhancing Antibody Responses and Unmasking CD8⁺ T Cell Epitopes. *Vaccines (Basel)* **2**, 581–600 (2014).
238. Lanzavecchia, A. & Sallusto, F. Progressive differentiation and selection of the fittest in the immune response. *Nat Rev Immunol* **2**, 982–987 (2002).
239. Olsen, A. W., Rosenkrands, I., Holland, M. J., Andersen, P. & Follmann, F. A *Chlamydia trachomatis* VD1-MOMP vaccine elicits cross-neutralizing and protective antibodies against C/C-related complex serovars. *NPJ Vaccines* **6**, 58 (2021).
240. Collar, A. L., Linville, A. C., Core, S. B. & Fritze, K. M. Epitope-Based Vaccines against the *Chlamydia trachomatis* Major Outer Membrane Protein Variable Domain 4 Elicit Protection in Mice. *Vaccines (Basel)* **10**, (2022).
241. Roe, S. K. *et al.* Structural Assessment of *Chlamydia trachomatis* Major Outer Membrane Protein (MOMP)-Derived Vaccine Antigens and Immunological Profiling in Mice with Different Genetic Backgrounds. *Vaccines (Basel)* **12**, (2024).
242. Huynh, D. T. *et al.* Intranasal delivery of *Salmonella* OMVs decorated with *Chlamydia trachomatis* antigens induces specific local and systemic immune responses. *Hum Vaccin Immunother* **20**, (2024).
243. Kastenmuller, W. *et al.* Cross-competition of CD8⁺ T cells shapes the immunodominance hierarchy during boost vaccination. *J Exp Med* **204**, 2187–2198 (2007).
244. Tang, X., Zhang, W. & Zhang, Z. Developing T Cell Epitope-Based Vaccines Against Infection: Challenging but Worthwhile. *Vaccines* **2025**, Vol. 13, Page 135 **13**, 135 (2025).
245. Muschaweckh, A. *et al.* Antigen-dependent competition shapes the local repertoire of tissue-resident memory CD8⁺ T cells. *Journal of Experimental Medicine* **213**, 3075–3086 (2016).
246. Pal, S., Peterson, E. M. & de la Maza, L. M. Vaccination with the *Chlamydia trachomatis* Major Outer Membrane Protein Can Elicit an Immune Response as Protective as That Resulting from Inoculation with Live Bacteria. *Infect Immun* **73**, 8153–8160 (2005).
247. Gill, N., Wlodarska, M. & Finlay, B. B. The future of mucosal immunology: studying an integrated system-wide organ. *Nature Immunology* **2010** *11:7* **11**, 558–560 (2010).

248. Nizard, M. *et al.* Mucosal vaccines: Novel strategies and applications for the control of pathogens and tumors at mucosal sites. *Hum Vaccin Immunother* **10**, 2175 (2014).
249. Pal, S., Peterson, E. M. & De la Maza, L. M. Intranasal immunization induces long-term protection in mice against a Chlamydia trachomatis genital challenge. *Infect Immun* **64**, 5341–5348 (1996).
250. Nguyen, N. D. N. T. *et al.* Parenteral vaccination protects against transcervical infection with Chlamydia trachomatis and generate tissue-resident T cells post-challenge. *NPJ Vaccines* **5**, 7 (2020).
251. Nguyen, N. D. N. T. *et al.* Th1/Th17 T cell Tissue-Resident Immunity Increases Protection, But Is Not Required in a Vaccine Strategy Against Genital Infection With Chlamydia trachomatis. *Front Immunol* **12**, (2021).
252. Rotrosen, E. & Kupper, T. S. Assessing the generation of tissue resident memory T cells by vaccines. *Nat Rev Immunol* **23**, 655–665 (2023).
253. Kastenmuller, W., Gasteiger, G., Stross, L., Busch, D. H. & Drexler, I. Cutting edge: mucosal application of a lyophilized viral vector vaccine confers systemic and protective immunity toward intracellular pathogens. *J Immunol* **182**, 2573–2577 (2009).
254. Bissett, C. *et al.* Systemic prime mucosal boost significantly increases protective efficacy of bivalent RSV influenza viral vectored vaccine. *npj Vaccines* **2024 9:1 9**, 1–14 (2024).
255. Schulze, K. *et al.* A prime-boost vaccination protocol optimizes immune responses against the nucleocapsid protein of the SARS coronavirus. *Vaccine* **26**, 6678 (2008).
256. Bošnjak, B. *et al.* Intranasal Delivery of MVA Vector Vaccine Induces Effective Pulmonary Immunity Against SARS-CoV-2 in Rodents. *Front Immunol* **12**, 772240 (2021).

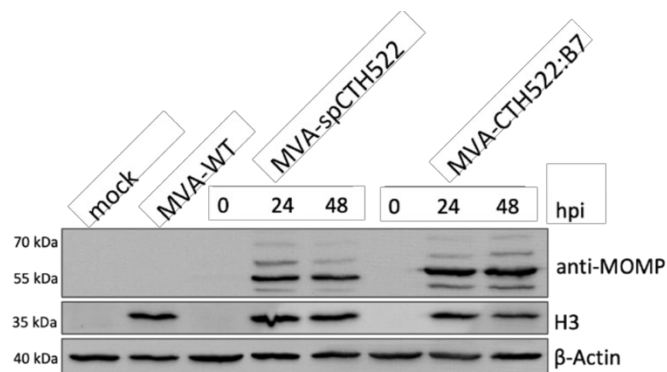
8. Appendix

8.1. Supplementary material



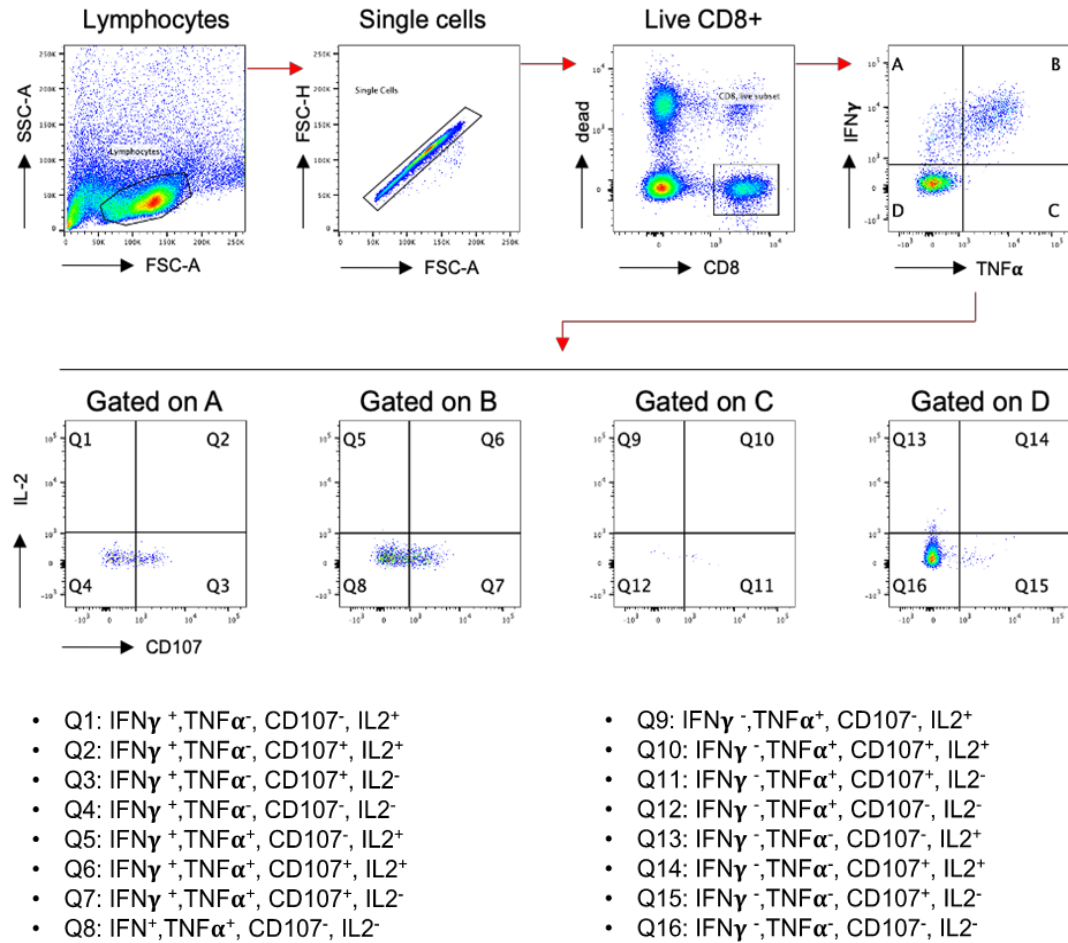
Supplementary figure 1. CTH522:B7 expressed by rec MVA localizes to the cell surface membrane.

Immunofluorescence microscopy was used to determine the localization of CTH522:B7 proteins in HeLa cells infected with MVA-spCTH522, MVA-CTH522:B7 or MVA-WT (as shown in Fig. 16) at a MOI of 5, fixed 6 hours post infection and stained under non-permeabilized conditions. The cell surface was labelled with a WGA probe conjugated to Alexa Fluor 594 (red), while MOMP protein was detected with a mouse monoclonal anti-MOMP antibody and visualized with a mouse secondary antibody conjugated to Alexa Fluor 488 (green). Cell nuclei were counterstained with DAPI (blue). Scale bars: 10 µm.



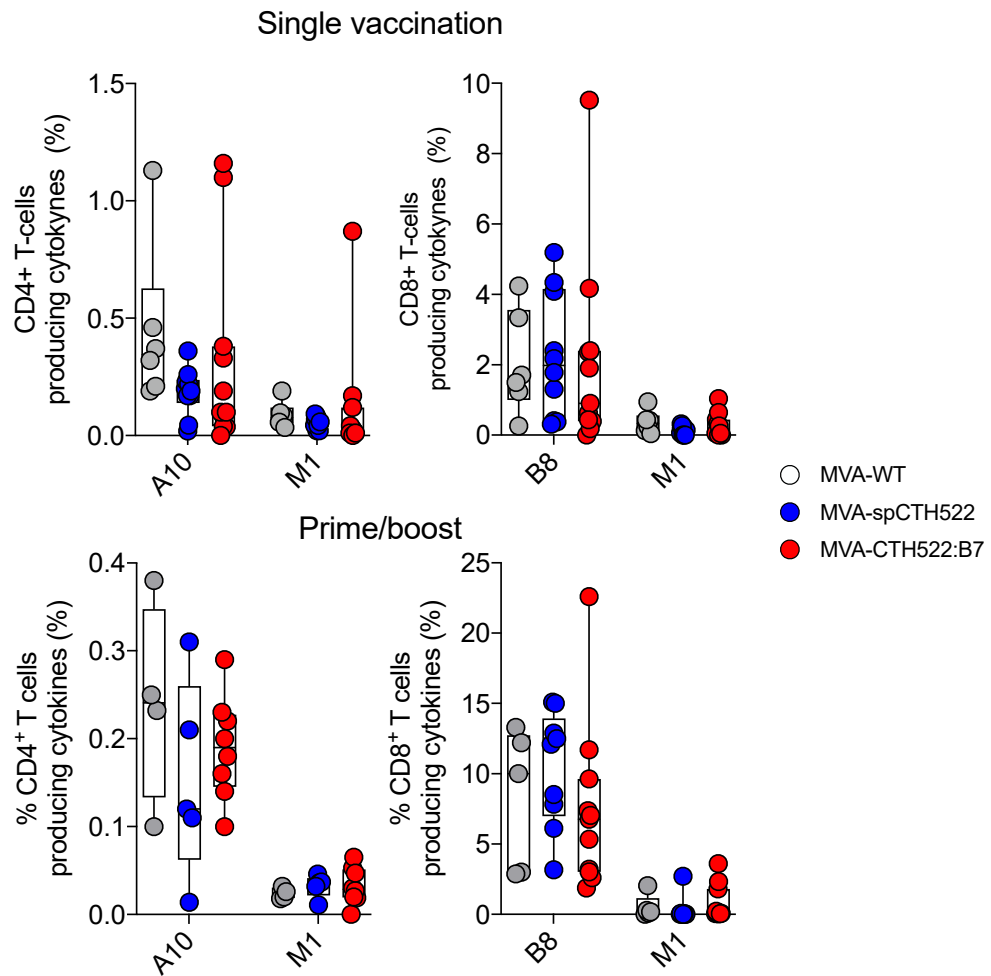
Supplementary figure 2. MVA-spCTH522 and MVA-CTH522:B7 synthesized recombinant antigens upon *in vitro* infection.

HeLa cells were mock-infected or infected with MVA-WT, MVA-spCTH522 or MVA-CTH522:B7 (MOI = 5). Cells were lysed at 0, 24 or 48 h.p.i. (MVA-spCTH522 or MVA-CTH522:B7) or at 48 h.p.i. (mock or MVA-WT). Whole cell lysates were analyzed by western blotting with antibodies against MOMP-SvD, displaying recombinant proteins with an expected size of ~57.4 kDa for spCTH522 and ~63.9 kDa for CTH522:B7. Vaccinia virus H3 protein (~37.5 kDa) and b-actin (~42 kDa) were used as infection and loading controls, respectively.



Supplementary figure 3. Representative flow cytometry plots demonstrating the gating strategy for the analysis of epitope-specific multifunctional CD8⁺ T-cells in the spleen.

Splenocytes from MVA-CTH522:B7 immunized HLA-A2.DR1 mice following the prime/boost (Fig.17) regimen were restimulated *in vitro* with MOMP₂₈₂₋₂₉₀ for 5-6h. After ICS, splenocytes were analyzed by flow cytometry by gating on lymphocytes, single cells, and CD8⁺ live cells (upper plots). CD8⁺ T-cells were then plotted regarding IFN- γ (x-axis) and TNF- α (y-axis) production, resulting in four populations, A (IFN- γ ⁺, TNF- α ⁻), B (IFN- γ ⁺, TNF- α ⁺), C (IFN- γ ⁻, TNF- α ⁺), and D (IFN- γ ⁻, TNF- α ⁻). (Lower plots) A, B, C, and D populations were further plotted regarding IL-2 (x-axis) and CD107 (y-axis) production. This strategy allowed to analyze all the possible combinations of IFN- γ , TNF- α , IL-2, and CD107 producing cells, resulting in 16 different populations, Q1 to Q16. Each population was then calculated as a percentage of total CD8⁺ live cells using FlowJo software.



Supplementary figure 4. Single dose and prime/boost vaccination regimens with MVA-spCTH522 and MVA-CTH522:B7 induce MVA-specific CD8⁺ and CD4⁺ T-cell responses.

HLA-A2.DR1 mice were immunized i.p. with 10^7 TCID₅₀ of MVA-WT (n=6), MVA-spCTH522 (n=10), or MVA-CTH522:B7 (n=11) in a single vaccination (as shown in Fig. 17) in four independent experiments or primed with 10^7 TCID₅₀ of MVA-WT (n=5), MVA-spCTH522 (n=9), or MVA-CTH522:B7 (n=11) and boosted with 10^8 TCID₅₀ on day 28 (as shown in Fig. 24) in four independent experiments. Splenocytes from immunized mice were restimulated with MVA-derived B8₂₀₋₂₇ or A10₂₉₃₋₃₀₇ peptides for CD8⁺ or CD4⁺ T-cell activation, respectively. Cytokine production (IFN- γ and TNF α) was measured by ICS assay followed by FACS analysis. Overall percentage of CD8⁺ and CD4⁺ T-cells producing IFN- γ and TNF- α , here referred as cytokines (calculated by summing the percentages of CD8⁺ or CD4⁺ T cells positive for IFN γ only, TNF α only, and double positive for both IFN γ and TNF α). These populations were determined by using Boolean combination of gates, as shown in supplementary fig. 4). Peptides derived from Matrix protein 1 (M1) of Influenza virus were used as negative controls for CD8⁺ (M1₅₈₋₆₆) and CD4⁺ (M1₁₇₋₃₀) T-cell responses.

>Amino acid sequence of CTH522

MGDAISM RVGYGDFV FDRVLKTDVNKEFQMGAKPTTDTGNSAAPSTLT
ARENPAYGRHMQDAEMFTNAACMALNIWDRFDVFCTLGATSGYLKGN
SASFNLVGLFGDNENQKTVKAESVPNMSFDQSVVELYTDTTFAWSVGAR
ALWECGCATLGASFQYAQSKPKVEELNVL CNAAEFTINKPKGYVGKEFPL
DLTAGTDAATGTKDASIDYHEWQASLALSYRLNMFTPYIGVKWSRASFD
ADTIRIAQPKSATAIFDTTTTLNPTIAGAGDVKTGAEGQLGDTMQIVSLQLN
NMFTPYIGVKWSRASFDADTIRIAQPKSATAIFDTTTTLNPTIAGAGDVKAS
AEGQLGDTMQIVSLQLNNMFTPYIGVKWSRASFDSDTIRIAQPRLVTPVVD
ITTLNPTIAGCGSVAGANTEGQISDTMQIVSLQLNNMFTPYIGVKWSRAS
FDSNTIRIAQPKLAKPVVDITTLNPTIAGCGSVVAANSEGQISDTMQIVSLQL
N*

>Amino acid sequence of spCTH522

MKKLLKSVLVFAALSSASSLQALPVG NPAEPSLMIDGILWEGFGGDPCDP
CATWCDAISM RVGYGDFV FDRVLKTDVNKEFQMGAKPTTDTGNSAAP
STLTARENPAYGRHMQDAEMFTNAACMALNIWDRFDVFCTLGATSGYL
KGN SASFNLVGLFGDNENQKTVKAESVPNMSFDQSVVELYTDTTFAWSV
GARAALWECGCATLGASFQYAQSKPKVEELNVL CNAAEFTINKPKGYVG
KEFPLDLTAGTDAATGTKDASIDYHEWQASLALSYRLNMFTPYIGVKWSR
ASFDADTIRIAQPKSATAIFDTTTTLNPTIAGAGDVKTGAEGQLGDTMQIVS
LQLNNMFTPYIGVKWSRASFDADTIRIAQPKSATAIFDTTTTLNPTIAGAGD
VKASAEGQLGDTMQIVSLQLNNMFTPYIGVKWSRASFDSDTIRIAQPRLVT
PVVDITTLNPTIAGCGSVAGANTEGQISDTMQIVSLQLNNMFTPYIGVKWS
RASFD SNTIRIAQPKLAKPVVDITTLNPTIAGCGSVVAANSEGQISDTMQIV
SLQLN*

Supplementary table 1. Amino acid sequences of CTH522 and spCTH522 antigens

Pool 1			Pool 2			Pool 3			Pool 4			Pool 5								
N°	Peptide sequence	N°	Peptide sequence	N°	Peptide sequence	N°	Peptide sequence	N°	Peptide sequence	N°	Peptide sequence	N°	Peptide sequence							
1	MKLLKSLVFAALS	2	LKSVLVFAALSASS	3	LVFAALSASSLQAL	4	ALSSASSLQALPVGN	5	ASSLQALPVGNPAEP											
16	DAISMVRVGYGDFV	17	MRVGYGDFVDRVL	18	YVGFVDRVLKTDV	19	FVDRVLKTDVNFKEF	20	RVLKTDVNFKEFMGA											
30	HMQDAEMFTNAACMA	31	AEMFTNAACMALNIW	32	TNAACMALNIWDRFD	33	CMALNIWDRFDVFT	34	NIWDRFDVFTLGTAT											
44	VKAESVPMFSFDQSV	45	SVPMFSFDQSVVELY	46	MSFDQSVVELYDIT	47	OSVVELYDITTFAWS	48	ELYDITTFAWSVGAR											
58	EELNVLCNAAEFTIN	59	VLNAAEFTINKPKG	60	AAEFTINKPKGVGK	61	TINKPKGVGKPEPL	62	PKGVGKPEPLDLTA											
72	YRLNMFTPIGVKWS	73	MFTPIGVKWSRASFD	74	YIGVKWSRASFDADT	75	KWSRASFDADTIRIA	76	ASFADDTIRIAQPKS											
86	GQLGDTMQIVSLQLN	87	DTMQIVSLQLNMF	88	IVSLQLNMFPIYG	89	QLNMFPIYIGVKWS	90	MFTPIYIGVKWSRASFD											
100	IAGADVKASAEGL	101	GDVKASAEGLGDTM	102	ASAEGLGDTMQIVS	103	GQLGDTMQIVSLQLN	87	DTMQIVSLQLNMF											
114	TPVVDITLNPITAG	115	DITLNPITAGCGSV	116	LNPTIAGCGSVAGAN	117	IAGCGSVAGANTEGQ	118	GSVAGANTEGQISDT											
128	DSNTIRIAQPKLAKP	129	IRIAQPKLAKPVVDI	130	QPKLAKPVVDITLNP	131	AKPVVDITLNPITIA	132	VDITLNPITIAAGCGS											
Pool 6		Pool 7		Pool 8		Pool 9		Pool 10		Pool 11		Pool 12		Pool 13		Pool 14				
N°	Peptide sequence	N°	Peptide sequence	N°	Peptide sequence	N°	Peptide sequence	N°	Peptide sequence	N°	Peptide sequence	N°	Peptide sequence	N°	Peptide sequence	N°	Peptide sequence	N°	Peptide sequence	
6	QALPVGNPAEPLIMI	7	VGNPAEPLIMIDGIL	8	AEPMLIMIDGILWEGF	9	LMIDGILWEGFGDP	10	GILWEGFGDPCDPC											
21	TDVNFQMGAKPTT	22	KEFQMGAKPTTDTGN	23	MGAKPTTDTGNSAAP	24	PTTDTGNSAAPSTLT	25	TGNSAAPSTLTAREN											
35	RFDFVCTLGATSGYL	36	FCTLGATSGYLGKNS	37	GATSGYLGKNSASFN	38	GYLKNSASFNVLGL	39	GNSASFNVLGLFGDN											
49	DTTFAWSVGARAALW	50	AWSVGARAALWECGC	51	GARAALWECGCATIL	52	ALWECGCATILGASF	53	CGCATILGASFQYAQ											
63	VGKEFPLDITAGTDA	64	FPLDITAGTDAATGT	65	LTAGTDAATGKSDAS	66	TDAATGKSDASIDYH	67	TGKSDASIDYHEWQA											
77	ADTIRIAQPKSATAI	78	RIAQPKSATAIFDIT	79	PKSATAIFDITLNP	80	TAIFDITLNPITAG	81	DTLNPITIAAGADV											
91	YIGVKWSRASFDADT	92	KWSRASFDADTIRIA	93	ASFADDTIRIAQPKS	94	ADTIRIAQPKSATAI	95	RIAQPKSATAIFDIT											
105	IVSLQLNMFPIYIG	106	QLNMFPIYIGVKWS	107	MFTPIYIGVKWSRASFD	108	YIGVKWSRASFDSDT	109	KWSRASFDSDTIRIA											
119	GANTEGQISDTMQIV	120	EGQISDTMQIVSLQL	121	SDTMQIVSLQLNMF	122	QIVSLQLNMFPIYI	123	LQLNMFPIYIGVKKW											
133	TLNPITIAAGCGSVAA	134	TIAGCGSVVAANSEG	135	CGSVVAANSEGQISD	136	VAANSEGQISDTMQI	137	SEGQISDTMQIVSLQ											
Pool 11		Pool 12		Pool 13		Pool 14														
N°	Peptide sequence	N°	Peptide sequence	N°	Peptide sequence	N°	Peptide sequence	N°	Peptide sequence	N°	Peptide sequence	N°	Peptide sequence	N°	Peptide sequence	N°	Peptide sequence	N°	Peptide sequence	
11	EGFGDPCDPCATWC	12	GDPCDPCATWCDAIS	13	DPCDPCATWCDASMRVG	14	TWCDAISMRVGYG													
26	AAPSTLTARENPAYG	27	TLTARENPAYGRHMVQ	28	RENPAYGRHMVQDAEM	29	AYGRHMVQDAEMFTNA													
40	SFNLVGLFGDNEQK	41	VGLFGDNEQKTVKA	42	GDNEQKTVKAESVP	43	NQKTVKAESVPMNSF													
54	TILGASFQYAOQPK	55	ASFQYAOQPKVEEL	56	YAOQPKVEELNVLC	57	KPKVEELNVLCNAAE													
68	DASIDYHEWQASLAL	69	DYHEWQASLALSYRL	70	WQASLALSYRLNMF	71	LALSYRLNMFPIYG													
82	LNPTIAGAGDVKTGA	83	IAGAGDVKTGAEGQL	84	GDVKTGAEGQLGDTM	85	TGAEGQLGDTMQIVS													
96	PKSATAIFDITLNP	97	TAIFDITLNPITAG	98	DTLNPITIAAGADV	99	LNPTIAGAGDVKASA													
110	ASFSDTIRIAQPKL	111	SDTIRIAQPKLPTPV	112	RIAQPKLPTPVVDIT	113	PRLVVDITLNP													
124	NMFTPIYIGVKWSRAS	125	PIYIGVKWSRASFDSDN	126	VKWSRASFDSDNTRI	127	RASFDSDNTRIQAQPK													
138	GQISDTMQIVSLQLN	15	MGDAISMRVGYGDF																	

Supplementary table 2. Sequences of the 15-mer peptides overlapping every 11 amino acids. The peptides span the entire sequence of spCTH522 antigen.

Table 3. *Chlamydia* spp. with 100% identity of NMFTPYIGV and ALWECGCATL epitopes within MOMP*

NMFTPYIGV	ALWECGCATL
<i>Chlamydia abortus</i>	<i>Chlamydia muridarum</i>
<i>Chlamydia gallinacea</i>	<i>Chlamydia suis</i>
<i>Chlamydia muridarum</i>	<i>Chlamydia trachomatis</i>
<i>Chlamydia pecorum</i>	<i>Chlamydia trachomatis</i> 434/Bu
<i>Chlamydia psittaci</i>	<i>Chlamydia trachomatis</i> A/363
<i>Chlamydia suis</i>	<i>Chlamydia trachomatis</i> A/5291
<i>Chlamydia trachomatis</i>	<i>Chlamydia trachomatis</i> A/7249
<i>Chlamydia trachomatis</i> C/TW-3	<i>Chlamydia trachomatis</i> A/HAR-13
<i>Chlamydia trachomatis</i> L3/404/LN	<i>Chlamydia trachomatis</i> A2497
<i>Chlamydia trachomatis</i> A2497	<i>Chlamydia trachomatis</i> B/Jali20/OT
<i>Chlamydia trachomatis</i> A/363	<i>Chlamydia trachomatis</i> B/TZ1A828/OT
<i>Chlamydia trachomatis</i> A/5291	<i>Chlamydia trachomatis</i> C/TW-3
<i>Chlamydia trachomatis</i> A/7249	<i>Chlamydia trachomatis</i> D/UW-3/CX
<i>Chlamydia trachomatis</i> A/HAR-13	<i>Chlamydia trachomatis</i> E/CS88
<i>Chlamydia trachomatis</i> G/9768	<i>Chlamydia trachomatis</i> F/SotonF3
<i>Chlamydia trachomatis</i> G/11074	<i>Chlamydia trachomatis</i> G/11222
<i>Chlamydia trachomatis</i> G/9301	<i>Chlamydia trachomatis</i> G/9301
<i>Chlamydia trachomatis</i> G/11222	<i>Chlamydia trachomatis</i> G/9768
<i>Chlamydia trachomatis</i> G/SotonG1	<i>Chlamydia trachomatis</i> G/SotonG1
<i>Chlamydia trachomatis</i> B/Jali20/OT	<i>Chlamydia trachomatis</i> L1/115
<i>Chlamydia trachomatis</i> L2/434/Bu	<i>Chlamydia trachomatis</i> L1/1322/p2
<i>Chlamydia trachomatis</i> L2c	<i>Chlamydia trachomatis</i> L1/224
<i>Chlamydia trachomatis</i> B/TZ1A828/OT	<i>Chlamydia trachomatis</i> L1/440/LN
<i>Chlamydia trachomatis</i> L1/224	<i>Chlamydia trachomatis</i> L2c
<i>Chlamydia trachomatis</i> D/UW-3/CX	<i>Chlamydia trachomatis</i> L3/404/LN
<i>Chlamydia trachomatis</i> L1/115	
<i>Chlamydia trachomatis</i> L1/440/LN	
<i>Chlamydia trachomatis</i> L1/1322/p2	

*based on the BLAST tool in NCBI Entrez Protein Database (nr)

Supplementary table 3. Prevalence of HLA-A*02:01 restricted MOMP peptides in *Chlamydia* species

8.2. List of Figures

Figure 1. Schematic structure of antibodies.....	7
Figure 2. Pathways of antigen processing and presentation.....	10
Figure 3. The multifaceted role of CD4 ⁺ T-cells in CD8 ⁺ T-cell activation.....	12
Figure 4. The life cycle of <i>C. trachomatis</i>	18
Figure 5. Schematic representation of the HHD and HLA-DR1 molecules.....	21
Figure 6. The mucosal immune response to <i>C. trachomatis</i> infection.....	22
Figure 7. Schematic representation of the CTH522 antigen.....	25
Figure 8. Schematic representation of the CTH522 and spCTH522 antigen and schematic map of the pVI-PmH5-CTH522 and pVI-PmH5-spCTH522 shuttle vectors.....	51
Figure 9. Schematic map showing the recombination steps for the integration of the expression cassette from pVI-PmH5-CTH522 into the BAC-MVA genome.....	53
Figure 10. Screening of MVA-CTH522 and MVA-spCTH522 single clones derived from limiting dilution by PCR.....	54
Figure 11. Genetic stability analysis of MVA-CTH522 and MVA-spCTH522 by PCR.....	55
Figure 12. Analysis of antigen synthesis in MVA-CTH522 and MVA-spCTH522 infected DF1 cells.....	56
Figure 13. CTH522 and spCTH522 protein synthesis analysis.....	57
Figure 14. Proteasome-Ubiquitin system interferes with CTH522 protein stability in MVA-CTH522 infected cells.....	58
Figure 15. Viral growth kinetics of MVA-CTH522 and MVA-spCTH522.....	59
Figure 16. Localization of spCTH522 in infected cells.....	61
Figure 17. Schematic representation of the immunization scheme.....	62
Figure 18. Representative flow cytometry plots showing IFN- γ and TNF- α -producing CD8 ⁺ T-cells from the spleens of MVA-WT, MVA-spCTH522 or MVA-CTH522:B7 immunized mice.....	63
Figure 19. MVA-spCTH522 and MVA-CTH522:B7 failed to induce CTH522-specific CD8 ⁺ T-cell responses in mice.....	64
Figure 20. Representative flow cytometry plots showing IFN- γ and TNF- α -producing CD4 ⁺ T-cells from the spleen of MVA-WT, MVA-spCTH522 or MVA-CTH522:B7 immunized mice.....	65
Figure 21. MVA-spCTH522 and MVA-CTH522:B7 induced CTH522-specific CD4 ⁺ T-cell responses in C57BL/6J mice.....	66
Figure 22. MVA-CTH522:B7, but not MVA-spCTH522, induced CTH522-specific antibody responses in C57BL/6J mice.....	67

Figure 23. MVA-CTH522:B7 induced several IgG subtypes composing the CTH522-specific antibody response in C57BL/6J mice.....	69
Figure 24. Schematic representation of the immunization scheme.....	70
Figure 25. MVA-spCTH522 and MVA-CTH522:B7 failed to stably induce CTH522-specific CD4 ⁺ T-cell responses in HLA-A2.DR1 mice.....	71
Figure 26. MVA-spCTH522 induced CTH522-specific CD8 ⁺ T-cell responses in HLA-A2.DR1 mice.	72
Figure 27. Representative flow cytometry plots of epitope-specific CD8 ⁺ T-cells producing IFN- γ and TNF- α from the spleen of MVA-spCTH522 immunized HLA-A2.DR1 mice. ...	73
Figure 28. MVA-spCTH522 and MVA-CTH522:B7 induced epitope-specific CD8 ⁺ T-cell responses in HLA-A2.DR1 mice.	74
Figure 29. Representative flow cytometry plots showing IFN- γ and TNF- α -producing CD4 ⁺ T-cells from the spleen of MVA-WT, MVA-spCTH522 or MVA-CTH522:B7 immunized HLA-A2.DR1 mice.....	75
Figure 30. A booster dose of MVA-spCTH522 and MVA-CTH522:B7 induced reliable CTH522-specific CD4 ⁺ T-cell responses in HLA-A2.DR1 mice.	76
Figure 31. Representative flow cytometry plots showing IFN- γ and TNF- α -producing CD8 ⁺ T-cells from the spleen of MVA-WT, MVA-spCTH522 or MVA-CTH522:B7 immunized HLA-A2.DR1 mice.....	77
Figure 32. A booster dose of MVA-spCTH522 and MVA-CTH522:B7 only increased MOMP ₂₈₂₋₂₀₉ epitope-specific CD8 ⁺ T-cell responses in HLA-A2.DR1 mice.....	78
Figure 33. A booster dose of MVA-spCTH522 and MVA-CTH522:B7 increased MOMP ₂₈₂₋₂₉₀ -specific CD8 ⁺ T-cell responses in HLA-A2.DR1 mice.	78
Figure 34. Multifunctional CD8 ⁺ T-cells induced by MVA-spCTH522 and MVA-CTH522:B7 in HLA-A2.DR1 mice.	79
Figure 35. MVA-CTH522:B7, but not MVA-spCTH522, induced CTH522-specific antibody responses in HLA-A2.DR1 mice.	81
Supplementary figure 1. CTH522:B7 expressed by rec MVA localizes to the cell surface membrane.....	106
Supplementary figure 2. MVA-spCTH522 and MVA-CTH522:B7 synthesized recombinant antigens upon <i>in vitro</i> infection.	106
Supplementary figure 3. Representative flow cytometry plots demonstrating the gating strategy for the analysis of epitope-specific multifunctional CD8 ⁺ T-cells in the spleen. ...	107
Supplementary figure 4. Single dose and prime/boost vaccination regimens with MVA-spCTH522 and MVA-CTH522:B7 induce MVA-specific CD8 ⁺ and CD4 ⁺ T-cell responses.	108

8.3. List of Tables

Table 1. Reaction components for the Phusion PCR of CTH522 or spCTH522 open reading frames.....	36
Table 2. Reaction components for the digestion of PCR derived DNA and pVI-PmH5-dVI plasmid DNA	36
Table 3. Reaction components for the colony PCR of pVI-PmH5-CTH522 or pVI-PmH5-spCTH522 transformed XL-1 blue <i>E. Coli</i> cells.....	37
Table 4. Reaction components for the <i>PacI</i> restriction digest of pVI-PmH5-CTH522 or pVI-PmH5-spCTH522 plasmid DNA	38
Table 5. Reaction components for the colony PCR of GS1783 single colonies carrying recombinant BAC	39
Table 6. Reaction components for the PCR analysis of MVA-CTH522 and MVA-spCTH522 single clones.....	41
Table 7. Reaction components for the Phusion PCR specific for deletion VI of MVA-CTH522 and MVA-spCTH522.....	43
Table 8. Polyacrylamide gel components for SDS-PAGE, with volumes calculated for a single 10% gel.....	45
Table 9. Sequences of peptides containing CD8 ⁺ T-cell epitopes recognized by CTL in the spleens of MVA-spCTH522 immunized HLA-A2.DR1 mice.....	73
Supplementary table 1. Amino acid sequences of CTH522 and spCTH522 antigens.....	109
Supplementary table 2. Sequences of the 15-mer peptides overlapping every 11 amino acids. The peptides span the entire sequence of spCTH522 antigen.....	110
Supplementary table 3. Prevalence of HLA-A*02:01 restricted MOMP peptides in <i>Chlamydia</i> species	111

Acknowledgement

This research was conducted at the Institute of Virology in the research group of Prof. Dr. med. Ingo Drexler and was supported by the European Union's Horizon 2020 Research and Innovation Program under the Marie Skłodowska-Curie Grant Agreement No. 812915.

First and foremost, I am deeply grateful to my supervisor, Prof. Dr. Ingo Drexler, for accepting me as his Ph.D. student and giving me the opportunity to explore the fascinating topic of MVA vaccines within his research group. Thank you for your support, guidance, time, and in-depth scientific discussions that have greatly enhanced my research skills.

I would also like to sincerely thank Prof. Dr. Rainer Kalscheuer for serving as my mentor and for his valuable insights and advice during our meetings.

A special thanks to Ylenia and Sara, who became more than just lab colleagues, they became true friends. I deeply appreciate the wonderful moments we shared in the office, in the lab, and at conferences, as well as your endless generosity in providing snacks during difficult times! It has been an absolute pleasure working with you.

I am also grateful to Sarah, Lena, Judi, Esma, and Kartikan, the students I had the privilege to supervise during their undergraduate and graduate work. Thank you for the joy and fun we had together, and I wish you all the best as you pursue your dreams.

My appreciation extends to the lab members, Sha and Ronny, as well as the PI members of the VacPath consortium. A special thanks to the other PhD students in VacPath, especially Lobna and Emanuele, for their support and for making our time in Siena and Utrecht so enjoyable.

I would like to express my heartfelt gratitude to my lifelong best friends - Riccardo, Martina, Oriana, Valeria and Elena - who are like a second family to me. Their constant presence and support mean the world to me. I would also like to thank all the wonderful people I have had the pleasure of meeting over the years: Piergiuseppe, Irene, Federica, Sophia, Anthea, Arlen, Martina, Antonia, Alex, Nico, Flaminia, Angelina, and Eleonora. Thank you for your patience, your encouragement, and for putting up with me during my never-ending chlamydia talks!

Finally, my deepest gratitude goes to my family-my parents, my sisters, my brothers-in-law, and my little nieces, Angela and Benedetta. Your unwavering love, encouragement, and support in every way have been my greatest source of strength.

I love you all.

Declaration

I declare that I have independently written this thesis, submitted for the degree of Dr. rer. nat. at the Heinrich Heine University Düsseldorf, in accordance with the principles of Good Scientific Practice.

Düsseldorf, 01.04.2025

Giuseppe Andreacchio